CIVIL ENGINEERING STUDIES
Illinois Center for Transportation Series No. 13-023
UILU-ENG-2013-2024
ISSN: 0197-9191

BRIDGE DECKS: MITIGATION OF CRACKING AND INCREASED DURABILITY

Prepared By

Piyush Chaunsali
Seungmin Lim
Paramita Mondal
Douglas Foutch
University of Illinois at Urbana-Champaign

Douglas Richardson
Ying Tung
Riyadh Hindi
St. Louis University

Research Report FHWA-ICT-13-023

A report of the findings of
ICT-R27-88
Bridge Decks: Mitigation of Cracking and Increased Durability

Illinois Center for Transportation

July 2013

Technical /Report Documentation Page

1. Report No.	2. Government Accession No.	3. Recipient's Catalog No.
FHWA-ICT-13-023		

4. Title and Subtitle
Bridge Decks: Mitigation of Cracking and Increased Durability

5. Report Date
July 2013

6. Performing Organization Code

8. Performing Organization Report No.
ICT-13-023
UILU-ENG-2013-2024

7. Author(s)
Piyush Chaunsali, Seungmin Li, Paramita Mondal, Douglas Foutch, Doug Richardson, Ying Tung, and Riyadh Hindi

9. Performing Organization Name and Address

Illinois Center for Transportation
Department of Civil and Environmental Engineering
University of Illinois at Urbana-Champaign
205 N. Mathews, MC 250
Urbana, IL 61801

10. Work Unit (TRAIS)

11. Contract or Grant No.
R27-88

13. Type of Report and Period Covered

12. Sponsoring Agency Name and Address

Illinois Department of Transportation
Bureau of Materials and Physical Research
126 E. Ash St.
Springfield, IL 62704

14. Sponsoring Agency Code

15. Supplementary Notes

16. Abstract

This report discusses the application of expansive cements (Type K and Type G) and shrinkage-reducing admixtures (SRAs) in reducing the cracking due to drying shrinkage. The Type K expansive cement contained portland cement and calcium sulfoaluminate-based component whereas the Type G expansive system was made of portland cement and CaO-based component. The restrained expansion test in accordance with ASTM C 878 demonstrated that Type K and Type G concretes had minimal shrinkage at the end of 100 days. The Type K bridge deck model also exhibited a reduction in tensile strain on the order of 40-50 microstrains and reduction in excess shrinkage potential which showed its effectiveness in reducing the tensile stress due to drying shrinkage. The effect of mineral admixtures on expansion characteristics of Type K and Type G system is also discussed. The effectiveness of SRA was assessed using ASTM C 1581 that clearly showed the delay in cracking time due to addition of an SRA. The increase in SRA dosage reduced the drying shrinkage, but also resulted in reduction of compressive strength.

17. Key Words	18. Distribution Statement
Expansive cement, shrinkage-reducing admixture	No restrictions. This document is available to the public through the National Technical Information Service, Springfield, Virginia 22161.

19. Security Classif. (of this report)	20. Security Classif. (of this page)	21. No. of Pages	22. Price
Unclassified	Unclassified	72 pp. plus appendices	

Form DOT F 1700.7 (8-72) **Reproduction of completed page authorized**

ACKNOWLEDGMENT, DISCLAIMER, MANUFACTURER'S NAMES

This publication is based on the results of ICT-R27-088, **Bridge Decks: Mitigation of Cracking & Increased Durability**. ICT-R27-088 was conducted in cooperation with the Illinois Center for Transportation and the Illinois Department of Transportation.

Members of the Technical Review panel were the following:

Daniel H. Tobias, IDOT Bureau of Materials and Physical Research (TRP Chair)
Julie A. Beran, IDOT Bureau of Materials and Physical Research
James M. Krstulovich, Jr., Bureau of Materials and Physical Research
Brian D. Lokaitis, IDOT Bureau of Materials and Physical Research
Matthew W. Mueller, IDOT Bureau of Materials and Physical Research
Megan Swanson, IDOT Bureau of Materials and Physical Research
Solomon W. Wab-Lumor, IDOT Bureau of Materials and Physical Research
Melinda S. Winkelman, IDOT Bureau of Materials and Physical Research
David L. Greifzu, IDOT Bureau of Bridges and Structures
Douglas A. Dirks, IDOT Bureau of Construction
Justan W. Mann, IDOT Bureau of Operations
Gary J. Welton, IDOT District 7
Steven Gillen, Illinois Tollway
Randell Riley, Illinois Chapter, American Concrete Pavement Association
Dan Brydl, Federal Highway Administration
Brian Pfeifer, Federal Highway Administration
Abraham Ramirez, Federal Highway Administration
Hal Wakefield, Federal Highway Administration

EXECUTIVE SUMMARY

Concrete elements that have large surface-to-volume ratios, such as bridge decks, are vulnerable to cracking as a result of drying shrinkage. This study examined the two mitigation techniques that use shrinkage-compensating cements and shrinkage-reducing admixtures (SRAs) to reduce the extent of shrinkage cracking. Shrinkage-compensating cements develop compressive stress in concrete during hydration that later counteracts tensile stresses induced by shrinkage, whereas shrinkage-reducing admixtures reduce the surface tension of pore water and thereby decrease the capillary stress and shrinkage induced by drying. Both of these materials were used with the goal of developing specifications for the Illinois Department of Transportation (IDOT).

Two different shrinkage-compensating cements were used in this study. The first was based on calcium sulfoaluminate (Type K), and the second was based on calcium oxide (Type G).The expansion in Type K and Type G systems is driven by the formation of ettringite and calcium hydroxide, respectively. Concrete incorporating 15% of Type K component exhibited 7-day restrained expansion of ~0.05%, which was found in small-scale testing to be sufficient to compensate for shrinkage (according to ASTM C878). Even after 100 days, concrete prisms showed minimal shrinkage strain. A similar magnitude of restrained expansion was observed in concrete with a 6% Type G component. The main difference between Type K and Type G concretes was in the rate of expansion: Type G concrete expanded at a faster rate than Type K concrete. The 28-day strength of both Type K and Type G concretes was comparable to the control concrete mix (without any expansive component).

The effect of mineral admixtures such as fly ash on the expansion of concrete mixes was also studied in this project. Addition of Class F fly ash increased expansion in both expansive concretes (with Type K and Type G), whereas silica fume reduced the extent of expansion. Addition of Class C fly ash initially increased expansion, but expansion stopped earlier than usual in the Type K–based mix. However, addition of Class C fly ash to the Type G mix increased expansion. The research showed that the effects on expansion by adding mineral admixtures are due to both the changes in the chemistry of the reaction products and the material resistance offered against expansion. It is recognized that any expansion before the setting of concrete is not effective in mitigating shrinkage. This research showed that any admixture that alters setting time can alter the effective expansion of a concrete mix; hence, the test method in accordance with ASTM C878 may not be sufficient for predicting effective expansion.

The presence of a high amount of calcium hydroxide in Type G–based concrete led to an investigation of the susceptibility for an alkali-silica reaction (ASR) in concrete with Type G. The length change measurements according to ASTM C227 did not show any firm evidence of higher likelihood of ASR in Type G concrete. Moreover, the pore solution analysis showed lower alkali concentration when Type G was used, which again does not suggest higher susceptibility for ASR.

Shrinkage-reducing admixtures were also found to be effective in reducing the shrinkage cracking of concrete. A ring test (in accordance with ASTM C1581) was performed to determine the cracking tendency of a concrete mix by counting the number of days before cracks appear on concrete rings. Concrete rings cracked beyond 30 days when an SRA was used. An increase in SRA dosage was found to increase the time for cracking to occur, but it also reduced compressive strength. A reduction of approximately 50% in free (drying) shrinkage was observed when a high dosage of one specific type of SRA was used.

Running concurrently with the small-scale materials tests were large-scale lab tests that monitored the strains within a 10 x 7-ft. prototypical Illinois bridge bay. Though the small-scale materials test showed the effectiveness of Type K, Type G, and SRA in mitigating shrinkage, it was important to check whether the same were true for a laboratory-scale model bridge bay before this technology is applied in the field. The bay was first poured with a control mixture similar to what is currently used by IDOT practitioners. Strain and temperature were monitored for several months. Once this step was completed, a second bay was created with the same specifications, but this time using a Type K concrete mixture based on the results of the small-scale materials tests. Similar to the small-scale tests, Type K concrete expanded at the early age; however, the expansion in this case was much smaller because of the higher amount of restraint provided by the steel reinforcement and end restraint used to mimic a long, continuous bridge deck. Therefore, instead of a 400-microstrain difference in expansion observed in small-scale testing between the concrete mixes without and with Type K, only a 30- to 50-microstrain difference in strain in the reinforcing bar was observed. Later on, as the bridge bay started to shrink, tensile stress started to develop. At the end of the test period, a difference of ~10 to 30 microstrains in tension was observed between the bridge bay with the control mixture and the bridge bay with Type K. Furthermore, careful observation showed that the resulting strain due to cracking caused by the release of the stored tensile stress in concrete was smaller for the Type K bridge bay. However, quantifying the potential benefits of Type K with respect to cracking mitigation will require further analysis correlating the small-scale and large-scale test results to understand the mechanism behind the reduction in shrinkage strain potential. For example, by comparing the small-scale test results with the large-scale test results, it was also found that the excess shrinkage potential due to the higher restraint against movement in the large-scale model was reduced in the Type K bridge bay which is hypothesized to reduce stored tensile stress in concrete compared to conventional non-expansive concrete.

On the basis of the experimental data, a finite element model was created for the experimental decks using SAP2000. Temperature loads were found using ratios based on the recorded strain values. These loads were then applied to the SAP2000 model and modified to appropriately match the recorded data. The model was refined until the difference between the experimental strains and the strains predicted by the finite element models were less than 15%, with most being differences in the range of 5% to 10%.

The possibility of a heated girder creating cracks in the concrete deck was also investigated using the SAP2000 and Abaqus models. Thermal loads of 10°F to 30°F were applied to the girder and the resultant strains in the deck were investigated. Though the 30°F temperature differential between the girder and concrete is high, a maximum of 30 microstrains developed in the reinforcing bars.

Once these initial steps were taken to model the laboratory experiments, a full bridge was modeled in Abaqus using the same procedures. This full bridge model is expected to provide reliable information on future bridge deck strains, thus proving useful in a predictive capacity. This final model culminates the cycle from small-scale material testing to large-scale lab testing and modeling to full-scale models. Through this process, the control and Type K mix designs were studied. In the future, SRAs and other materials will be used in mix designs studied through this same process.

CONTENTS

CHAPTER 1 INTRODUCTION

Mitigation of cracking in concrete bridge decks is a challenging problem across the United States. The dominant pattern of cracking in Illinois is transverse along the deck and occurs at fairly regular intervals. Figure 1 shows transverse cracking under bridge decks caused by shrinkage. Concrete decks, especially because of their large surface/volume ratio, are more vulnerable to shrinkage cracking. The widespread occurrence of shrinkage cracking calls for development of superior concrete with a low potential for cracking.

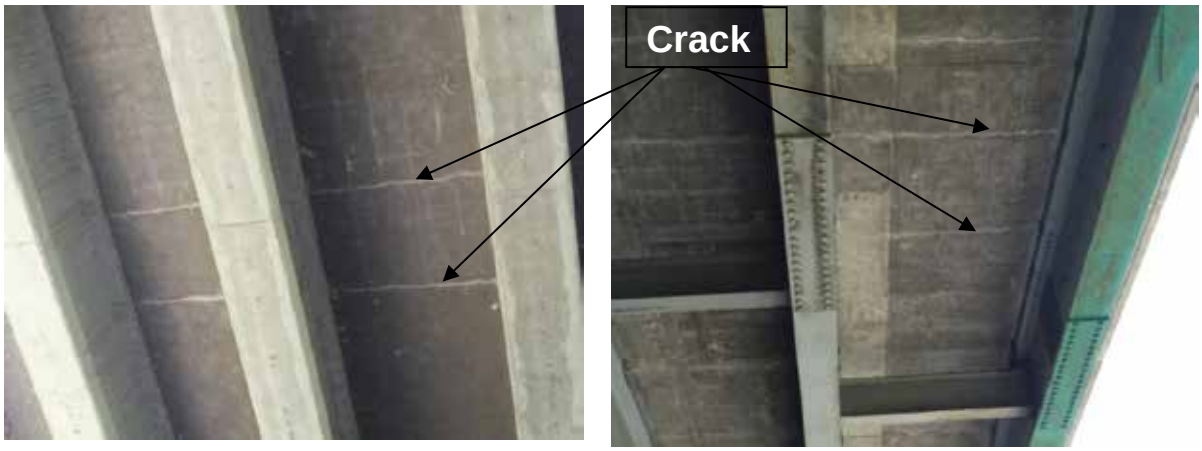

Figure 1. Transverse cracking in concrete bridge (left), and steel girder bridge (right).

Restrained shrinkage that occurs soon after pouring is theorized to be one of the primary causes of this cracking. It is important to note, however, that regular transverse crack patterns occur in both positive and negative moment regions, even though bridge decks in Illinois are typically constructed to not be fully composite in negative moment regions over piers. Consequently, it is thought that the effects of intermittent structural restraint in combination with long distances without expansion joints along bridge decks produce what can be considered a net relatively uniform global tension acting longitudinally along bridge decks. This net uniform tension is also thought to be present (and is a contributing factor to the creation and/or exacerbation of transverse deck cracking) as superstructure beams expand and contract because of normal temperature fluctuations in service. In both cases (restrained shrinkage, and thermal expansion and contraction), the deck can be thought of as essentially “subject to the whims” of the superstructure beams because of its lack of flexibility in conjunction with tensile strength.

Significant research has been conducted on assessment of cracking in bridge decks through field investigation (Eppers et al. 1998; French et al. 1999a, 1999b); new approaches to concrete mix designs, particularly using local aggregates and other concrete constituent materials (Streeter 1996; Lawler et al. 2006; Brown et al. 2007); using steel or polymer fibers or other additives (e.g., Whiting et al. 2000; Altoubat and Lange 2001; Subramaniam et al. 2005; Naik et al. 2006); structural design configuration and the potential influence on restraint of the deck (Le et al. 1998; French et al. 1999a, 1999b); improved curing procedures (Deshpande et al. 2007); and development of laboratory procedures to validate whether specific mixes used in the field are susceptible to premature cracking (Brown et al. 2007).

Consensus has been developed in prior research, with the following general findings:

- Bridge deck cracking is primarily caused by shrinkage of the deck concrete. Drying shrinkage is often considered the dominant form of shrinkage that leads to this cracking, but plastic shrinkage, autogenous shrinkage, and thermal shrinkage are also contributing factors. A variety of mix designs or additives have been investigated to mitigate this problem. It is often emphasized that local aggregates or other materials influence the choice of concrete mix. In addition, casting conditions (such as weather) may influence deck cracking. Thus, success at mitigating cracking across the United States often varies from state to state.
- Other effects have been studied and shown to contribute to reduce cracking (French et al. 1999a); however, these recommendations may not be easy to implement for the type of bridges constructed in Illinois:
    - Minimizing the restraint on the bridge (e.g., by minimizing the use of shear connectors or large transverse reinforcement)
    - Using cast-in-place or newly precast concrete girder bridges rather than steel girder bridges (steel girder bridges tend to exhibit more cracking)
    - Pouring the deck only when ambient temperature is neither too cold nor too hot

In the late 1990s, the Illinois Department of Transportation (IDOT) began using high-performance concrete (HPC) mixes for bridge decks on selected projects. It was expected that use of HPC in Illinois would produce less cracking of bridge decks. As a consequence, less chloride penetration (i.e., a less permeability) and a more durable performance than conventional mixes (Aitcin 2003) was expected, thereby producing bridge decks with significantly increased life spans in Illinois. Unfortunately, this was not the case for a significant portion of the selected structures. Some of the HPC bridge decks constructed in Illinois cracked with greater frequency and increased severity than conventional mixes used by IDOT. So, there remains a need to review the state-of-the-art research on premature deck cracking and investigate the best solutions for Illinois, with a focus on the use of HPC and, as appropriate, local aggregates and other constituent materials in the concrete.

The objective of the proposed research project was to develop procedures that mitigate premature cracking in concrete bridge decks. A corollary benefit of this research is that bridge deck durability should increase when cracking is decreased. Specific objectives include the following:

- Determine whether recommendations from earlier national research are applicable to Illinois.
- Document the shrinkage and premature cracking behavior of common mixes used in Illinois, as well as propose mixes that mitigate deck cracking; these mixes will be based on use of constituent ingredients commonly used in Illinois.
- Develop design and construction recommendations to help mitigate premature cracking in concrete bridge decks.

Various methods have been suggested to mitigate shrinkage cracking, such as the use of shrinkage-compensating cements, shrinkage-reducing admixtures, and lightweight aggregate. The current work focused on evaluating the potential of two expansive cements: a calcium sulfoaluminate cement (or Type K component) and a CaO-based component (Conex, or Type G) to mitigate shrinkage. Early-age and hardened properties of expansive

pastes/concretes were examined. In addition, the potential of shrinkage-reducing admixtures was investigated. In addition to small-scale materials testing, large-scale laboratory model and finite element modeling was used to fully understand the potential of expansive additives before applying those technologies in the field.

CHAPTER 2 LITERATURE REVIEW

This chapter provides a detailed review of previous research on the factors influencing the shrinkage of concrete and its mitigation techniques. The following sections include a summary of the effects of different concrete mix constituents that are reported to affect autogenous and drying shrinkage of concrete and hence should be considered for crack mitigation of bridge decks. A comprehensive literature review on use of expansive cements and concrete is also presented.

2.1 AUTOGENOUS SHRINKAGE

Autogenous deformation of cement paste is defined as "the bulk deformation of a closed, isothermal, cementitious material system not subjected to external forces" (Jensen and Hansen 1996). The reduction in internal relative humidity (RH) without any loss of moisture to the external environment causes autogenous shrinkage of cement paste. The factors that have been found to affect the autogenous shrinkage of concrete are discussed in detail in the following subsections.

2.1.1 Influence of Water-to-Cementitious Material Ratio (w/cm)

High-performance concrete is expected to have increased autogenous shrinkage because of higher cement content and the pozzolanic mineral admixtures that consume additional water in a reaction to form secondary calcium silica hydrate (C-S-H) (Jensen and Hansen 1996). A low w/cm ratio causes a reduction in internal RH, which thereby increases capillary tension. This increase in capillary tension results in self-desiccation, which causes autogenous shrinkage (Bentz et al. 2001a). Autogenous shrinkage continues as long as the cement hydrates. With the decrease in w/cm ratio, autogenous shrinkage increases (Tazawa and Miyazawa 1995; Holt 2005). It is observed most often in concrete with a w/cm ratio less than 0.42 and in concrete with a high silica fume content.

2.1.2 Influence of Aggregate Content

As the paste shrinks, the aggregate offers a restraint. Hence, the volume of aggregate plays a crucial role in influencing shrinkage. An increase in aggregate volume reduces autogenous shrinkage (Tazawa and Miyazawa 1995; Holt 2005). Aggregate stiffness also influences shrinkage of concrete. As aggregate stiffness increases, it offers higher resistance to volume change and reduces shrinkage.

2.1.3 Influence of Mineral Admixtures

At present, the use of supplementary cementitious materials such as fly ash, ground granulated blast-furnace slag, and silica fume has become a common practice. Silica fume addition has been reported to increase the autogenous shrinkage of cement paste (Jensen et al. 1996). In their study, Jensen and Hansen (1996) reported an increase of 1000με shrinkage for 10 % silica fume addition. A mechanism was proposed to explain the considerable increase in autogenous shrinkage with the addition of silica fume. The consumption of calcium hydroxide during the secondary C-S-H formation was attributed for the increase in autogenous shrinkage as calcium hydroxide in plain concrete can act as restraining components to volume change (and hence reduce shrinkage). Furthermore, refinement of pore structure was observed that causes self-desiccation (Jensen and Hansen 1996) and additional shrinkage. Slag also has been found to increase the autogenous shrinkage of paste (Tazawa and Miyazawa 1995). The role of fly ash in influencing autogenous shrinkage is still not clear. Setter and Roy (1978) did not observe any significant

effect on autogenous shrinkage of cement paste with the addition of fly ash. However, in another study, autogenous shrinkage increased with the addition of Class F fly ash (Justnes et al., 1998).

Autogenous shrinkage of concrete mixtures consisting of silica fume and slag or fly ash has also been investigated (Subramaniam and Agrawal 2009). A concrete mixture with silica fume and fly ash had lower autogenous shrinkage than the mixture consisting of silica fume and slag.

2.1.4 Influence of Fineness

Fineness of cement greatly influences the autogenous shrinkage. With the increase in fineness of cement, an increase in autogenous shrinkage was observed in previous studies (Tazawa and Miyazawa 1995; Bentz et al. 2001a). Finer cement reduces internal relative humidity, which increases tensile stresses and causes more autogenous shrinkage.

2.1.5 Effect of Shrinkage-Reducing Admixtures

Weiss (1999) showed that the addition of SRAs significantly reduce autogenous shrinkage of HPC measured from the time of set. Approximately 50% of shrinkage was reduced at 90 days (Weiss 1999). In a different study, autogenous shrinkage of cement mortar containing a w/cm ratio of 0.35 was reduced substantially with the addition of SRA (Bentz et al. 2001b).

2.2 DRYING SHRINKAGE

Drying shrinkage is caused by evaporation of free water from the capillary pores of concrete. Drying is a surface phenomenon and proceeds only if the relative humidity of air is less than the humidity within the capillary pores. The pore structure features, surface-to-volume ratio, and ambient environmental conditions (temperature, relative humidity, wind speed) influence drying shrinkage behavior significantly. Drying shrinkage alone would not be of any concern if the concrete were allowed to shrink freely. However, in the presence of restraint provided by surrounding structural components, internal tensile stresses develop. When the internal tensile stress exceeds the tensile strength of concrete, it cracks. Once cracks are formed within concrete, durability and load-carrying capacity are significantly reduced. Most of the factors that influence autogenous shrinkage also affect drying shrinkage. The following section presents in detail the factors that have been found to affect the drying shrinkage of concrete.

2.2.1 Effect of w/cm Ratio

Drying shrinkage has been found to be influenced by the w/c ratio. El Hindy et al. (1994) observed a significant influence of w/cm ratio and curing period on the drying shrinkage of HPC. An increase in w/c ratio increased the drying shrinkage, while the longer curing period caused a reduction in drying shrinkage. Aktas et al. (2007) also observed an increase in drying shrinkage of concrete with an increase in w/c ratio.

Bloom and Bentur (1995) investigated the drying shrinkage of concrete mixtures with w/cm ratios of 0.33, 0.40, and 0.50. There was no clear trend observed with regard to the effect of w/c ratio on drying shrinkage, especially for low w/c ratio mixtures. Lange et al. (2003) observed that the difference in free shrinkage of concrete mixtures containing low w/cm ratios (0.44 and 0.39) was not significant. It was hypothesized that the decrease in drying shrinkage was counteracted by an increase in autogenous shrinkage when the w/cm ratio was lowered from 0.44 to 0.39. Deshpande et al. (2007) evaluated the drying shrinkage

of concrete mixtures that had different aggregate contents and w/cm ratios. For a given aggregate content, no significant effect on drying shrinkage was observed with the change in w/cm ratio.

2.2.2 Effect of the Aggregate Type and Content

Babaei and Purvis (1995) examined the effect of mineralogy of aggregate on the drying shrinkage. Concrete with sandstone coarse aggregate (low stiffness) was found to have higher drying shrinkage than concrete with dolomite coarse aggregate (high stiffness). The absorption capacity of aggregate also affected the drying shrinkage. A higher absorption capacity led to increased shrinkage (Babaei and Purvis 1995). Aktas et al. (2007) investigated the influence of different coarse-to-fine aggregate (CA/FA) ratios on the free shrinkage of concrete mixtures. Concrete with a low CA/FA ratio showed high drying shrinkage. Deshpande et al. (2007) reported a decrease in drying shrinkage with an increase in the aggregate content of the mix. Concrete with granite coarse aggregates showed lower shrinkage than limestone coarse aggregates.

2.2.3 Effect of Mineral Admixtures

The effect of mineral admixtures on the drying shrinkage has been investigated previously by many researchers. Babaei and Purvis (1995) reported an increase in drying shrinkage with the addition of fly ash. Lange et al. (2003) investigated drying shrinkage of HPC mixtures. Free shrinkage was determined using prismatic and uniaxial specimens. The expansion of uniaxial specimens containing mineral admixtures was found to be more than that of the control mix. Drying shrinkage was observed to be the maximum for silica fume, which was attributed to its high silica content and fine particle size. However, the long-term (40 days) drying shrinkage of concrete prisms mineral admixtures was found to be lower than the control mix. Deshpande et al. (2007) reported that the addition of Class C fly ash and ground granulated blast-furnace slag increased early-age drying shrinkage compared with the control mix. However, the ultimate shrinkage was not found to be significantly affected in the case of ground granulated blast-furnace slag. Subramaniam and Agrawal (2009) evaluated the influence of ternary cement blends using silica fume, fly ash, and slag. Drying shrinkage of concrete mix containing silica fume and fly ash was observed to be more than the concrete mixtures with silica fume and slag.

2.2.4 Effect of Shrinkage-Reducing Admixtures

Concrete shrinks as a consequence of losing water from its pore space. The difference in relative humidity when exposed to the atmosphere creates a RH gradient that triggers the loss of water, resulting in generation of capillary stresses. The addition of an SRA does not appear to change the total loss of water (Weiss 1999; Sant et al. 2007). However, SRAs significantly lower the surface tension of water, which in turn lowers shrinkage strain at a low RH (Sant et al. 2007).

2.3 EXPANSIVE AND SHRINKAGE-COMPENSATING CEMENTS

Expansive cements utilize the early-age expansion of cement by inducing a compressive stress that later counteracts the tensile stresses developing from drying shrinkage. The following sections discuss the two types of expansive cements that were used in this study.

2.3.1 Type K (Calcium Sulfoaluminate-Based System)

Type K cement contains ordinary portland cement and calcium sulfoaluminate (CSA) cement. The main constituents of CSA cement are calcium sulfoaluminate or ye'elimite [$(CaO)_4(Al_2O_3)_3(SO_3)$], calcium sulfate ($CaSO_4$) and belite (C_2S). The expansion necessary for inducing compressive stress is achieved through formation of ettringite crystals. Though developed for shrinkage-compensating concrete, CSA cement also provides a sustainable alternative to portland cement by reducing CO_2 production during manufacturing. The main ingredient of CSA cement is ye'elimite ($C_4A_3\hat{S}$), which, on reaction with gypsum, forms ettringite. The formation of ye'elimite requires a kiln temperature of 1250°C, which is lower than 1400°C for portland cement (Ali et al. 1994). The lower temperature requirement significantly reduces energy demand. At the same time, manufacture of CSA clinker requires a lower amount of lime than required for portland cement. Both of these factors significantly reduce the CO_2 production associated with these cements. Furthermore, the CSA clinker is more friable than portland cement clinker, which also lowers the energy required for its grinding.

Many studies have dealt with the hydration of CSA cement and the factors influencing its expansion. The main cause of expansion in these cements is the formation of ettringite. The following reactions can be attributed to the formation of ettringite (Collepardi et al. 1972; Kasselouri et al. 1995):

$$C_4A_3\dot{S} + 2\,C\dot{S}H_2 + 34\,H \longrightarrow C_3A.3C\dot{S}.32H + 2AH_3 \quad (1)$$

$$C_4A_3\dot{S} + 6\,Ca(OH)_2 + 8\,C\dot{S}H_2 + 74\,H \longrightarrow 3\,C_3A.3C\dot{S}.32H \quad (2)$$

$$AH_3 + 3Ca(OH)_2 + 3\,C\dot{S}H_2 + 20H \longrightarrow C_3A.3C\dot{S}.32H \quad (3)$$

$$C_2S + 2H \longrightarrow C\text{-}S\text{-}H + CH \quad (4)$$

where

C = CaO

A = Al_2O_3

$\dot{S}$ = SO_3

H = H_2O

AH_3 can also form in absence of lime. In the presence of lime, AH_3 can take part in a reaction and can form ettringite, as shown in Reaction 3. The presence of lime is expected to make Reaction 2 (which is basically a combination of Reactions 1 and 3) more favorable than Reaction 1, resulting in formation of larger amount of ettringite. Therefore, the hydration of CSA results in larger amount of ettringite following Reaction 2 in a C_3S-based system, compared with a C_2S-based system where Reaction 1 is favored (Collepardi et al. 1972). Mehta (1973) studied the influence of lime on the hydration of $C_4A_3\hat{S}$ and found that the ettringite formed in the presence of lime is colloidal compared with the lath-like morphology seen in the absence of lime. It was also observed that the presence of lime retards the hydration of $C_4A_3\hat{S}$ during the first 6-hr period.

There exist two schools of thought on the proposed mechanism of expansion resulting from ettringite formation. According to the first school of thought, the expansion is driven by the crystallization pressure induced by ettringite formation, which can take place either topo-chemically (around the CSA particle) or in the solution. The crystal growth theory

as an expansion mechanism has been reported in studies by Kalousek and Benton (1970), Bentur and Ish-Shalom (1974), and Cohen and Richards (1982). The second school of thought emphasizes on the swelling of ettringite gel for the expansion (Mehta 1973). In portland cement, ettringite is usually colloidal because of the presence of lime. Colloidal ettringite is reported to adsorb water and cause significant swelling and expansion (Mehta and Hu 1978).

Expansion has been found to be greatly influenced by the particle size distribution. The fine particle size of $C_4A_3\hat{S}$ has shown a higher rate and shorter duration of expansion than the coarse particle size (Cohen and Richards 1982; Chen et al. 2012). The fine CSA particles deplete at a faster rate than the coarser particles because of the large number of distributed expansive sites (Cohen and Richards 1982). A lower w/cm ratio is reported to result in incomplete hydration of $C_4A_3\hat{S}$, leaving scope for delayed hydration of the remaining unhydrated $C_4A_3\hat{S}$ particle. The expansion caused by delayed hydration can pose significant damage to concrete. In a study, the compressive strength and the dimensional stability of $C_4A_3\hat{S}$-$C_5S_2\hat{S}$-$C\hat{S}$ system were investigated by varying the water-to-solid (w/s) ratio and the $C_4A_3\hat{S}$ content (Beretka et al. 1996). At a low w/s ratio, the performance was adversely affected as a result of less water for the hydration of $C_4A_3\hat{S}$ and, at the same time, a higher fraction of $C_4A_3\hat{S}$ led to cracking caused by large expansion.

Various factors have been found to affect the expansion of Type K cements. The predominant ones are cement composition, fineness, cement content, aggregate type, admixtures, mixing time, curing, temperature, and restraint (Polivka 1973). Lobo and Cohen (1991) observed that the addition of silica fume lowered the expansion in silica fume–modified Type K cement pastes. In same study, silica fume was found to increase the ettringite formation rate and magnitude at early age along with a reduction in duration of expansion. Folliard et al. (1994) also observed a reduction in restrained expansion and chloride permeability when Type K cement was replaced by silica fume and fly ash. Although silica fume increased the compressive strength of Type K cements, fly ash addition decreased the compressive strength, especially at early age.

The restraint (external or internal) influences the extent of expansion and rate of stress development in expansive concretes. Gulyas et al. (2008) reported that the use of Type K cement with lightweight aggregate for internal curing improved performance of bridge decks. The study also highlighted the importance of expansion joint design in fully reaping the benefits of expansive cement because it allows the necessary expansion required for shrinkage compensation.

2.3.2 Type G (CaO-Based System)

Type G cement is In a CaO-based system, however, the formation of calcium hydroxide ($Ca(OH)_2$) crystals results in an expansion that has been attributed to the crystal growth pressure of $Ca(OH)_2$ (Chatterji 1995). A very limited number of studies pertaining to CaO-based cement are available in the literature (Russell et al. 2002). The reaction involving the precipitation of calcium hydroxide is expressed as follows:

$$CaO + H_2O \longrightarrow Ca(OH)_2$$

2.4 SUMMARY OF INVESTIGATION BY OTHER DOTS

The New York DOT (Subramaniam and Agrawal 2009) investigated the potential of ternary cement blends using silica fume and fly ash on shrinkage cracking of HPC. The

study showed that the concrete incorporating slag and silica fume exhibited the maximum autogenous shrinkage within first day; however, it had lower drying shrinkage at any age when compared with concrete having silica fume and fly ash. Concrete with fly ash and silica fume showed a very low potential for cracking under restrained shrinkage. This can be attributed to the lower magnitude of elastic modulus with a slower rate of increase, which in turn is responsible for lower stress under restrained conditions and a slower rate of stress development, even though there was a high shrinkage rate. The study recommended use of Type I/II or Type II cement and careful examination of blast-furnace slag before implementation.

KANSAS DOT (Deshpande et al. 2007) examined effects of various factors on the drying shrinkage behavior of concrete mixtures. Drying shrinkage was found to be increased with a reduction in the aggregate content and curing period, and with the addition of mineral admixtures (Class C fly ash and blast-furnace slag). In addition, Type II cement showed lower shrinkage than Type I. The recommendations of the Kansas study included reduction in paste content, use of granite coarse aggregate over limestone, selection of coarser cement, increase in curing period, and careful use of mineral admixtures.

NEW JERSEY DOT (Aktas et al. 2007) evaluated the restrained shrinkage properties of HPC mixes. The results showed that total coarse aggregate content and the CA/FA ratio had the greatest effect on both free and restrained shrinkage. The CA/FA ratio of more than 1.48 reduced the restrained shrinkage cracking in HPC. The high cementitious material content also increased the cracking potential. Free shrinkage rate prior to cracking was found to correlate directly with the restrained shrinkage prior to cracking and time to cracking for a given mix. The final recommendations included the limitation of cementitious material to 700 lb/yd^3, high CA/FA ratio (more than 1.48), and a maximum percentage of silica fume of 5%.

TEXAS DOT (Folliard et al. 2003) evaluated the potential benefits of using innovative materials to control shrinkage cracking, both in small- and large-scale laboratory testing. To provide the best resistance to drying shrinkage cracking in concrete bridge decks, the use of SRA, CSA, fiber, and high-volume fly ash (HVFA) were recommended.

ILLINOIS DOT (Lange et al. 2003) investigated early-age thermal, shrinkage, creep, and cracking behavior of various HPC bridge decks. Concrete mixtures with mineral admixtures caused an increase in unrestrained shrinkage. Specifically, silica fume had greater effect on shrinkage than fly ash. However, the long-term (40 days) drying shrinkage of concrete prisms with mineral admixtures was found to be lower than the control mix. An increase in w/cm from 0.44 to 0.50 increased the shrinkage; however, a mix with w/cm 0.39 showed even higher shrinkage. It was proposed that for w/cm as low as 0.39, the benefit of reduced drying shrinkage from lower w/cm was probably counteracted by an increase in autogenous shrinkage.

PENNSYLVANIA DOT (Babaei and Purvis 1995) examined the influence of aggregate source, cement source, and fly ash on drying shrinkage. The study revealed that the higher absorption of the aggregate resulted in higher shrinkage. Furthermore, the cement replacement with fly ash increased the drying shrinkage.

A COLORADO DOT study (Shing and Abu-Hejleh 1999) focused on changes in material specifications and construction practices to reduce the severity of deck cracking. The use of Type II cement and Class F fly ash was suggested to reduce heat of hydration and early-age strength (fast strength gain is considered detrimental). A maximum 6 % silica

fume by weight of cement and large-size, well-graded aggregate were recommended to avoid shrinkage cracking.

OHIO DOT (Lefchik 1994) investigated the performance of bridge decks with regard to rapid permeability testing, strength testing, and chloride ion testing. The results showed that the Type K concrete is inferior to Class S and Class C with respect to permeability, chloride penetration, scaling susceptibility, and delaminations. The addition of microsilica to Type K concrete reduced the average permeability to that equal to Class S concrete, but other durability parameters were not improved. The high variability in cracking indicated that the cracking might be sensitive to construction practices, placement, and curing conditions.

CHAPTER 3 DRYING SHRINKAGE OF CEMENTS

IDOT receives Type I portland cement from 12 different suppliers; however, the shrinkage characteristics of the various cements were unknown. On the basis of the suggestion made by the TRP for this project, the first task was to determine whether any specific cement provides particularly favorable or adverse behavior with respect to shrinkage. The following sections present the preliminary investigation of the shrinkage characteristics of 12 cements.

3.1 SHRINKAGE AND MASS LOSS

Shrinkage of mortar bars made out of the 12 cements was measured according to ASTM C596 (see Section A.3.6 in Appendix A for details on the test method). Figure 2 (a) shows the drying shrinkage of 12 different cements as a function of drying period. It is evident that for all cements, shrinkage strain increased with the drying period. The rate of shrinkage was higher at an early age, and it slowed down later. However, at the end of 25 days of the drying period (28 days after casting, which includes 3 days curing in saturated lime water), shrinkage of all mixes were still increasing. It is clear from Figure 2 (a) that no cement showed drastically different behavior. All mixes had final shrinkage strain after 25 days within the range of 800 to 1050 microstrains.

It should be noted that all cements used in this investigation were Type I portland cements. Along with shrinkage measurements, the weight of the individual mortar bar was also measured at various time intervals. As expected, the weight of the samples decreases as water evaporates from them during drying. It can be seen in Figure 2 (b), total weight loss at the end of the drying period varied between 3% and 3.75%. As drying shrinkage occurs as a result of loss of water from the sample, it is expected that measured weight loss would be related to the measured shrinkage for each beam.

By comparing Figure 2 (a) and (b), it is clear that both shrinkage and weight loss vary the same way with drying period. To explore this relationship better, shrinkage was plotted against weight loss for each mortar bar, as shown in Figure 3 (a). Furthermore, when both shrinkage and weight loss measurements were normalized with respect to the final value of the shrinkage and weight loss measured at the end of 25 days of drying for each bar, as plotted in Figure 3 (b), a non-linear expression (R^2 = 0.99) could be used to relate the normalized shrinkage with the normalized weight loss. This empirical relationship between the drying shrinkage and weight loss can be used to determine shrinkage behavior by measuring weight loss only.

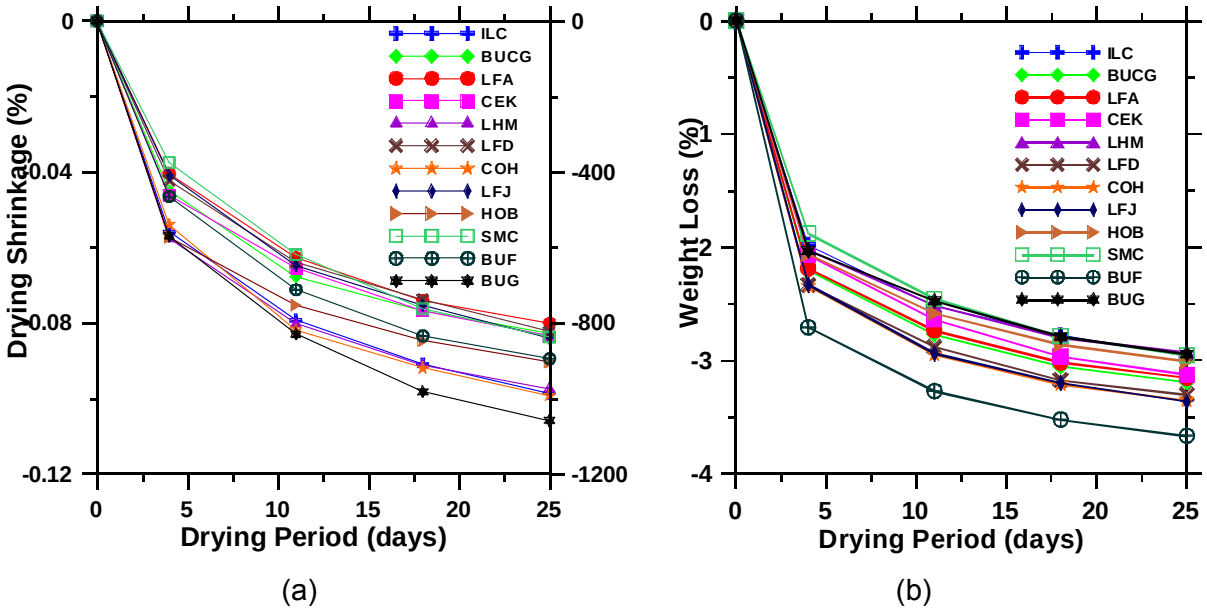

(a) (b)

Figure 2. Effect of drying period on (a) drying shrinkage, and (b) weight loss of prismatic mortar bars.

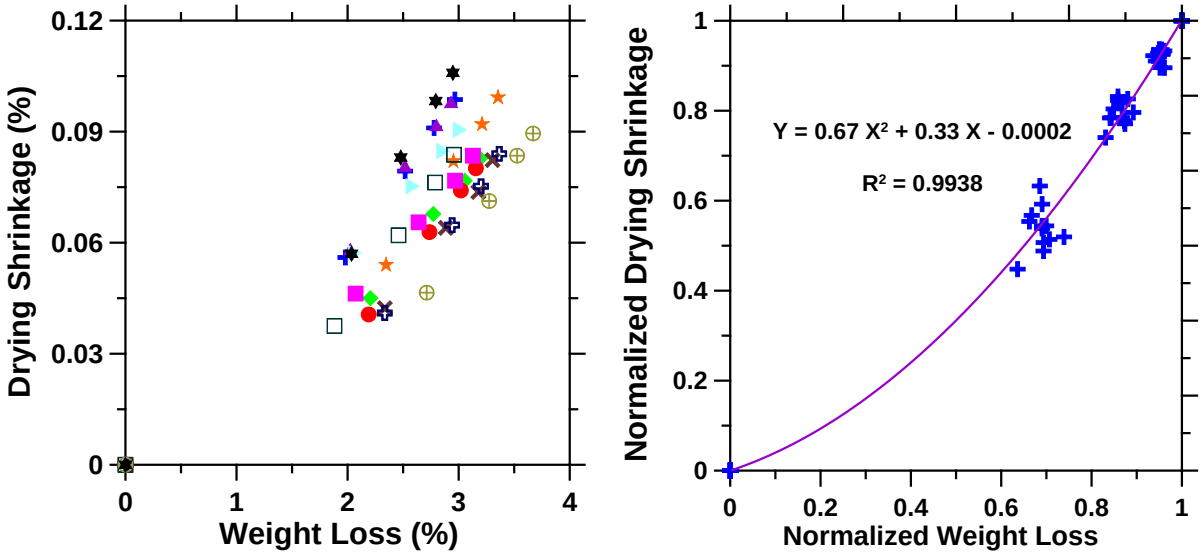

(a) (b)

Figure 3. (a) Drying shrinkage vs. weight loss, and (b) normalized (with respect to maximum shrinkage) drying shrinkage vs. normalized (with respect to maximum weight loss) weight loss.

3.2 SUMMARY

The 12 cements showed shrinkage strain in the range of 800 to 1050 microstrains after 25 days of drying. As expected, the drying shrinkage was found to be proportional to the weight loss. After preliminary tests, Type I cement from Continental Hannibal (abbreviated as COH in this report) was selected for use in the subsequent study, based on its availability, and its use by IDOT.

CHAPTER 4 DRYING SHRINKAGE OF CONCRETE WITHOUT AND WITH SHRINKAGE-REDUCING ADMIXTURES

SRAs are widely used to mitigate the shrinkage cracking of concrete. The mechanism behind the effectiveness of an SRA lies in the fact that it reduces the surface tension of pore water. Since the capillary stresses induced during the drying depend on the surface tension and pore size radius, the reduction in surface tension significantly decreases the magnitude of capillary stresses, leading to lower shrinkage. This chapter compares the shrinkage and strength characteristics of concrete with and without SRA and discusses the suitability of SRA concrete for mitigating shrinkage of bridge decks.

4.1 FREE SHRINKAGE AND MASS LOSS

On the basis of IDOT concrete mix design specification for concrete bridge decks, a control mix was designed for testing shrinkage and strength characteristics in the laboratory. The detail of the mix design is given in the Table A.3 in Appendix A. Low cement content (610 lb/yd^3) was used because it is known to reduce shrinkage. A mortar factor of 0.86 was used for the control mix. Concrete prisms 3 x 3 x 11.25 in. (75 x 75 x 285 mm) in size were made in accordance with ASTM C157 (see Section A.3.6 in Appendix A for details on the test method) using the control mix and also with various dosage of SRA. An SRA (Tetraguard AS20) manufactured by BASF was used in this study. The typical range of dosage for this particular SRA is 2.5 to 7.5 L/m^3. In our study, four different dosages, 3.5 L/m^3 (0.71 gal/yd^3), 4.45 L/m^3 (0.9 gal/yd^3), 6.35 L/m^3 (1.28 gal/yd^3), and 7.5 L/m^3 (1.5 gal/yd^3) of SRA were used to determine how shrinkage and strength varies with SRA dosage.

Three prisms were prepared for each batch of concrete mixture. Figure 4 shows the free shrinkage and mass loss of concrete for various dosages of the SRA. All mixtures showed little expansion during the first 7 days of saturated limewater curing. Drying shrinkage measurements were taken for up to 100 to 120 days. It is evident from Figure 4 (a) that addition of SRA significantly reduced the magnitude of shrinkage of plain concrete. An approximately 50% reduction in free shrinkage was observed with a high dosage (7.5 L/m^3) of SRA. The mass loss of samples was also monitored at various time periods. The concrete prisms with SRA exhibited similar mass loss during drying (at 23°C and 50% relative humidity) as the prisms without SRAs.

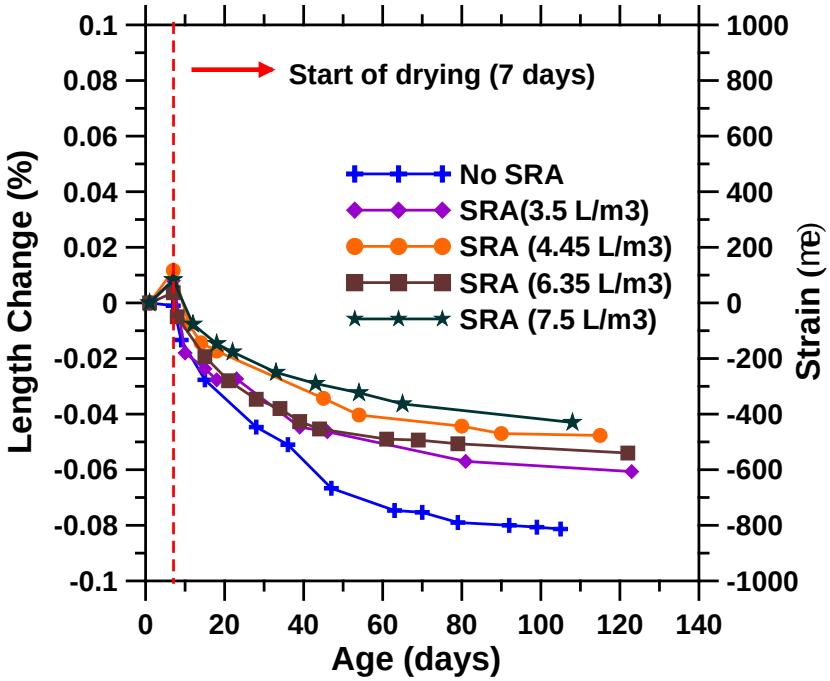

(a)

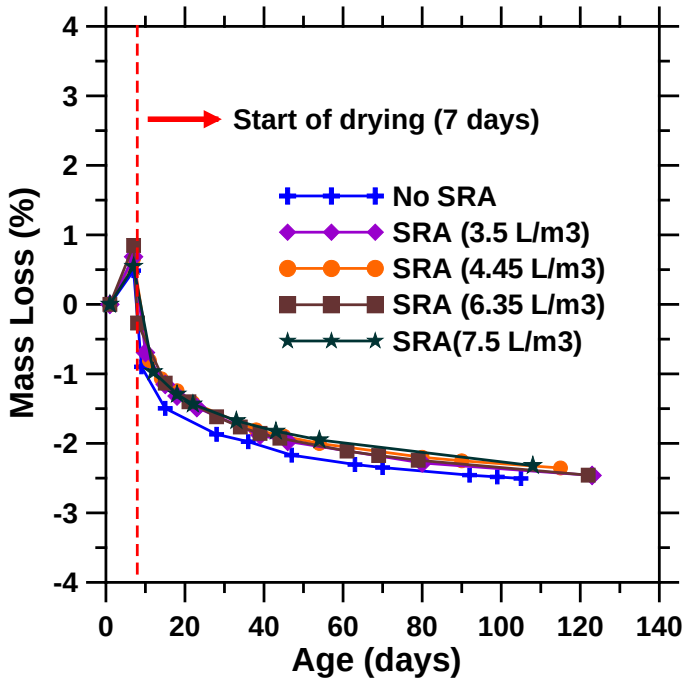

(b)

Figure 4. Effect of SRA dosage on (a) free shrinkage, and (b) weight loss of plain concrete [cement factor (CF) 610, mortar factor (MF) 0.86, w/cm 0.44].

4.2 RESTRAINED SHRINKAGE

Concrete in bridge decks is always restrained by reinforcement, supports, shear studs, etc. Although free shrinkage test results reported in the previous section showed that SRA can effectively reduce shrinkage, it may not necessarily mean better performance of SRA concrete or less cracking caused by shrinkage in real bridge decks. Therefore, it is important to examine the restrained shrinkage of concrete, which was determined using ASTM C1581 (also called a ring test). The ring test setup (see Section A.3.7 in Appendix A for details) comprises a steel ring that offers a uniform restraint against the concrete ring cast outside it. The circumferential tensile strain (measured through the strain gages mounted on the inner surface of the steel ring) increases as concrete presses against the wall of the steel ring during drying. A sudden decrease in strain value indicates formation of a crack.

The concrete mixtures prepared for this test had aggregates with maximum nominal size 0.5 in. (12.5 mm) instead of 0.75 in. (19 mm), which was used in all other mixtures. The smaller size was used because of the limitation on aggregate size suggested in ASTM C1581.Two rings were cast for each concrete mixture.

Figure 5 shows the variation in strain measured on the steel ring with time for four different concrete mixtures. The two control mixtures (without SRA) were compared with two SRA-based mixtures. Clearly, the use of SRA increases the onset time of cracking in concrete rings. The concrete rings without SRA cracked in 15 to 17 days, whereas SRA-based concrete rings cracked after 28 days. ASTM C1581 defines a concrete with low potential for cracking when the cracking occurs beyond 28 days. An increase in SRA dosage also delays the onset of cracking. The difference between the times of cracking for two rings with same concrete mix was within 3 days, indicating good repeatability, except for the concrete mixture with the high SRA dosage: one ring did not show any sign of cracking.

It is evident from the ring test that use of SRA can significantly reduce the cracking potential. It is suggested that the optimal SRA dosage for future use should be arrived after trial batching with the particular concrete mix because cement type, aggregate type, and quantities of each ingredient (cement, water, and aggregate) will influence shrinkage.

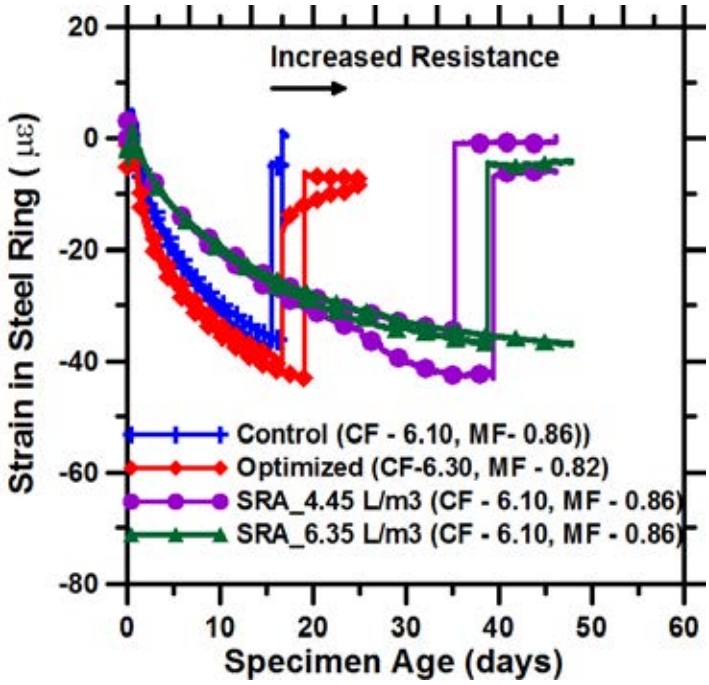

Figure 5.The strain in steel ring as a function of time in the presence of various dosages of an SRA (w/cm - 0.44); a sudden drop in strain indicates cracking (CF = cement factor, MF = mortar factor).

4.3 COMPRESSIVE STRENGTH OF SRA CONCRETE

Concrete containing SRA has been shown to have 5% to 10% lower strength than plain concrete (Weiss 1999). The influence of SRA on strength also becomes important, especially when the concrete has to meet specified strength requirement [for example, 4000 psi (27.6 MPa) for Class BS (bridge superstructure) concrete]. The 28-day strength of 4 x 8 in. (100 x 200 mm) cylinders (size chosen for convenience in the laboratory) was determined according to ASTM C39.

Figure 5 shows that the compressive strength was not influenced much when the SRA dosage was low. However, at a high dosage of SRA, the compressive strength was found to be lower than the plain concrete. Overall, the strength was higher than 4000 psi (27.6 MPa) at the end of 28 days; however, it should be remembered that 4 x 8 in. (100 x 200 mm) cylinders, in general, provide higher strength than full-size 6 x 12 in. (125 x 250 mm) cylinders.

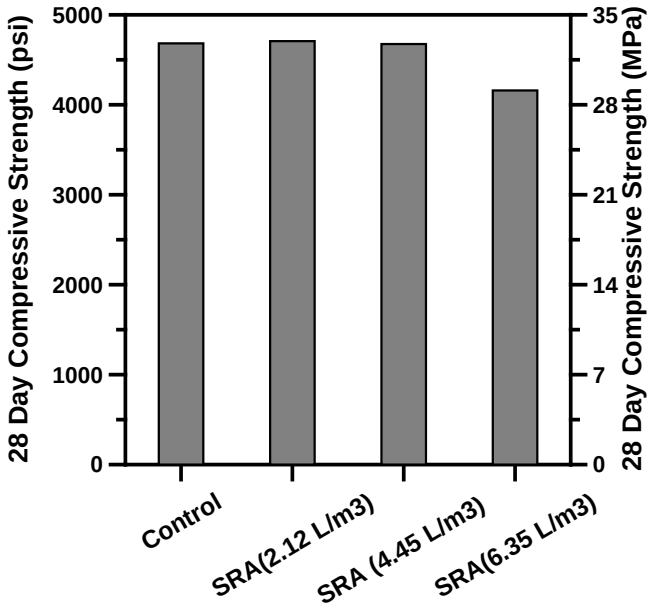

Figure 6. Effect of SRA dosage on compressive strength of plain concrete.

4.4 OPTIMIZATION OF CONCRETE MIX DESIGN

To determine how the control mix can be optimized to reduce shrinkage even without addition of any SRA, two new concrete mixes (see Table A.5 in Appendix A) were designed with higher coarse-aggregate-to-fine aggregate-ratio (CA/FA).

Previous studies by Atkas et al. (2007) and Deshpande et al. (2007) reported a reduction in drying shrinkage with increasing CA/FA content. So, one of the two new concrete mixtures was designed by lowering the mortar factor from 0.86 to 0.82 and keeping the cement factor the same as that of the control mix. The second mix was designed by increasing the cement factor from 610 to 630 and reducing the mortar factor from 0.86 to 0.82. Though an increase in cement content can increase shrinkage, the cement factor was increased in the second optimized mix to make sure the strength of the concrete was sufficient in spite of the change in the mortar factor. Figure 7 compares the unrestrained drying shrinkage of the control mix (CF 610, MF 0.86) with two new optimized mixes with varying cement and mortar factors. The drying shrinkage exhibited by the two new optimized mixes was lower than the control concrete mix because the optimized mixes had lower mortar factor which resulted in a higher CA/FA ratio.

Once the reduction in free shrinkage was observed, the effectiveness of the optimized mix in reducing cracking tendency in ring test was studied. Between the two optimized concrete mixtures, the one with a 630 cement factor and 0.82 mortar factor was selected for comparison with the control mix. This mix with higher cement factor was selected based on the expectation that the one with lower cement factor and lower mortar factor may not meet the minimum strength requirement of 4000 psi (27.6 MPa). However, 28-day strength results suggested that both of the mix produced much higher strength: the mix with CF 610 and MF 0.82 had 5148 psi (35.5 MPa), and the mix with CF 630 and MF 0.82 had 5496 psi (37.9 MPa).

The reduction in restrained shrinkage was also observed for the optimized mix (CF 630, MF 0.82). The cracking time increased by about 2 days in the restrained ring test, as shown in Figure 5. However, this improvement was not as significant as what was observed

when SRA was used. Further optimization of mix proportion can be done by changing aggregate grading, w/cm ratio, and using pozzolans, which has potential to impact the shrinkage characteristics per the studies reviewed in the previous chapter. However, this was outside the scope of the current study.

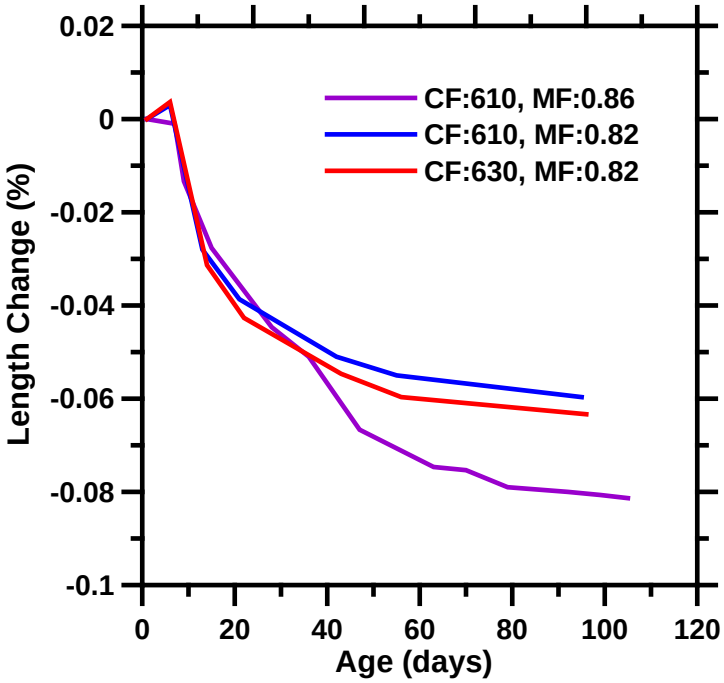

Figure 7. Free drying shrinkage of concrete mixtures with varying cement and mortar factors at w/cm 0.44.

4.5 SUMMARY

The shrinkage-reducing admixture (Tetraguard AS 20) used in this study was effective in reducing the drying shrinkage of concrete mixtures. An approximately 50% reduction in free drying shrinkage was achieved with a high dosage of SRA.

The use of SRA also delays the onset of cracking when strain caused by shrinkage was restrained, which was clearly demonstrated by the ring test. At the same time, about a 10% reduction in compressive strength was observed at a high dosage of SRA, but this reduction was not significant at lower dosage.

It is also clear that a greater reduction in shrinkage can be achieved by using shrinkage-reducing admixtures rather than through mix optimization. A approximately 50% reduction in free shrinkage was achieved with a high dosage of SRA, whereas a reduction of only about 25% was observed with the optimized mix.

The effectiveness of SRA in reducing the drying shrinkage in both unrestrained and restrained conditions was clearly demonstrated in this study.

CHAPTER 5 EARLY-AGE AND LONG-TERM PROPERTIES OF EXPANSIVE CONCRETES

Expansive concretes have the potential to reduce shrinkage cracking. The early-age expansion caused by formation of ettringite or calcium hydroxide crystals induces compressive stress in these concretes that helps counteract tensile stress generated during drying shrinkage. This chapter discusses the early-age properties of two kinds of expansive concretes: Type K (ettringite-based) and Type G (calcium hydroxide-based). In addition, the influence of pozzolans such as Class C fly ash, Class F fly ash, and silica fume on expansion and strength characteristics is discussed.

5.1 RESTRAINED EXPANSION AND SHRINKAGE CHARACTERISTICS OF TYPE K SYSTEM

The restrained expansion and shrinkage of Type K concrete was measured according ASTM C878 (see Section A.3.3 in Appendix A for details on the test method). Figure 8 compares length change (expansion and shrinkage) of concrete containing Type K component with the control mix (see Table A.3 in Appendix for mixture proportion).

The Type K component (sold as Komponent by CTS Cement Manufacturing Co.) was used as 15% replacement of the total cementitious material. Two different w/cm ratios (0.44 and 0.5) were used because of higher water demand of Komponent (calcium sulfoaluminate-based additive). The net expansion at the end of the 7-day period was about 0.05%, irrespective of the w/cm ratio. When exposed to drying conditions, concrete with Type K exhibited similar shrinkage characteristics with time as that of the control mix (both concretes shrunk the same amount). The major difference between the control and Type K concrete lies in early-age expansion. In this small-scale laboratory testing, a difference of about 400 microstrains was observed in concrete prisms, which compensated for the strain subsequently developed as a result of shrinkage for Type K concrete (Figure 8). Concrete without Type K expands at early age as well, but this expansion is not nearly enough to compensate shrinkage strain. On the basis of this small-scale testing, use of Type K seemed promising for reducing shrinkage cracking of bridge deck concrete because the restrained concrete prisms with Type K concrete showed minimal shrinkage strain at the end of 100 days (see Figure 8).

However, in an actual bridge deck, the early-age expansion and stress development, and hence, the shrinkage-compensating benefit of the Type K concrete, will depend on the restrain against expansion. Reinforcement in concrete acts as internal restraint, whereas exterior boundary conditions (adjacent slab, shear studs, etc.) provide external restraint as in jointless bridge deck. It is also important that concrete be cured for at least 7 days to achieve complete expansion.

A large-scale laboratory test was done as part of this project that has potential to capture the actual field behavior of concrete better (see Chapter 6). The large-scale testing also highlighted the difference in strain measured in the longitudinal rebar between the control and the Type K concrete deck (about 40 to 50 microstrains; see Figures 40, 41, and 43). The difference is, of course, much smaller compared with the small-scale testing because of higher restraint against expansion (see Chapter 6 for more detail).

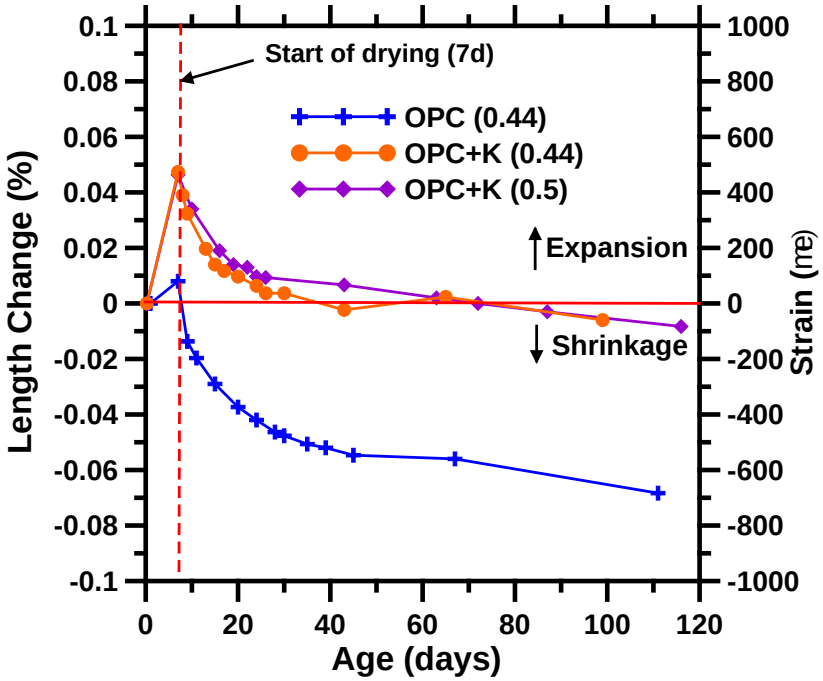

Figure 8. Expansion and shrinkage characteristics of Type K concrete in comparison with ordinary portland cement concrete, at two different w/cm ratios.

5.2 RESTRAINED EXPANSION AND SHRINKAGE CHARACTERISTICS OF TYPE G SYSTEM

The expansion in a Type G system is driven by the formation of calcium hydroxide crystals. This section discusses the early-age deformation of concrete in the presence of Type G component (sold as Conex by Euclid Chemical Co.). Restrained expansion/shrinkage of Type G concrete was measured according to ASTM C878 (see Section A.3.3 in Appendix A for details).The mixture proportion of Type G concrete is presented in Table A.3 of Appendix A.

Figure 9 shows the beneficial effect of Type G concrete in compensating for the shrinkage. Similar to the Type K component, addition of Type G component to concrete also increases early-age expansion. It can be seen from the two dosages of Type G component that increasing the amount of Type G also increases the magnitude of expansion. The restrained expansion increased by 0.15% as the amount of Type G was increased from 4.5% to 6% of total cementitious material. The lower dosage (4.5% addition) resulted in ~0.03% expansion, which was not sufficient to completely compensate the drying shrinkage strain. Therefore, the dosage of Type G was increased to 6%, which in turn increased the expansion to 0.05%. Therefore, a smaller percentage of Type G resulted in a similar level of expansion as was achieved by addition of a higher percentage of Type K.

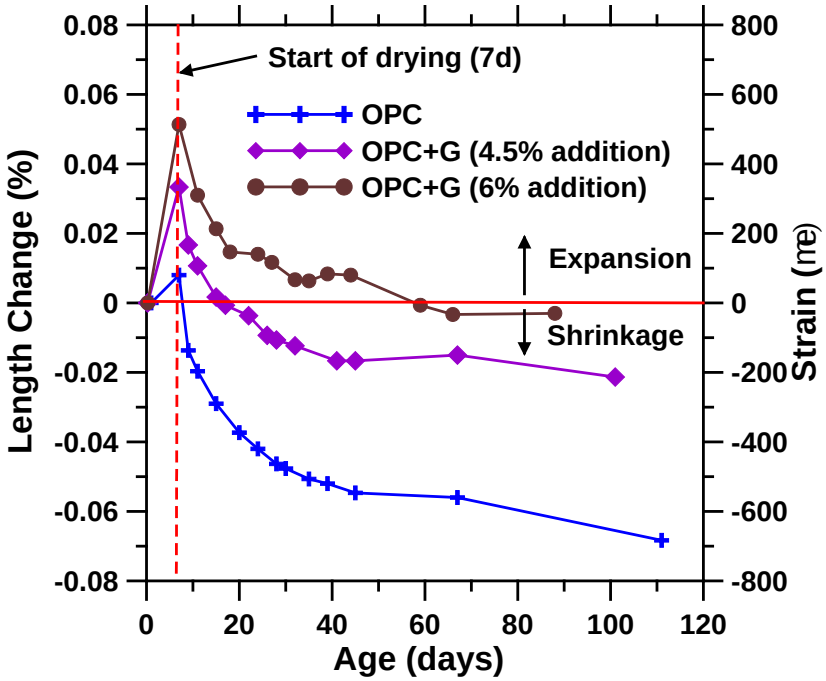

Figure 9. Influence of Type G on restrained shrinkage of concrete at two different dosages and comparison with plain concrete at w/cm 0.44.

5.3 EFFECTS OF POZZOLANS ON RESTRAINED EXPANSION OF CONCRETE

5.3.1 Effects of Fly Ash Addition on Restrained Expansion of Type K Concrete

Fly ash is widely used by DOT in bridge deck concrete for mitigating ASR. Because addition of fly ash changes the concrete mixes physically as well as chemically, it is important to know how fly ash addition can affect early-age expansion of Type K concrete. For this purpose, three mineral admixtures: (1) Class C fly ash, (2) Class F fly ash, and (3) silica fume (for comparison purpose) were used as 15%, 15%, and 5% replacement of total cementitious material, respectively. The mixture proportion of concrete incorporating mineral admixtures is presented in Table A.4 of Appendix. Figure 10 shows the expansion behavior of Type K concrete with three different mineral admixtures along with a close up for the first 7 days.

In addition to the expansion measurement at 7 days, one extra measurement at 3 days was performed. Both fly ashes (Class C and F) increased the expansion in comparison with silica fume, which reduced the expansion of the concrete compared with the mixture without any mineral admixture. Also, Class C fly ash mix showed a decrease in expansion after 3 days. The maximum expansion at the end of 7 days was found to be in the range of 0.44% to 0.06%. After exposing the samples to a drying environment, all samples exhibited shrinkage, which was found to be the highest in the silica fume–based concrete mixture at the end of 140 days. There was minimal tensile strain caused by shrinkage, even after 140 days, which highlights the beneficial effect of Type K concrete in compensating for shrinkage, even in the presence of mineral admixture.

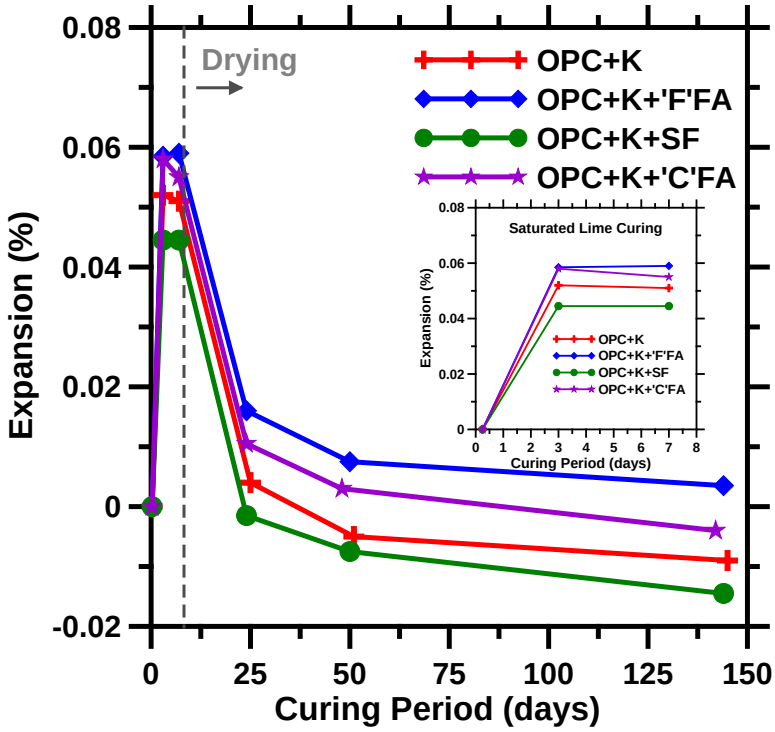

Figure 10.The influence of mineral admixtures on restrained expansion of Type K concrete (w/cm - 0.44).

5.3.2 Effects of Fly Ash Addition on Restrained Expansion of Type G Concrete

Restrained expansion/shrinkage of Type G concrete was also evaluated when pozzolans were used as the replacement of portland cement. Figure 11 shows the expansion characteristics of Type G concrete when mineral admixtures were added as a partial replacement of portland cement (see Table A.4 in Appendix A for mixture proportion). Both types of fly ashes (Class C and F) increased the restrained expansion of Type G concrete, whereas silica fume did not influence the expansion significantly. The maximum expansion at the end of 7 days was found to be in the range of 0.05% to 0.07%. All samples exposed to a drying environment exhibited shrinkage. There was minimal tensile strain (about 0.02%) caused by shrinkage, even after 140 days, which highlights the beneficial effect of Type G concrete in compensating for shrinkage, even in the presence of a mineral admixture.

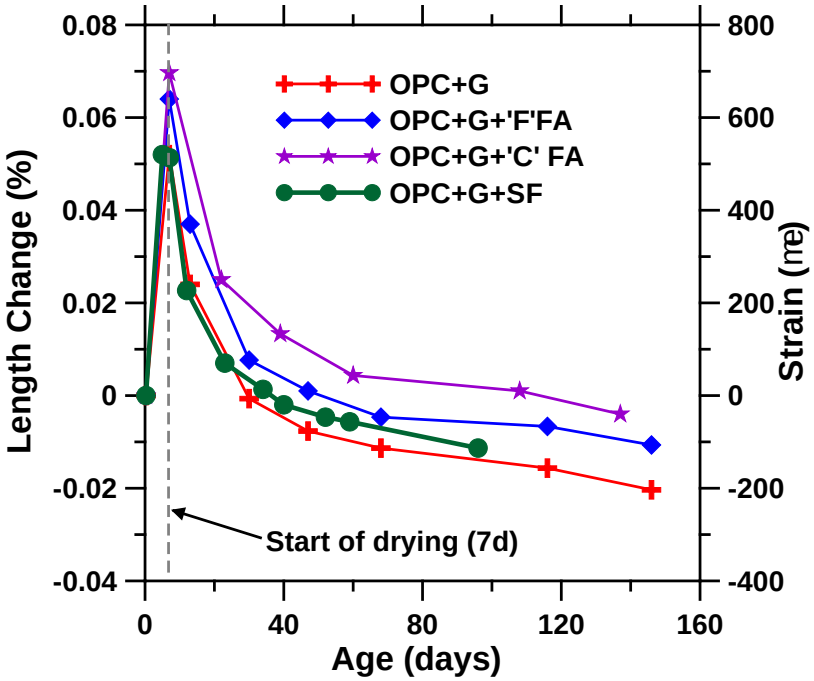

Figure 11. The influence of mineral admixtures on restrained expansion of Type G concrete at w/cm - 0.44.

5.4 UNRESTRAINED EXPANSION OF TYPE K AND TYPE G SYSTEMS

The restrained expansion test according to ASTM C878 recommends demolding of concrete prisms 6 hours after casting, and the length change is calculated based on the initial reading at 6 hours. However, the development of compressive stress when expansion is restrained starts only after concrete has hardened (at final set). So, strains measured according to ASTM C878 may over- or underestimate expansion because the setting time for all concrete mixes were not at 6 hours and changed, particularly when pozzolans such as fly ash were used. To consider this aspect, a corrugated tube test (ASTM C1698) was used to monitor the unrestrained expansion of Type K and Type G cement pastes, which accounts for the difference in the set time for different mixes in monitoring the length change. The unrestrained expansion using a corrugated tube was also used to examine the influence of the addition of pozzolans because they are expected to modify the setting characteristics.

5.4.1 Use of Corrugated Tube Test to Measure Unrestrained Expansion

Figure 12 shows the difference in the rate of expansion as measured by the corrugated tube test protocol (ASTM C1698; see Section A.3.4 in Appendix A for details) for the two different expansive binder systems. The Type K cement paste exhibited a slow rate of expansion and achieved most of the expansion within the first 8 days. However, Type G cement pastes expanded much faster and achieved most of the expansion within the first 24 hours. The difference in the expansion behavior can be explained by examining the hydration reactions. In a Type K system, the hydration of ye'elimite (constituent of Type K) takes place slowly, and it also depends on particle size and the availability of water. The slow hydration of ye'elimite results in formation of ettringite, causing a steady expansion. On

the other hand, in a Type G system, the precipitation of calcium hydroxide crystals derives the expansion. The formation of calcium hydroxide takes place rapidly, causing expansion to reach maximum within 24 hours.

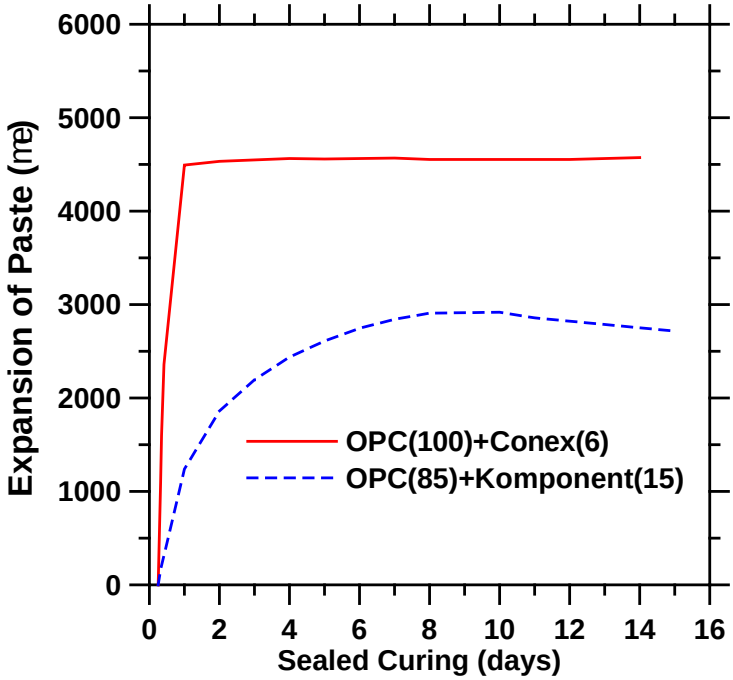

Figure 12. The rate of expansion of cement paste incorporating two expansive components.

5.4.2 Effect of Sealed Curing on Expansion: Corrugated Tube vs. Sealed Prism

To check the consistency of data from the corrugated tube test (ASTM C1698), additional prismatic paste samples were prepared in accordance to ASTM C157 and cured under sealed conditions. Figure 13 shows that the corrugated tube test data relate to prismatic beam test data reasonably well, ensuring the consistency of the data. The initial expansion within 24 hours from corrugated tube test was added to prismatic test data because the prisms were demolded after 24 hours. This comparative study emphasizes that the expansion can be monitored, even a using sealed prismatic bar (modified ASTM C157)—the only difference being the magnitude of expansion occurring within 24 hours.

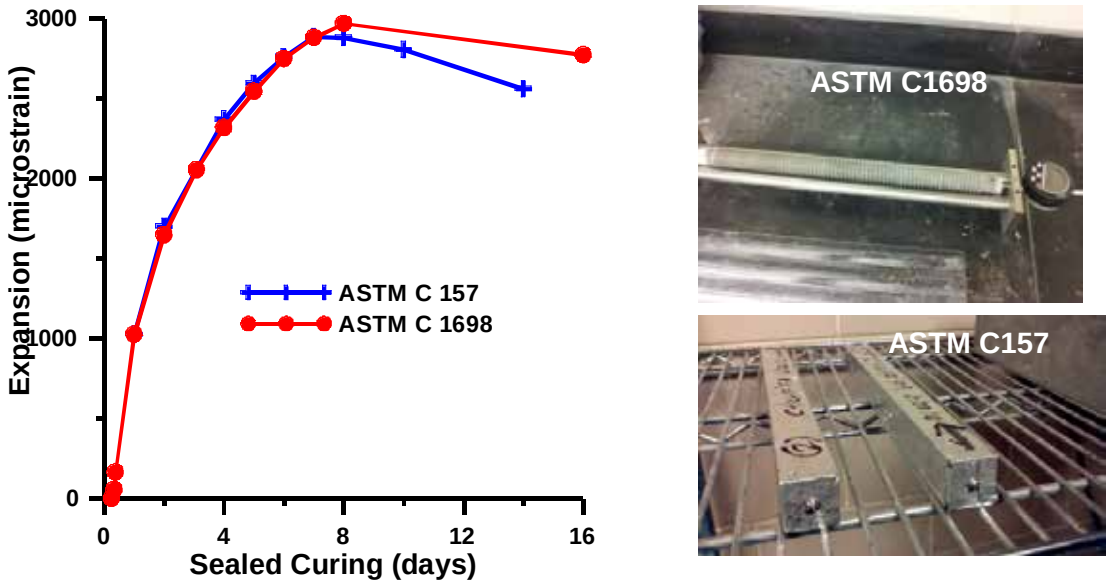

(a) (b)

Figure 13. (a) Expansion of sealed prismatic bars (ASTM C157) compared with corrugated tube (ASTM C1698), and (b) photographs showing the difference in test methods.

5.4.3 Effects of Fly Ash Addition on Unrestrained Expansion of Type K System

The corrugated tube test has advantage of accounting for the difference in setting characteristics, and hence, it was used to investigate the influence of fly ash addition on expansion. Figure 14 (a) shows the unrestrained expansion behavior of expansive cement pastes in the presence of Class C fly ash, Class F fly ash, and silica fume. The highest expansion was observed in the paste containing Class F fly ash, whereas silica fume reduced the expansion of the cement paste. The behavior of Class C fly ash was different: it increased expansion until 2 days, after which it exhibited shrinkage. The expansion of sealed samples could also have been influenced by the shrinkage of portland cement, which constitutes at least 70% (by mass) of total cementitious material. To isolate the effect of shrinkage (that occurs as a result of sealed curing) on expansion, an additional set of prismatic bars was prepared and kept in saturated limewater after 24 hours. The expansion occurring within 24 hours from the corrugated tube was added to the expansion of prismatic samples. Figure 14 compares the expansion in unsealed environment to the sealed environment. “Unsealed environment” refers to saturated limewater curing. A number of commonalities were observed in terms of expansion behavior: Class F fly ash exhibited the highest expansion in both curing conditions, whereas the silica fume reduced expansion of the Type K expansive cement paste. This behavior is the same as what was observed from the restrained expansion and shrinkage test done in accordance with ASTM C878 (see Section 5.3.1 of this report). The behavior of Class C fly ash was also found to be similar in a way that expansion stopped after 2 days when the samples were cured in saturated limewater.

The possible explanation for these observations lies in many factors, such as amount of ettringite, internal resistance offered by the material against expansion, and pore size features. But the material resistance seems to have governed the expansion behavior

because it can be used to explain the expansion characteristics. As an indirect measure of material resistance, compressive strength of different mixes was measured, as discussed in Section 5.8.The Class F fly ash seems to have reduced the material resistance that led to an increase in expansion, whereas silica fume increased the material resistance by densifying the microstructure and resulted in smaller expansion compared with other mixes. It was established that the faster consumption of ye'elimite in C fly ash–based mix caused the expansion to stop early. The presence of free lime and C_3A in Class C fly ash seems to have influenced the rate of ye'elimite consumption.

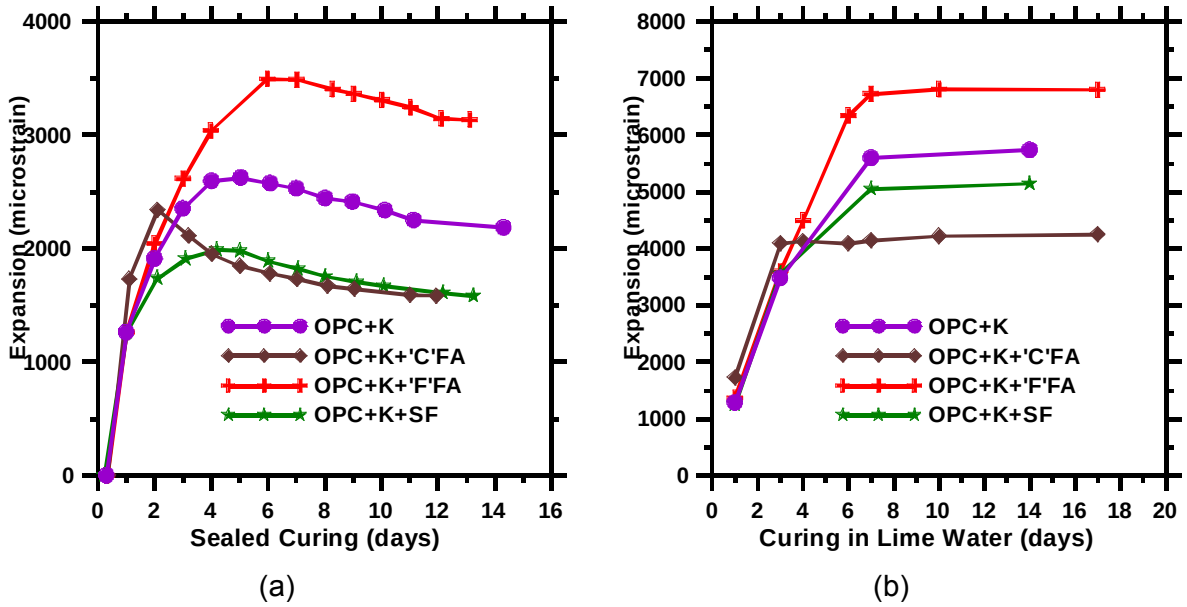

Figure 14. Unrestrained deformation of Type K cement paste (w/cm 0.44) with mineral admixtures under (a) sealed curing (using corrugated tube), and (b) saturated limewater curing (using prismatic beams).

Finally, the unrestrained expansion of Type K cement pastes could be correlated reasonably well with the restrained expansion of Type K concrete shown in Figure 10 except for the case of Class C fly ash, which showed higher expansion than the plain Type K concrete at the end of 7 days. It is evident from this study that mineral admixtures bring physico-chemical changes that also influence the expansion characteristics. Therefore, while using the mineral admixtures in the field, proper attention must be given to physical and chemical changes taking place in cementitious system.

5.4.4 Effects of Fly Ash Addition on Unrestrained Expansion of Type G System

The restrained expansion of Type G concrete showed that the addition of fly ash increased the expansion (Figure 11). Because the replacement of portland cement by pozzolans is expected to modify the setting characteristics of expansive cement, the unrestrained expansion of Type G cement paste was also examined using a corrugated tube test to verify the restrained expansion test results.

Figure 15 shows that when Class C and Class F fly ashes were used, the unrestrained expansion of plain Type G cement paste increased similar to what was

observed for concrete samples. The silica fume reduced the extent of expansion of plain cement paste by a small extent. The difference in expansion level was magnified in the study of cement pastes because aggregates act as a restraining agent in concrete, which is expected to reduce the expansion in addition to the restraining effect provided by the cage in the ASTM C878 setup. The behavior of mineral admixture in a Type G system can also be explained based on the difference in material resistance. Other factors (such as the amount of calcium hydroxide and pore structure features) may also influence expansion behavior.

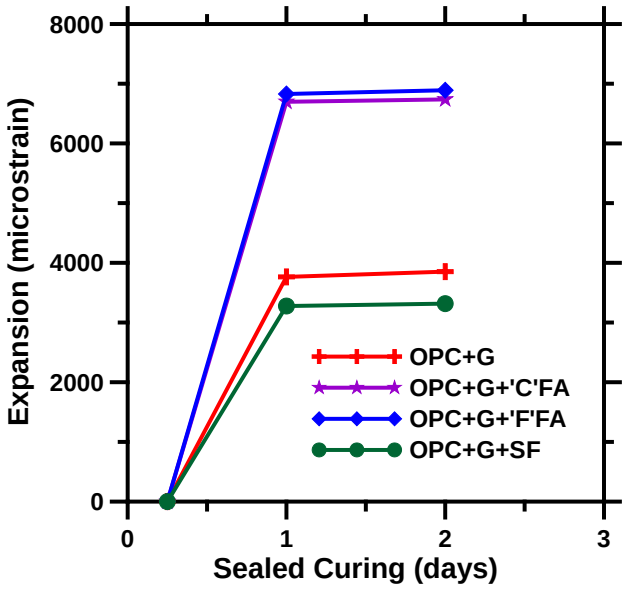

Figure 15. Unrestrained expansion of Type G cement pastes in presence of mineral admixtures at w/cm 0.44.

5.5 EFFECT OF RETARDER ON RESTRAINED EXPANSION OF TYPE K AND TYPE G CONCRETE

Retarders are often used in the field to account for transportation delay and for finishing purposes. The rapid loss of slump in expansive concrete (discussed in Section 5.7) makes it necessary to examine the influence of retarder on expansion characteristics. Preliminary experiments were performed to determine the effect of retarder (Delvo Stabilizer by BASF) on expansion.

Figure 16 shows that the effect of retarder on Type K concrete was not as pronounced as on Type G concrete. The expansion was found to have increased when retarder was added to Type G concrete. These tests were performed in accordance to ASTM C878, which requires the demolding of the samples after 6 hours. In fact, the use of retarder will delay the setting of concrete, which is expected to influence expansion, depending on the retarder's dosage. The development of compressive stress starts only after the concrete has hardened; hence, the effects of change in setting time on expansion measurement of Type G cement paste and concrete with retarder will be important in the future.

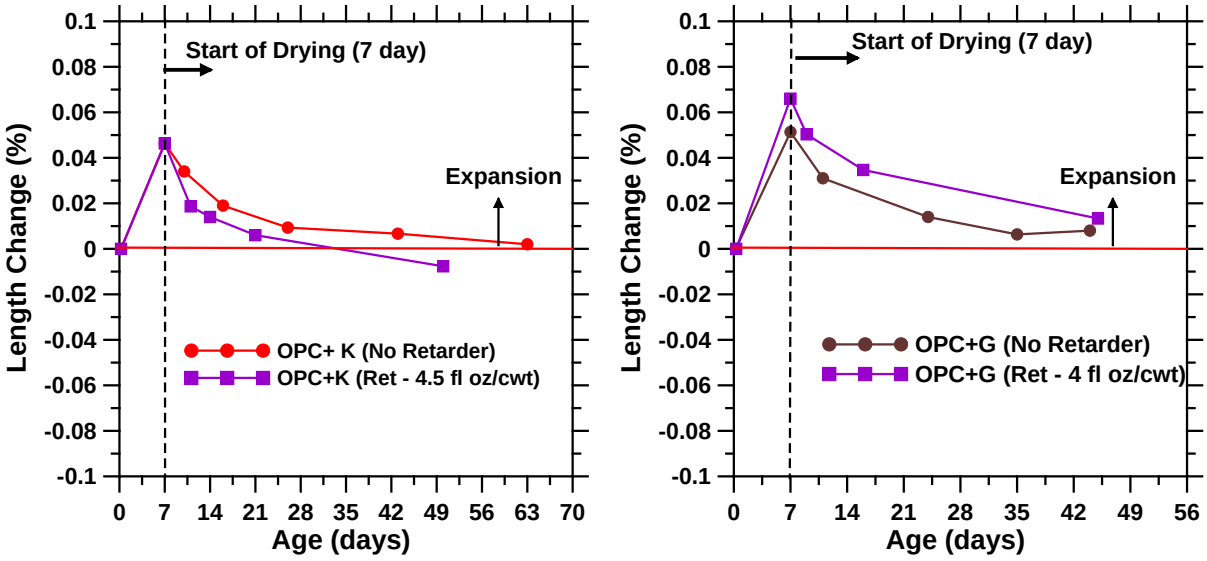

Figure 16. Effect of the addition of retarder (Delvo Stabilizer, BASF) on restrained expansion and shrinkage of (a) Type K concrete (w/cm 0.5), and (b) Type G concrete (w/cm 0.44).

5.6 EFFECT OF ENHANCED MIXING TIME ON THE RESTRAINED EXPANSION OF TYPE K SYSTEM

It is important to determine the influence of haul time between the concrete plant and job site on the extent of expansion. To simulate this influence, additional prismatic samples were prepared with an enhanced mixing time of 35 minutes for a Type K mix [OPC (66.9%) + K (14.7%) + C FA (18.4%); cement factor 6.80; w/cm 0.45]. This new mix design was used for this test because of some interest in using it for an actual bridge deck pour. It is evident from Figure 17 that the additional mixing resulted in a decrease of about 12% in 7-day expansion of the mix. The slump at the end of 35 minutes measured 3 in. The mix was sticky as a result of the formation of ettringite during the additional mixing. No superplasticizer was used in this case, but use of it is expected to improve the workability of Type K concrete.

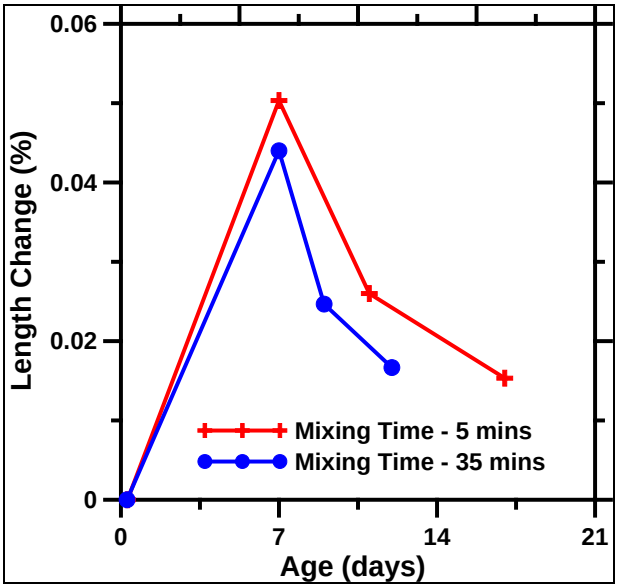

Figure 17. Effect of mixing time on the extent of expansion of Type K concrete [OPC (66.9%) + K (14.7%) + CFA (18.4%); cement factor 6.80; w/cm 0.45].

5.7 SLUMP LOSS IN EXPANSIVE CONCRETES

Although concretes with an expansive component significantly reduce shrinkage, low workability of these mixes must be addressed. The formation of various crystals (ettringite and calcium hydroxide), in the case of Type K and Type G, influences the fresh property of concrete such as slump value. As presented in Figure 18, Type K concrete showed approximately 50% slump loss within 30 minutes of the mixing period. The effect of retarder and superplasticizer on expansive concretes should be investigated in detail in the future because such a significant slump loss may not be desirable for practical considerations. The use of Delvo Stabilizer (294 ml/100 kg) delayed slump loss to a significant extent. The amount of retarder can be adjusted to achieve desirable workability of expansive concrete.

Also, it is important to design concrete with an expansive component that exhibits the desired slump of 5 to 8 in. at the job site, rather than after mixing. For example, concrete with a Type K component should have a slump around 8 or 9 in. right after mixing in order to obtain a slump of 5 or 6 in. after haul time to the job site.

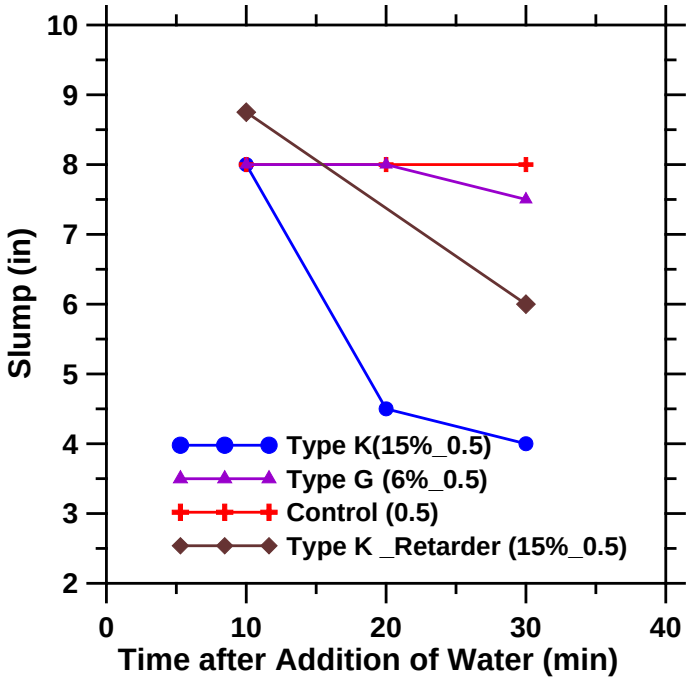

Figure 18. Slump loss in expansive concretes and influence of retarder, according to ASTM C143.

5.8 COMPRESSIVE STRENGTH

The compressive strength of expansive concretes was determined at 28 days using cylindrical samples of size 4 x 8 in. (100 x 200 mm), according to ASTM C39. As can be seen in Figure 19 (a), the compressive strength of expansive concretes was found to be similar or slightly higher than control mix (without Type K/G). Concrete with Type K component at w/cm ratio of 0.5 showed lower strength than the control mix at w/cm of 0.44, but it was still higher than 4000 psi (27.6 MPa); the typical minimum strength for bridge deck concrete.

The compressive strength of Type K and Type G concrete was also measured when the various mineral admixtures were used. The addition of fly ash (both C and F) reduced the 28-day compressive strength of Type K and Type G concrete, whereas strength was increased in presence of silica fume, as shown in Figure 19 (b) and (c). A decrease in strength highlights the difference in internal resistance offered by materials against the expansion (material resistance against deformation) that is expected to influence early-age expansion behavior.

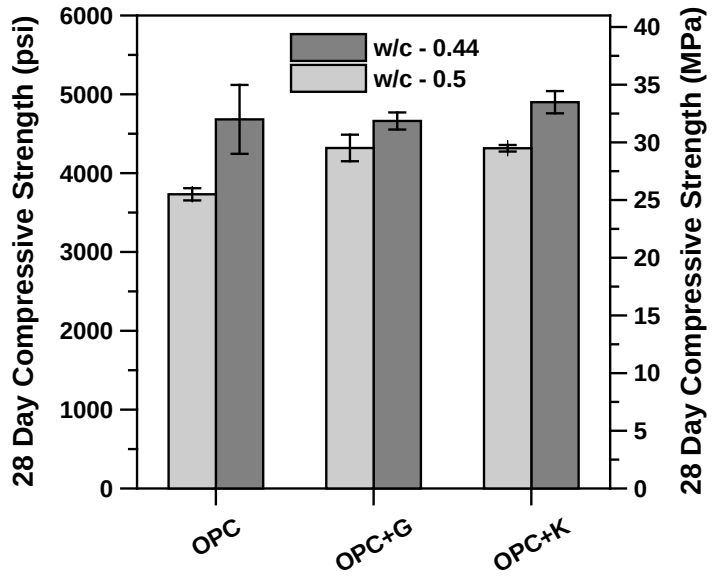

(a)

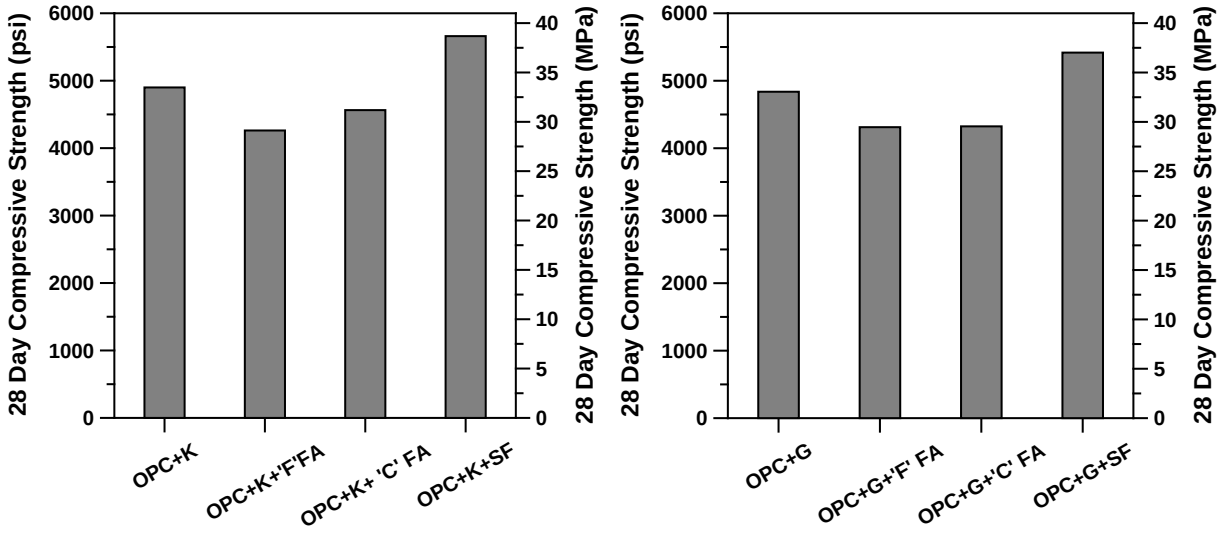

(b) (c)

Figure 19. (a) Comparison of strength between expansive and plain concrete at two different w/cm ratios (K and G refer to Komponent and Conex, respectively); (b) and (c) effect of mineral admixtures on compressive strength of Type K and Type G concrete at w/cm 0.44.

5.9 INVESTIGATION OF ALKALI-SILICA REACTION IN TYPE K ANDTYPE G SYSTEM

The use of fly ash is recognized to reduce the potential for ASR. The presence of CaO in Type G and Class C fly ash led to investigation of ASR potential in a Type G system. ASTM C227 (see Section A.3.9 in Appendix A for details of test method) was used to

determine the influence of Type G on length change of mortar bars with and without reactive sand.

Figure 20 (a) shows that the mortar bars with reactive sand had a similar percentage of length change after 400 days. The first reading of mortar bars was taken after 7 days, based on the assumption that the expansion caused by Type G would have been completed by then. The Class C fly ash initially exhibited highest expansion followed by a gradual decrease. The mortar bars with plain portland cement and Type G showed an increase in length beyond 250 days. In addition, the mortar bars with non-reactive sand exhibited length change on the order of 0.01%. The test results of ASTM C227 do not suggest higher vulnerability of Type G system to ASR.

In addition to ASTM C227, pore solution was extracted (see Figure A.6 in Appendix A for photos of the extraction device) from the cement paste to estimate the alkali content because it can provide useful information regarding vulnerability for ASR. Figure 20 (b) shows the total alkali concentration (Na_2O_{eq}) of various cement pastes. The pore solution was extracted from three paste samples: OPC (100%); OPC (85%) + Class C fly ash (15%); and OPC (80%) + Class C fly ash (15%) + Type G (5%), all of which were prepared at a w/cm of 0.5.

The pore solution analysis showed that the alkali concentration was initially higher in the cement paste with Class C fly ash, owing to the slow release of alkalis from fly ash. At a later age, the alkali concentration was found to be smaller than that in the plain portland cement, possibly as a result of alkali binding of calcium aluminosilicate hydrate (C-A-S-H) formed during pozzolanic reaction of fly ash. It can also be observed that the presence of Type G component did not increase the alkali concentration of the cement paste with C fly ash. It appears that addition of C fly ash starts to show the beneficial effect in reducing the alkalinity at later age.

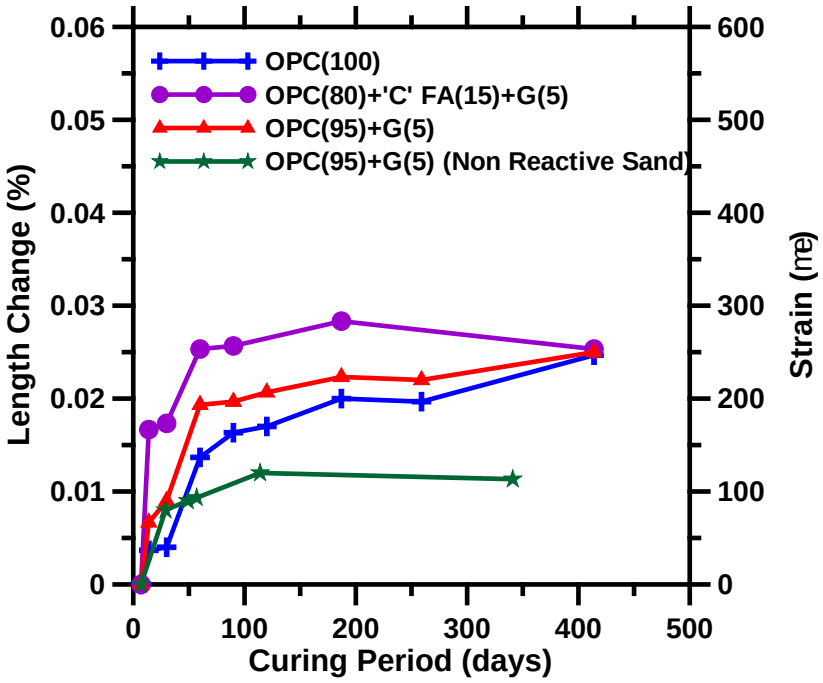

(a)

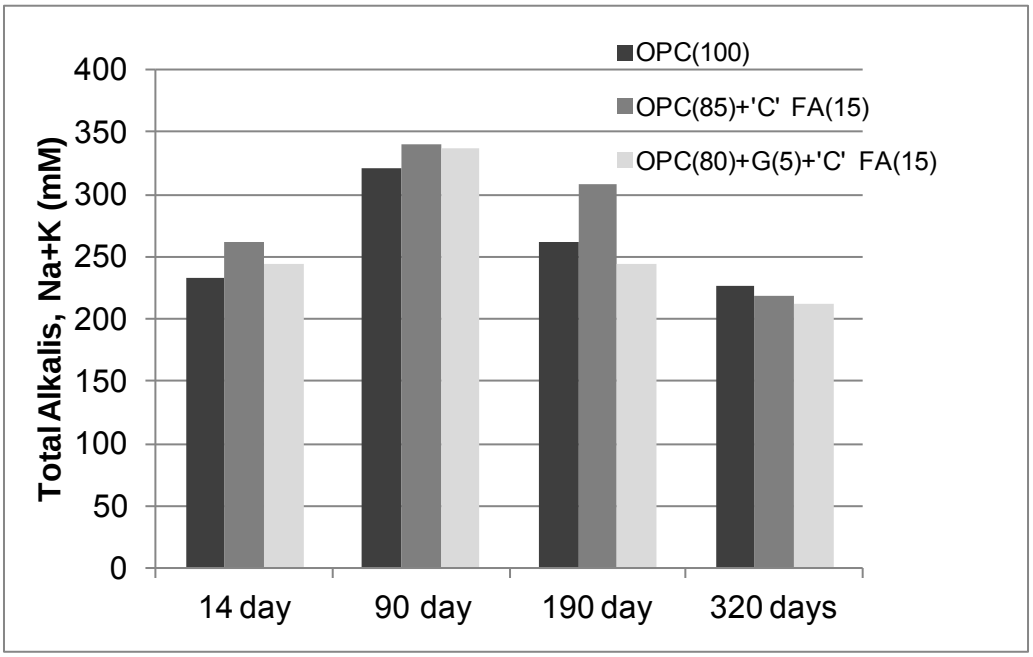

(b)

Figure 20. (a) The length change of mortar bars according to ASTM C227 (w/cm 0.44), and (b) total alkalis (Na + K) in the pore solution of the paste samples (w/cm 0.5).

5.10 HEAT OF HYDRATION OF EXPANSIVE CEMENTS

Susceptibility for thermal cracking in concrete depends on the heat evolved during cement hydration. The heat release during the hydration of expansive cement was examined using isothermal calorimetry (see Section A.3.8 in Appendix A for details of the test method).

Figure 21 (a) shows the rate of heat evolution of expansive cements in comparison with portland cement. Isothermal calorimeter was used to study the hydration behavior. Three paste samples: OPC (100%), OPC (85%) + Type K component (15%), and OPC (95%) + Type G component (5%) were prepared at w/cm 0.5. It was evident that the expansive cement pastes did not show any increase in rate of heat evolution in comparison with portland cement paste. The shoulder appearing in portland cement paste caused by gypsum depletion, and monosulfate formation disappears when Type K was used as 15% replacement of portland cement. The intensity of the acceleration peak in Type K cement paste was reduced due to the dilution effect.

Figure 21(b) shows the total heat release during the hydration of three cement pastes. Total heat released during the hydration of Type K cement was lower than plain portland cement at the end of 72 hours. Moreover, Type G and plain portland cements exhibited similar heat release at the end of 72 hours.

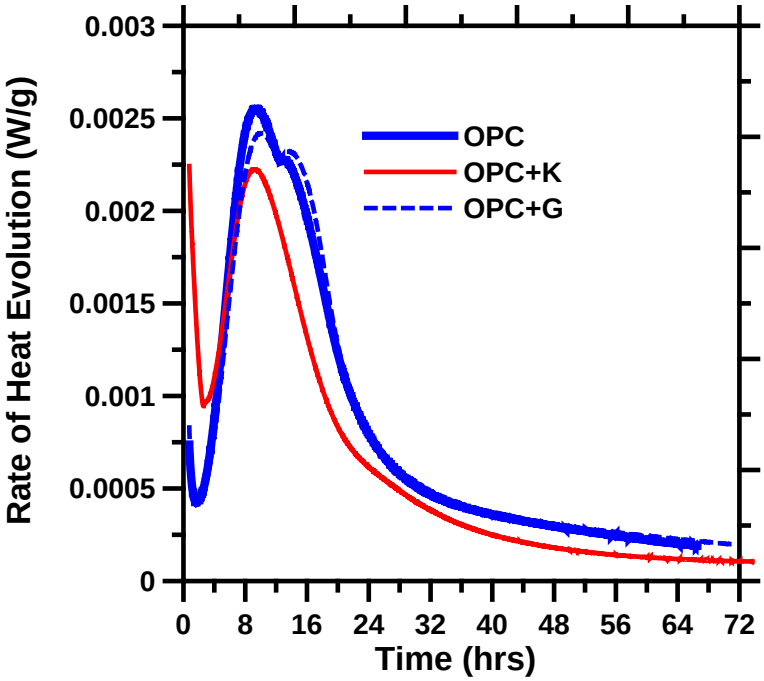

(a)

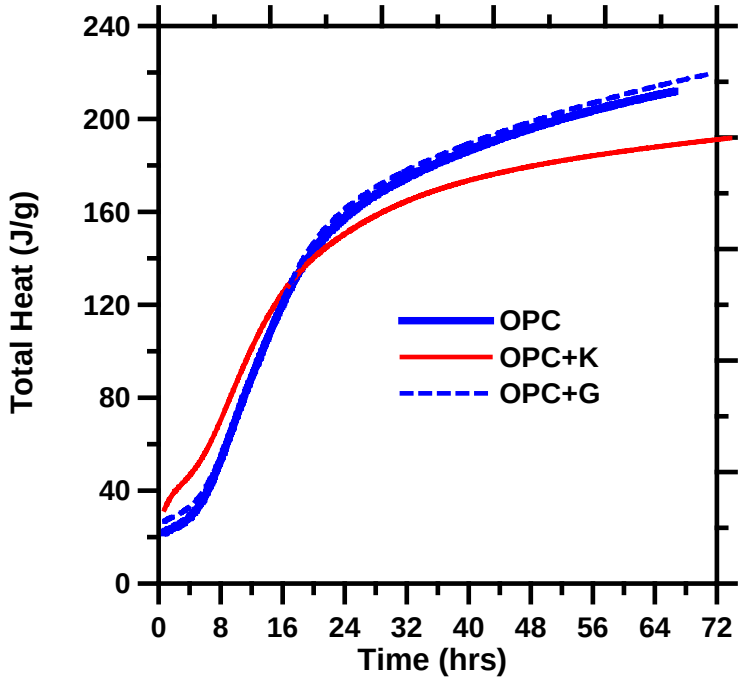

(b)

Figure 21 (a) Rate of heat evolution, and (b) total heat release in expansive cements in comparison with plain portland cement paste at w/cm 0.5.

5.11 SUMMARY

On the basis of the small-scale laboratory testing, it was found that Type K and Type G concretes shrank the same amount as a control mix without the expansive components. However, depending on the dosage of Type K or Type G in concrete, the early-age expansion can be sufficient to compensate for the shrinkage strain developed later on.

In the laboratory test, concrete prisms with a Type K or Type G component showed minimal shrinkage strain, even after 100 days. This shows the advantage for using these additives to mitigate shrinkage, which will be studied later during large-scale laboratory testing.

From the small-scale testing, it was also found that pozzolans such as fly ash and silica fumes change the expansion characteristics of concrete with Type K or G. Addition of fly ash decreases internal resistance offered by the material against expansion; hence, higher expansion was measured. Therefore, in determining the dosage of Type K, the effect of fly ash should be properly considered.

In addition, any admixture, including fly ash, which affects setting time of concrete, will also affect the effective expansion of concrete. It is important to note that Type K concrete showed significant slump loss at early age and that total expansion also reduced when increased mixing time (to account for haul time) was used.

It initially seemed possible that the slump loss could be mitigated by using retarder or superplasticizer. However, based on a preliminary study, these chemical additives seemed to affect expansion as well. In the future, these effects should be considered more carefully in order to design expansive concrete mixes that are more robust or, in other words, less susceptible to changes that can be hard to control in the field.

CHAPTER 6 BRIDGE DECK MODELS

The next step in the research was to move up the ladder from small-scale material tests to tests on a prototypical bridge bay. These larger tests could still be conducted within a lab environment, and they would provide insight into how different concrete mixes would behave in shrinkage before use in full-scale bridges. An initial deck was tested using a control mix suggested by IDOT engineers to provide control data to be compared later with a deck made from the modified mix.

After rigorously studying different possibilities (such as SRAs, Type G, and mix design optimization) in altering the control mix to reduce shrinkage-related cracking as detailed in the previous chapters, it was decided that a mix design based on use of a Type K additive was the strongest candidate for the next large-scale laboratory test. A second experimental bay was created using this Type K mix design to compare with the control data.

6.1 BAY DESIGN

The bay design for this study was determined based on IDOT recommendations and lab area restrictions. Using the bridge design provided by IDOT engineers, a 10 x 7 ft representative bridge bay with an 8-in. slab thickness was designed. This bay is supported by two 10-ft W12x79 steel girders at a spacing of 5 ft. The steel girders are connected to the reinforced concrete deck through shear studs spaced at 1 ft longitudinally along the girder. The girders are raised off the ground at their ends with 1-ft-long W12 shapes. These 1 ft long girders are used not only to simulate the bay being held in place at the corners but also to raise the deck off the ground for better study. The girders are also constrained by two C6x8.2 steel c-channels to keep them free from twisting.

Finally, along the perimeter of the concrete bay are four C10x15.3 steel c-channels. These c-channels have holes drilled in them, which give the G60 epoxy-coated rebar an attachment point in order to simulate the continuity of a real bridge superstructure. The rebar, meanwhile, is split into the top rebar and the bottom rebar. The top rebar is located 1 in. from the top of the concrete and is designed as shown in Figure 26. The bottom rebar is located 2 in. from the bottom of the concrete; its design is shown in Figure 27. Caution was taken when bolting the rebar to the c-channels to avoid creating pre-strain. See Figure 22 and Figure 23 for pictures of the first experimental deck before and after the pour. The bay design and construction were the same for both the control and the Type K models.

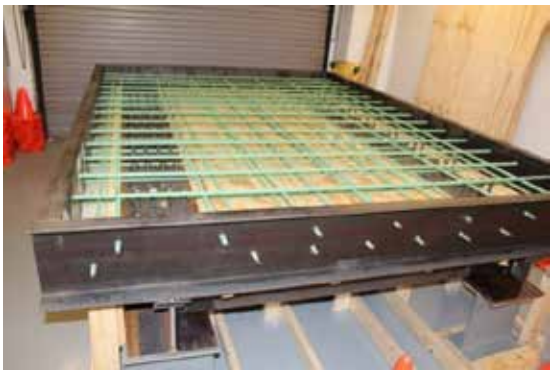

Figure 22. Deck with rebar and formwork.

Figure 23. Concrete deck after the pour.

6.1.1 Strain and Temperature Gage Location for the Control Model

Multiple gages within the model recorded the strain and temperature for 6 months. Twenty strain gages were interspersed throughout the top and bottom rebar in both longitudinal and transverse directions (see Figures 24 and 25; the strain gages are indicated by thick black lines). More gages were placed on the top layer of rebar because this is generally where a greater amount of cracking is found in the field and is of greater interest for this study. The gages were also centrally located so that any local fluctuations caused by the c-channels and girders would dissipate within the concrete before reaching the gages. Another three gages were placed on each girder to investigate the effects of concrete shrinkage on the steel girders, followed by another five gages that were placed along the top surface of the concrete.

The strain gages along the girders (Figure 26) were the same type as those used for the rebar, but the strain gages along the top surface of the concrete (Figure 27, the non-numbered gages) were much larger. The larger gages were necessary because of the non-homogeneous characteristics of concrete. Instead of merely studying the severe local fluctuations of strain at a certain location, these longer gages are able to find strain over a large area. This is a much better representation of what is going on in the superstructure. Thermocouples were placed along the top and bottom of the concrete and on the girders in much the same way as the strain gages (denoted with an S and a T in Figures 26 and 27).

An NI data acquisition system was used to collect strain and temperature data. This system was connected to a laptop, which then read and saved the data using a LabVIEW program. At first, data from the strain gages and the thermocouples were recorded at an interval of 5 seconds, but after an initial period of about 2 weeks, this delay was changed to every 5 minutes to decrease file size but still maintain accuracy. Once these files had been downloaded, a MATLAB program was used to quantify and graph the results for the strain and temperature readings.

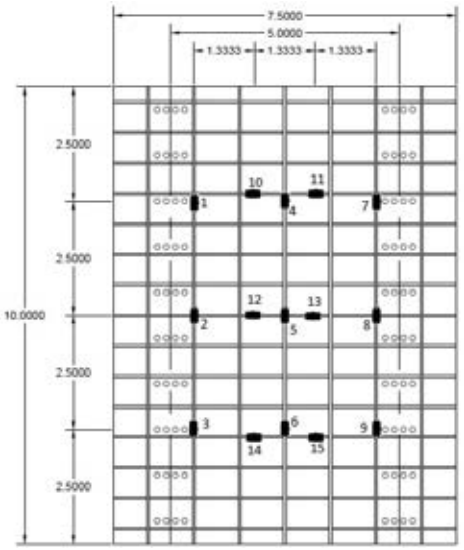

Figure 24. Strain gage location on top rebars.

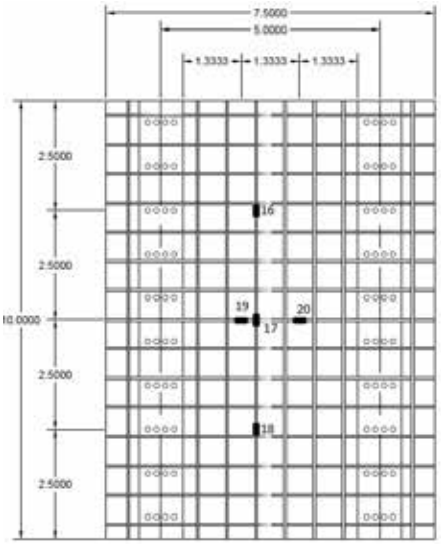

Figure 25. Strain gage location on bottom rebars.

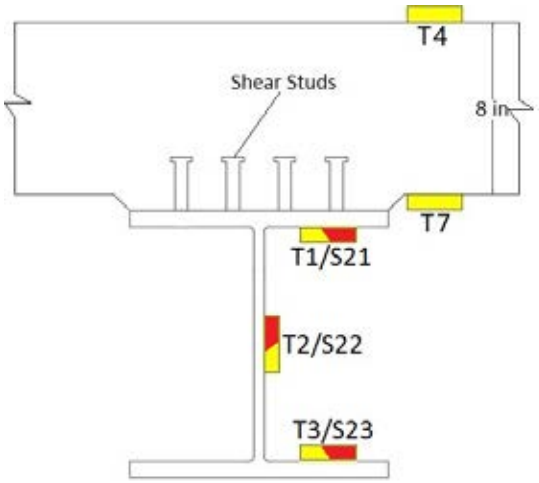

Figure 26. Strain gage (S) and thermocouple (T) location in section view.

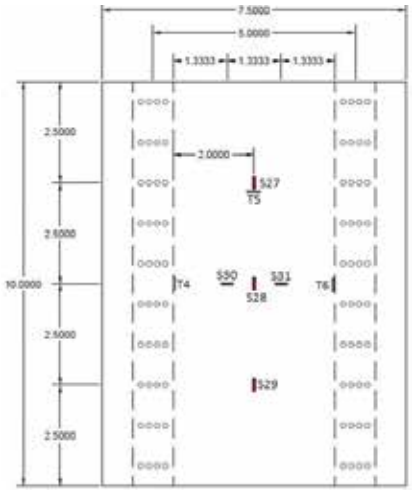

Figure 27. Strain gage (S) and thermocouple (T) location in overhead view

6.1.2 Strain and Temperature Gage Location for the Type K Model

The strain gage location for the Type K model was the same as that for the control model (see Figures 24 through 27). This setup created continuity between the two models and allowed for accurate comparisons. The thermocouples had locations similar to the control model, but for this experiment, additional thermocouples were placed inside the concrete as well. This was done to ensure accurate temperature readings at the location of the top and bottom rebar. This way, the strain caused by changing temperature could be determined and, along with the gravity strain, removed from the recorded strains. After removing these two strains, the strain caused solely by shrinkage is left, and an accurate measurement can be found. The thermocouples were located along the top and bottom rebar in vertical alignment with gages 4 and 7. This provides a very accurate representation of the temperature gradient through the cross-section of the deck.

6.1.3 ASTM Test Results and Mix Design

During the pour for both experiments, specified ASTM tests were done. This was to ensure that the concrete being used not only lived up to standards but that it also fit the intended mix properties. Multiple slump and air entrainment tests were done for both pours. Also, cylinders 6 x 12 in. (150 x 300 m) were used for strength testing later on.

For the control model, an initial slump of 3.5 in. and a final slump of 2.5 in. were recorded over the 1-hour pour. Meanwhile, two air entrainment tests were conducted at the beginning and end of the pour as well, with a resulting air content of 5.8% and 6.0% respectively. Finally, the cylinders were crushed at the specified 7-, 14-, and 28-day marks. The recorded 28-day compressive strength of 4555 psi (31.4 MPa) was well above the specified 4000 psi (27.6 MPa) mark.

These tests were then repeated for the Type K mix design during its pour. The initial and final slumps were the same at 7.5 in. This large slump for the Type K mix can probably be attributed to the higher w/c ratio in the type K mix. This higher ratio makes the concrete more workable and though the slump seems large, it was within the acceptable range. Three air entrainment tests were also done, with air contents of 5.9%, 5.5% and 5.7%.

Finally, the cylinders were crushed at the specified 7-, 14-, and 28-day marks. The recorded 28-day compressive strength of 4340 psi (30 MPa) was well above the specified 4000 psi (27.6 MPa) mark. The mix designs for both the control and Type K mixes can be seen in Table 1.

Table 1. Mix Designs

	Control Mix	Type K Mix
Water*	267	286
Type I Cement*	608	455
Type K Komponent*	—	90
Fine Aggregate*	1129	1069
Coarse Aggregate*	1825	1831
W/C Ratio	0.44	0.52

*Quantities are in lb/yd^3 (1 lb/yd^3 = 0.59 kg/m^3)

As can be seen when comparing Table 1 and Table A.3 in Appendix A, the mix design for the control mix is the same as that used during the small-scale testing. The Type K mix, though, differs slightly. The amount of aggregate and water is similar in the small-scale and large-scale lab tests, but there is slightly less cement in the mix design used for the large-scale lab testing. This was done to increase the workability (slump) of the mix.

As shown in Table 1, the reduction in the cement content increased the w/c ratio. Chapter 2 discussed the effects of w/c on drying shrinkage. Though some researchers report an increase in drying shrinkage caused by an increase in w/c, the effect is not always obvious, as reported by many other researchers. As will be seen in the results section of this report, the strain measured in this study actually decreased for the Type K mix. This means that either the Type K was effective enough to overcome the effect of this increased w/c ratio, or (more likely) the w/c ratio increase did not cause any major effects on shrinkage.

6.2 STRAIN AND TEMPERATURE VARIATION IN THE BRIDGE DECKS

6.2.1 Plain Concrete Deck

The first deck was built using the control mix design for the concrete. The strain gages and thermocouples were connected to a computer, which then read and recorded the data using a LabVIEW computer program. Afterward, the data were downloaded, and a MATLAB program was used to quantify and graph the results. During the first 2 weeks of curing, data were recorded every 5 seconds; after that, data were recorded every 5 minutes. This was done not only to cut down on file size but also because the strain was not changing nearly as rapidly as it did during the first 2 weeks. Recording data every 5 seconds for the entire experiment would provide unnecessarily refined data.

6.2.1.1 Strain Gages

Multiple gages were used to record the strain at several points throughout the bay for 6 months. To correct for any movement during the pour and any initial gage readings, different zero points were inspected from before, during, and after the pour. A zero point from 1.5 hours after the pour was chosen. This time was the closest found to the time of pour completion, and therefore was the closest to the beginning of the concrete cure, which provided graphs with reasonable results. Any readings taken before the chosen zero point caused strain fluctuation within the first few hours of curing as a result of the remaining

behavior from the pour. Figures 28 through 33 are graphs of the recorded microstrain vs. time. In these figures, positive strain designates tension, while negative strain indicates compression. For brevity's sake, one group from the top longitudinal rebar, top transverse rebar, bottom longitudinal rebar, bottom transverse rebar, and girders has been included. Refer to Figures 24 through 27 for gage locations.

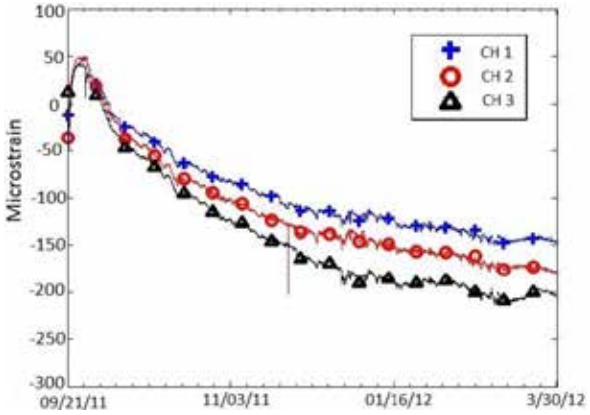

Figure 28. Top longitudinal rebar.

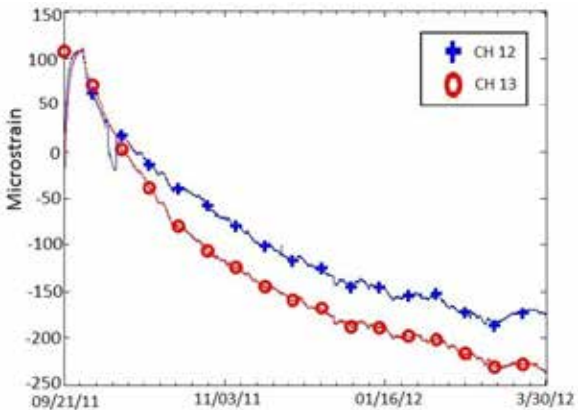

Figure 29. Top transverse rebar.

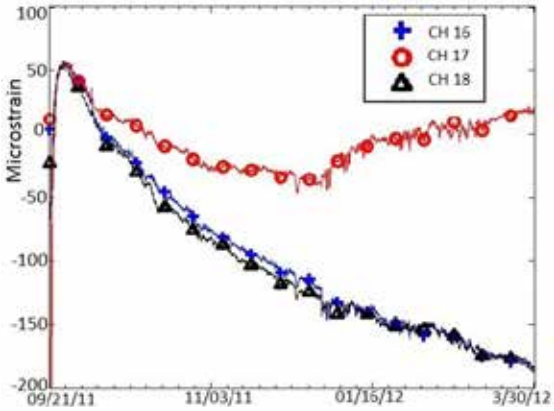

Figure 30. Bottom longitudinal rebar.

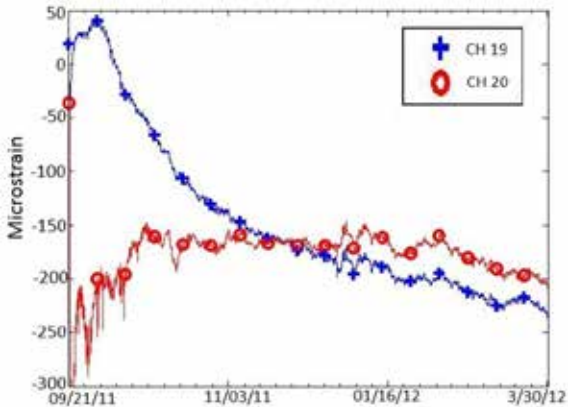

Figure 31. Bottom transverse rebar.

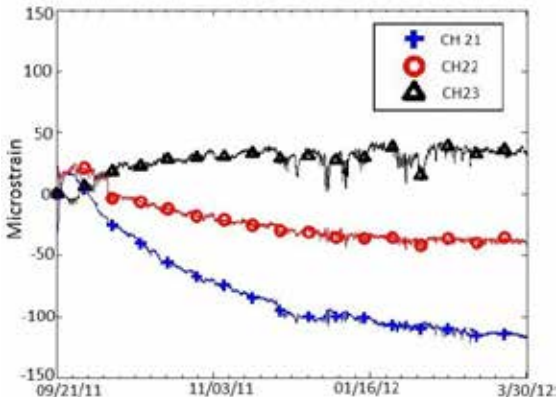

Figure 32. Girder strain gages.

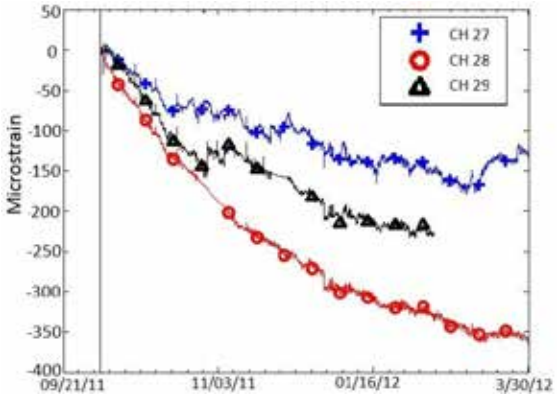

Figure 33. Top concrete longitudinal gages (placed 1 week after pour).

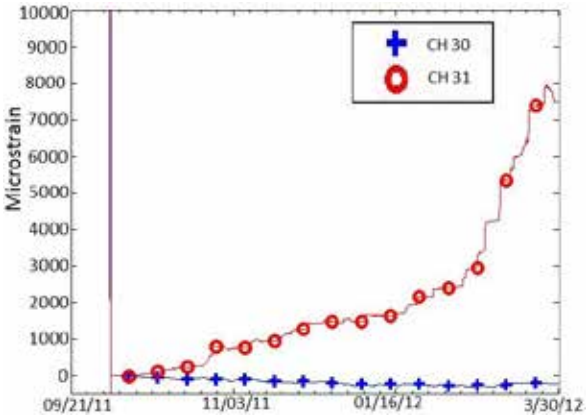

Figure 34. Top concrete transverse gages (placed 1 week after pour).

The gages located on the surfaces of the concrete (Figures 33 and 34) were instrumented at a later date than the others because, during the curing process, the concrete is very moist, which causes issues with gage bond and performance. This is why the initial expansion of the concrete indicated by the other gages was not captured by these gages.

As can be seen in Figures 28 through 34, most of these graphs follow the same general trend. All of the strain gages located along the rebar initially move up into tension. This is caused by the general expansion of concrete resulting from hydration of cement at an early age, as discussed in previous sections. As the expansive reaction dissipates, though, shrinkage begins to take over, and from about 2 weeks after the pour onward, the concrete is constantly shrinking. This causes the strain to move into compression. Meanwhile, the gages along the girders (Figure 32) followed a slightly different trend because of their location. Gage 21 is located along the top flange; therefore, it will expand initially and then compress as time goes on, following the same trend as the rebar strain gages. Gage 23, though will do the opposite because it is located along the bottom flange of the girder. Finally, gage 22 is in the middle of the web and will follow the same trend as gage 21 but at a lower loading rate.

Figures 33 and 34 provide insight into the strain values at the top surface of the concrete. The longitudinal gages shown in Figure 33 have an extreme amount of spread among them. This is probably due to the map cracking at the surface of the concrete caused by evaporation during the course of the experiment. Figure 34 shows that one of the transverse gages (gage 31) developed an extreme amount of tensile microstrain. After investigation of the concrete around the gage, it became apparent that a surface crack created by map cracking was located directly under the gage. Though this is not desirable, map cracking does not cause any structural deficiencies and therefore is not being studied in this research.

All of these gages provide insight into deck shrinkage and will be extremely helpful for later comparison, but the greatest knowledge can be gleaned from a gage that deviates from trend. Figure 35 shows the gages located along one of the top transverse rebars. Channel 10 deviated from the norm, but unlike some of the malfunctioning gages, it has the same initial negative slope as the other transverse gages. Once a crack forms at the location of the gage, its slope quickly turns as the shrinkage pulls the crack open. The tensile strain after the 6-month period is around 550 microstrains.

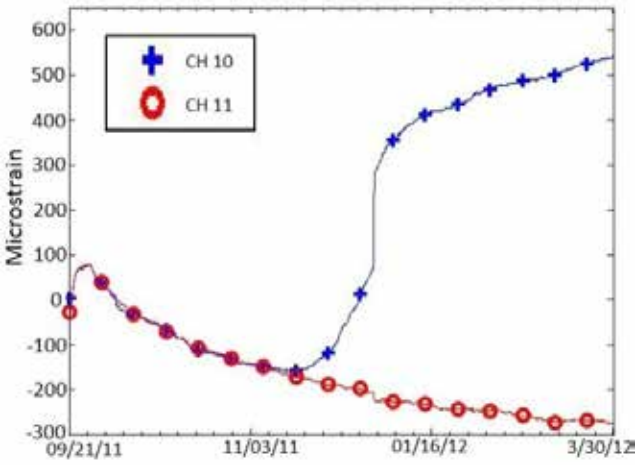

Figure 35. Top transverse rebar (gages 10 and 11).

6.2.1.2 Thermocouples

Unlike the strain gages, the thermocouples need not be zeroed to gain an accurate reading. The thermocouples were placed as described previously to keep track of deck temperature throughout the experiment. This is important for two reasons:

1. By removing from the experimental strain the strain caused by temperature and by gravity, one can find the pure shrinkage strain of the specimen. This process was done using SAP2000 during the finite element modeling portion of the research.
2. The temperature difference between the time the strain gages are placed and the temperature at the time of each reading causes the strain reading of the gage to be thrown off. This is due to the thermal expansion and contraction of the strain gage itself and the fact that the electrical resistivity of the grid conductor within the gage is temperature dependent as well. Therefore, adjustments must be made to the recorded strains to account for this error. These adjustments proved to be extremely small (~2 microstrains) because of the small temperature differential, but they were still included before creating the experimental strain plots (Figures 28 through 35).

The thermocouples located on the girder were placed at the onset of the experiment, but because of the moist environment, the thermocouple on the top of the concrete could not be placed until after the concrete had begun to solidify. (For the Type K mix, thermocouples were chosen that could endure the moist environment so that they could be placed at the outset of the experiment.)

At the end of November, it was decided to open and close the door of the laboratory to the outside to create a temperature differential. This was done to mimic the sun's warming effect on the deck. The bottom of most bridge decks is in the shade, while the top has the sun warming it. This can create temperature differentials that could theoretically cause cracking. To study this effect, more temperature gages were placed on the top and bottom of the concrete directly before the opening and closing of the doors began. See Figures 36 and 37 for the temperature graphs.

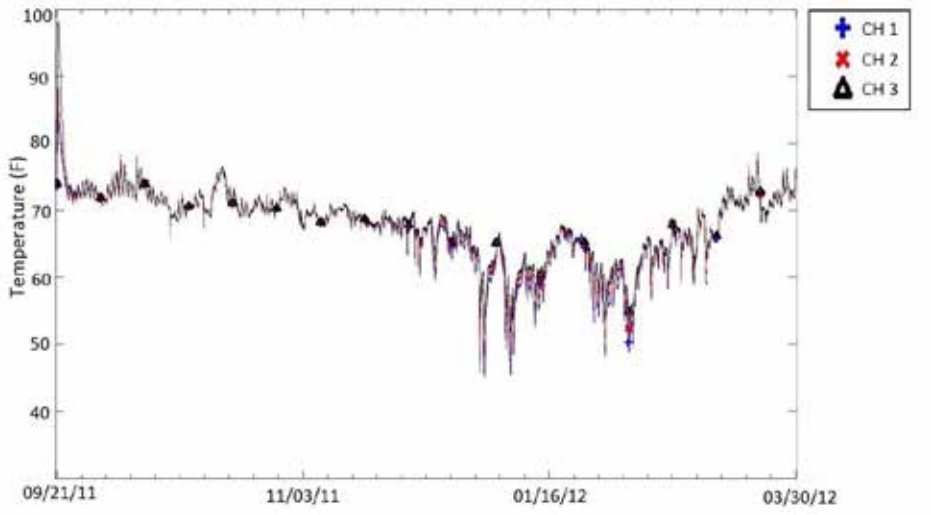

Figure 36. Temperature channels on girder.

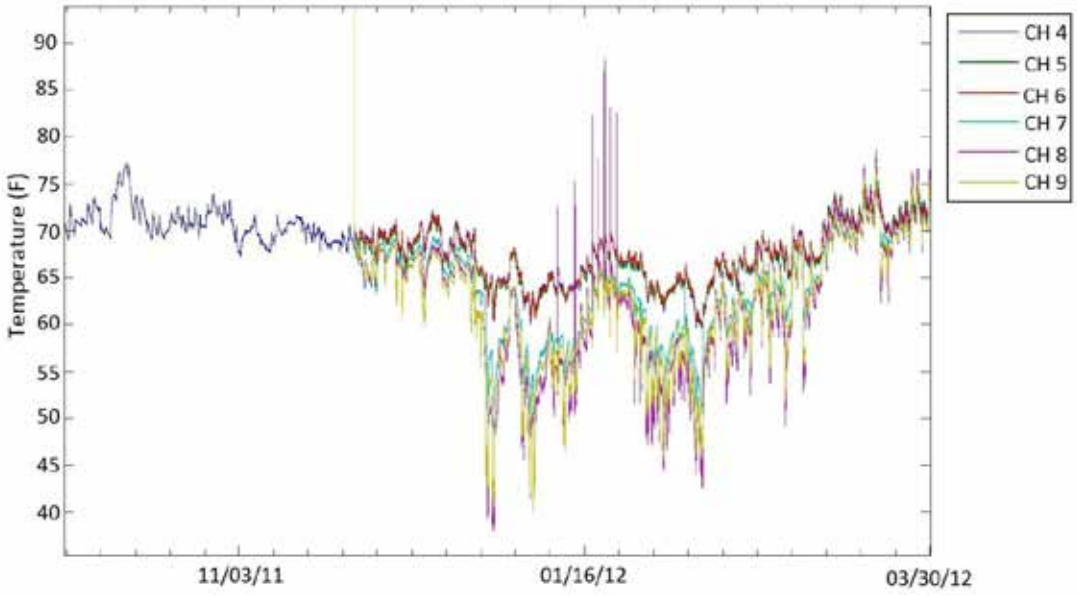

Figure 37. Top and bottom concrete temperature channels.

6.2.1.3 Core Samples

To satisfy curiosity and to look for cracks within the deck, core samples were drilled at various places throughout the concrete (Figure 38) after the control experiment was completed. The samples were all inspected for cracks, specifically samples N and B, because they were located so close to gage 10, which was the gage that was believed to be showing a crack. Core N was the only one that was showing a crack (Figure 39), which

makes sense because it was located so close to a gage that was reading a positive value. This crack, though, was very small and located along the edge of a piece of aggregate, which may indicate only slippage between the aggregate and the cement. There was also a larger than expected number of air pockets in this sample, which may indicate why the rebar began to slip. Though there was no definitive result from inspection, it does make sense that core N would have more cracking and air pockets than other cores removed from the deck.

The cores that did not have rebar inside them were also crushed to make sure that the concrete strength stayed above the required 4000 psi (27.6 MPa) level. The two that were crushed were samples A and J, which had compressive strengths of 4750 psi (32.8 MPa) and 4335 psi (29.9 MPa), respectively.

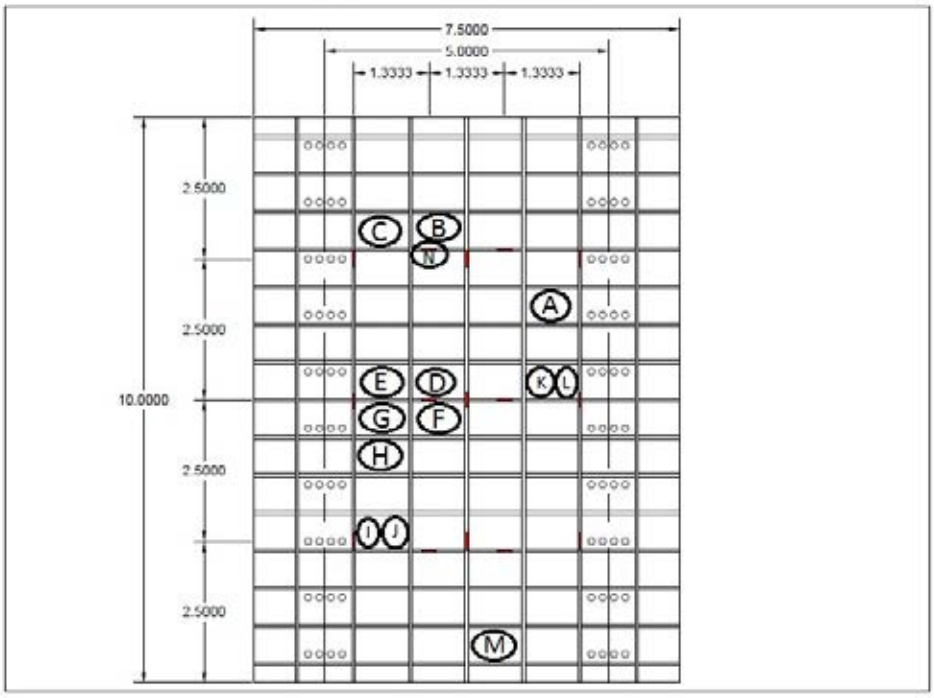

Figure 38. Core sample location.

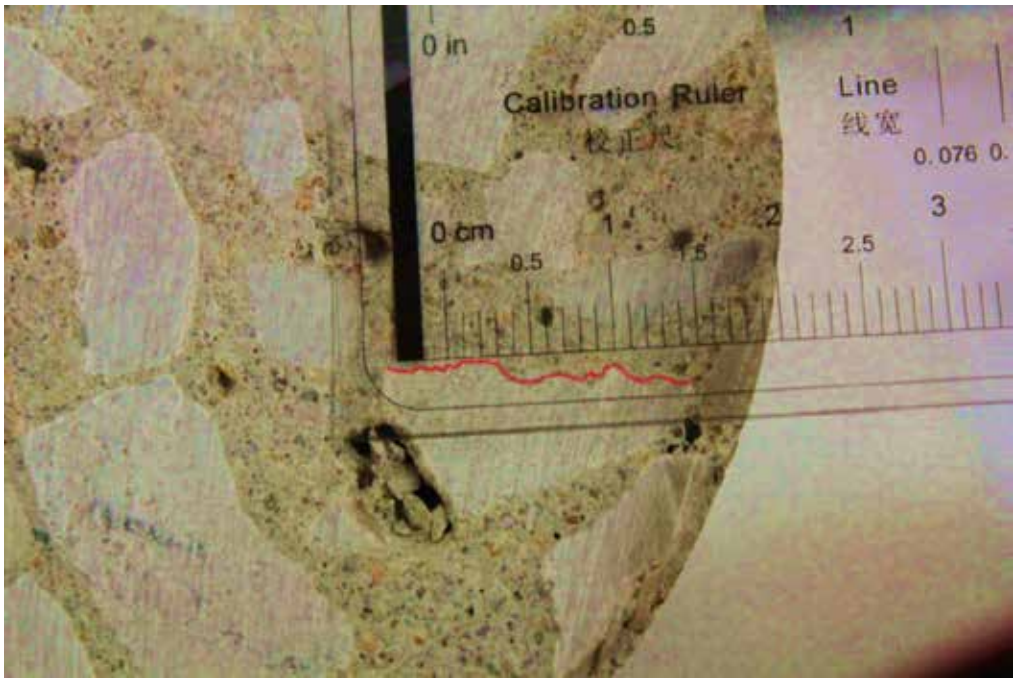

Figure 39. Core N showing a longitudinal microcrack (highlighted in red) and one of the larger air pockets.

6.3 TYPE K CONCRETE DECK

The LabVIEW program and National Instruments (NI) data acquisition setup for the Type K deck was the same as for the control deck. Unlike the control deck, however, strain and temperature readings were collected every 5 seconds during the first week of curing, instead of the first 2 weeks. After completing the control deck, it was decided that the volatility of the strains had dissipated enough to warrant this decreased rate of measurements after 1 week instead of 2. Afterward, the frequency of these readings was decreased to every 60 seconds to decrease the file size. Once the files had been downloaded, the same MATLAB program from before, with a few minor adjustments, was used to quantify and graph the results for the strain and temperature readings.

6.3.1 Strain Gages

The strain gages were placed in the same locations as in the control experiment. Yet again, to accurately graph the readings, a zero point was needed. Multiple zero points from the day of the pour were taken, including times before, during, and after the pour itself. The validity of each zero point was investigated, but it was determined that the readings from 1 hour after the pour was completed would be the most appropriate zero point. Unsurprisingly, both experiments had roughly the same amount of time pass between the beginning of the pour and the zero point reading, which was also taken into consideration for determining when to zero the Type K deck. Examples of the final graphs can be seen in Figures 40 through 45 (see Appendix B for full results) and correspond to the locations from Figures 24 through 27. They are overlaid with the graphs from the control mix experimental model for comparison.

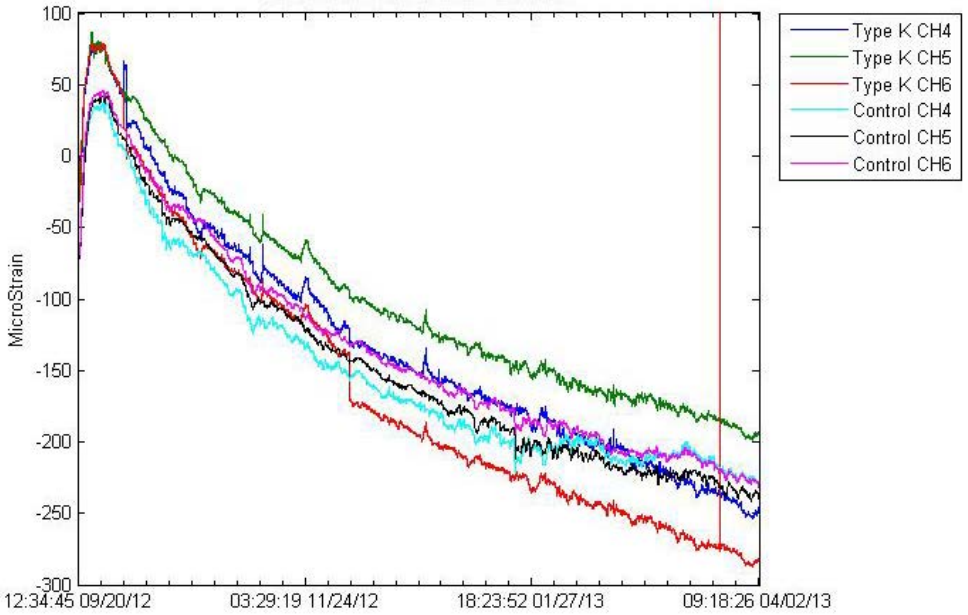

Figure 40. Top longitudinal rebar.

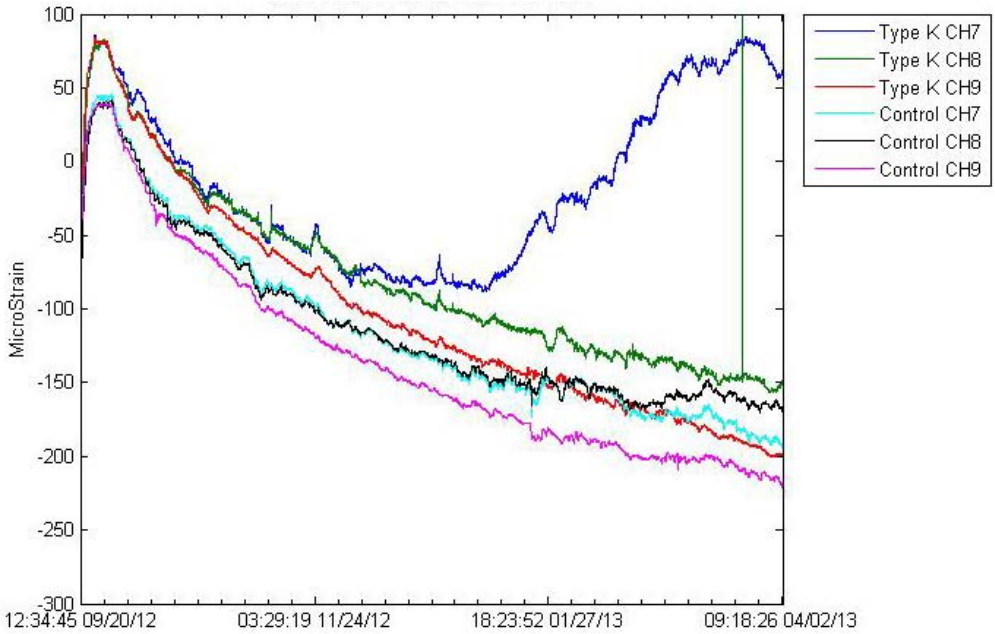

Figure 41. Top longitudinal rebar.

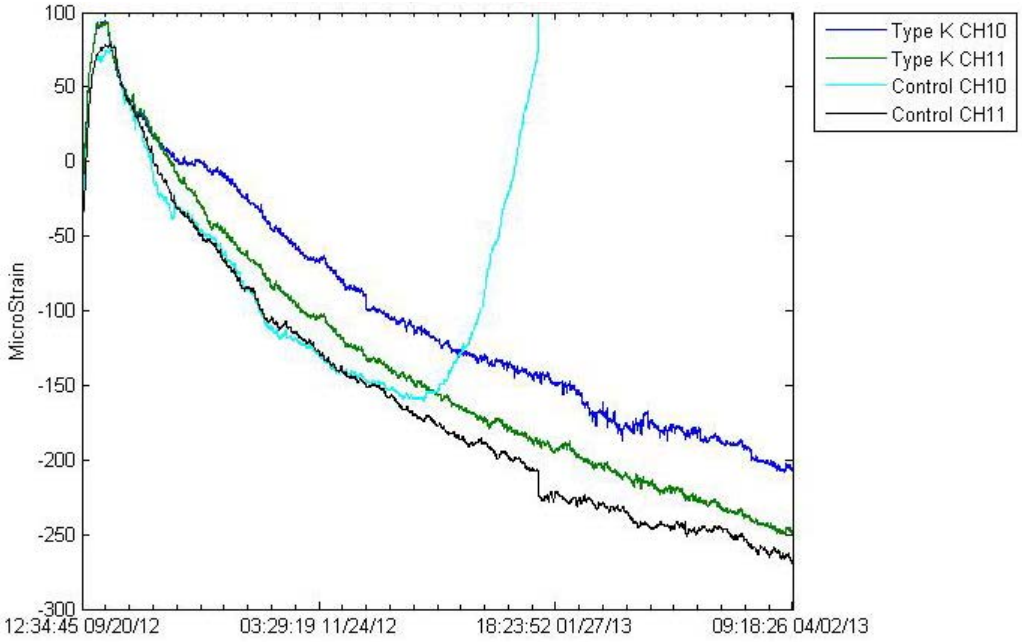

Figure 42. Top transverse rebar.

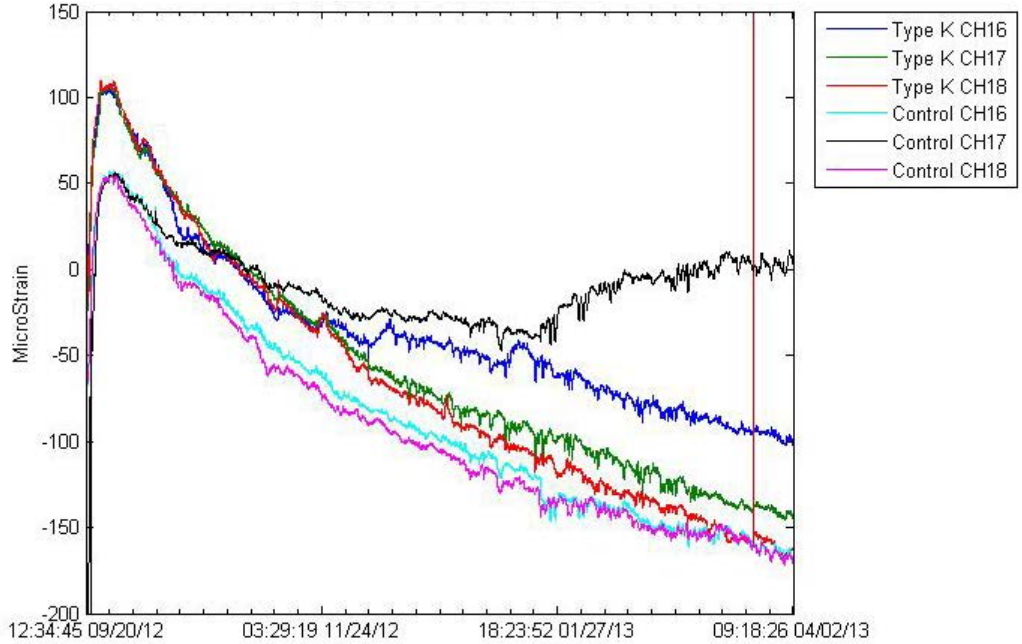

Figure 43. Bottom longitudinal rebar.

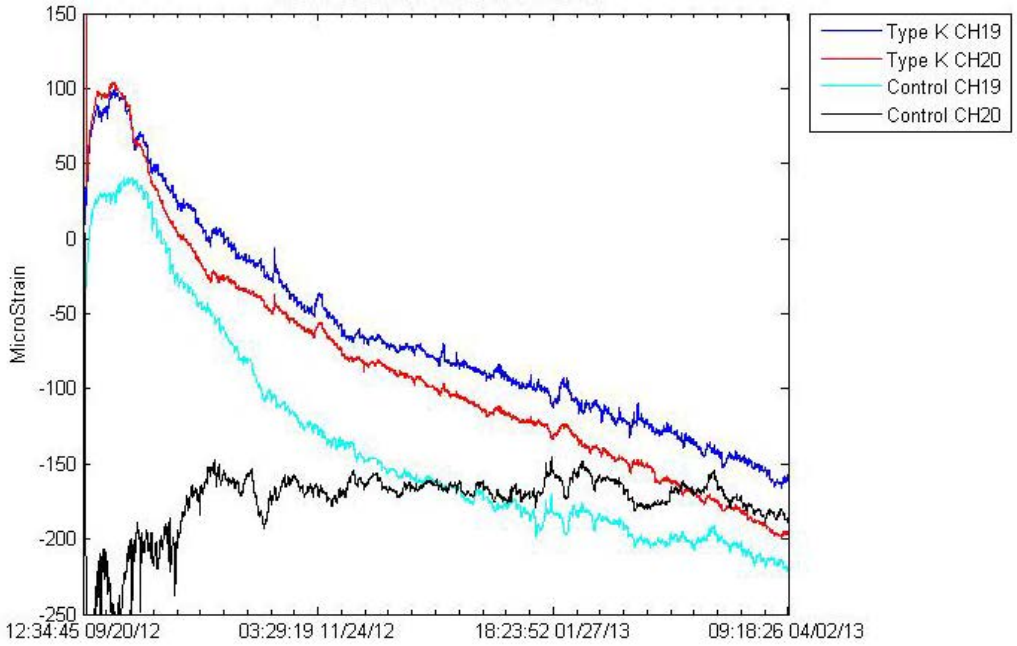

Figure 44. Bottom transverse rebar.

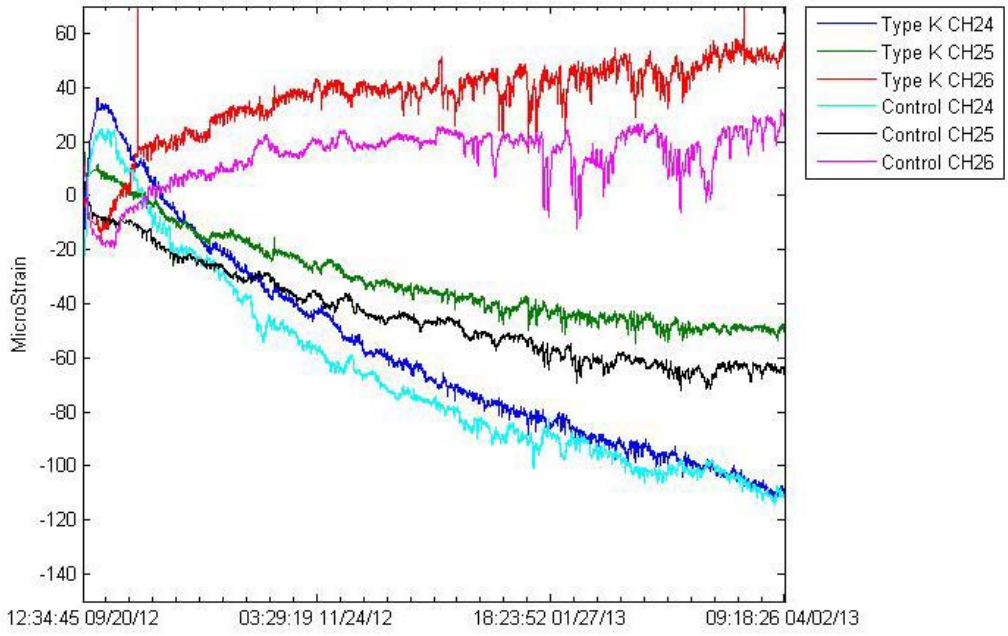

Figure 45. Girder strain gages.

As can be easily seen in the figures, the two mix designs provided fairly similar results. The trends were almost identical; the key difference between the two models was that the Type K mix was generally shifted upward, if at all. The main difference can be seen early in the curing process. While the deck is still in tension from the expansion caused by

development of different hydration products, the Type K additive creates a large difference between the two models, sending the second mix design much higher into tension (around 40 to 50 microstrains higher) for the gages located within the deck. This large tensile difference, though, quickly dissipates as time goes on. Most gages were shifted by +10 to 30 microstrains (a tensile shift, even though the gages were still in compression) by the end of the experiment, but some had reduced to about the same microstrain values.

The gage of the highest significance in this experiment was gage 7. This gage clearly trended with most of the other gages until the middle of December, at which point its gradient began to flip from negative to positive and the strain began to shoot into the tensile region. Just as before, this was most likely caused by a crack forming at or near the location of this gage.

6.3.2 Thermocouples

The thermocouple readings were recorded as discussed earlier and provided very similar results to those of the control model. The main difference between the two models was the location of some thermocouples on the inside of the concrete bridge deck. The results for the thermocouples can be seen in Figures 46 and 47. The corresponding locations can be seen in Figures 24 through 27 in Section 6.1.1. They are overlaid with the graphs from the control mix experimental model for comparison.

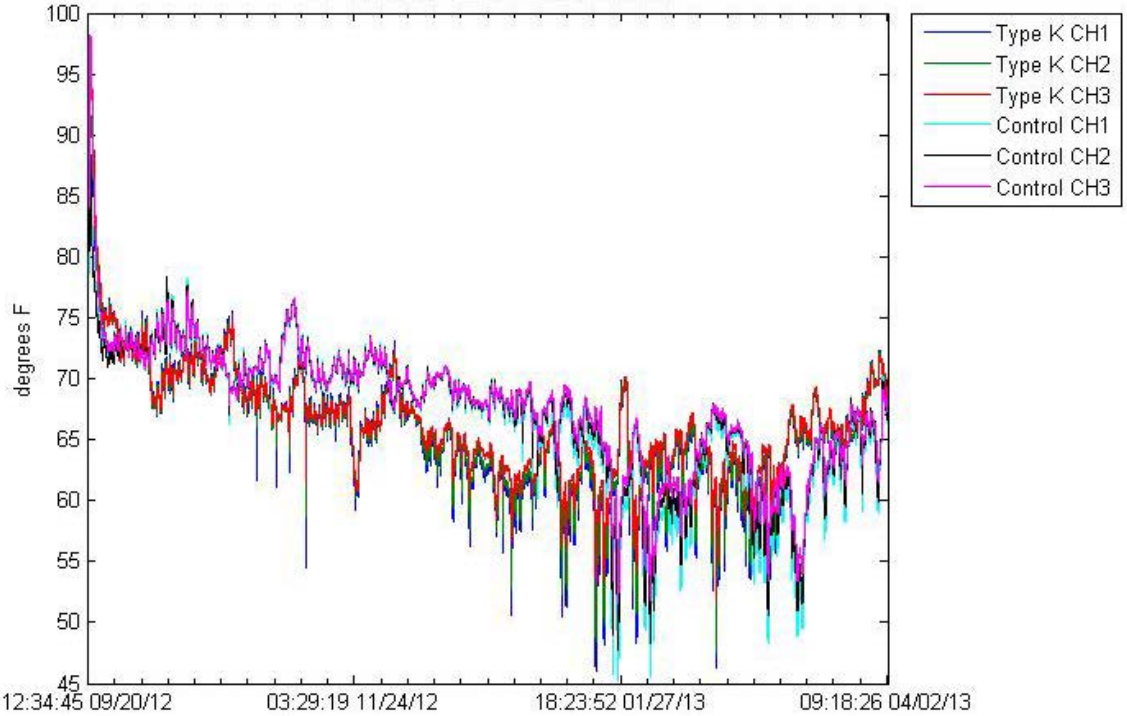

Figure 46. Girder thermocouple readings.

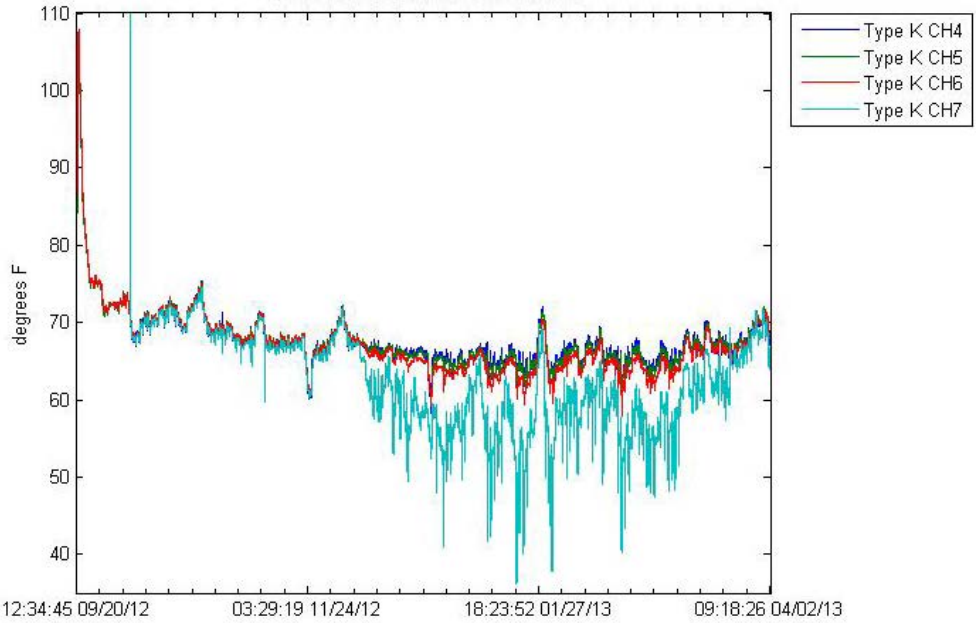

Figure 47. Concrete thermocouple readings (Type K only).

The girder temperatures recorded for the two models were fairly comparable. This makes sense because both were poured during late September. The Type K model temperatures were a little bit cooler because the winter of 2012–2013 was somewhat cooler than winter 2011–2012. Also, it should be noted that gages 5 and 6 were located within the concrete and did not exist during the control mix model; therefore no comparisons could be made.

The intense temperature fluctuations between December and March were caused by opening and closing the door to mimic the sun rising and setting each day. A maximum temperature differential of around 25°F was achieved between the top layer and bottom layer of the concrete. It can be seen, though, that even the thermocouple located along the bottom rebar only differed by a maximum of 3°F from the top of the concrete. This means that even though apparatus was exposed to the outside for about 9 hours a day, it was not enough time for the concrete sample to equilibrate. As the process repeats, the decks is left with a sharp temperature differential between the bottom of the concrete and the bottom rebar of around 23°F. This was most likely caused by the low thermal conductivity of concrete. Even though the temperature on the very edge of the concrete was much lower than the inside, this low thermal conductivity means that the concrete was not exposed to the temperature long enough for it to penetrate to even the level of the lower rebars.

6.4 EXPERIMENTAL CONCLUSIONS BY LINKING LARGE-SCALE MODEL DECK TESTING WITH SMALL-SCALE MATERIALS TESTING

The large-scale lab tests were performed as a stepping stone between the small-scale material tests and a real-world bridge deck. Because the laboratory bridge bay replicates a real-world deck, the cracking and strain within the deck should give a good indication of how each mix design will perform in the real world. A fairly obvious way to determine whether or not a mix design has improved performance is to observe the cracking

in each deck. Though an observable surface crack would have been beneficial to the research, it was not completely necessary to gain useful information as detailed below.

After comparing the two experiments, it can be seen that the addition of Type K decreased the absolute value of strain observed from most of the strain gages by 10 to 30 microstrains after the experiment had run its course. It was also observed that the time it took to form a crack in the Type K deck and the value of the tensile strain measured after cracking decreased compared to the control deck. Cracks formed at the location of gage 10 and gage 7 in the control deck and in the Type K deck respectively, with the Type K deck cracking almost 2 weeks later than the control deck. Furthermore, once the cracks formed, gage 7 (for Type K mix) saw an increase of 35 microstrains in tension whereas gage 10 (for control mix) saw an increase of 170 microstrains in tension. Though strain in gage 10 was measured for about 2 extra weeks, it can be easily seen that the gradient for strain increase in gage 10 is much steeper than that of the gage 7. This means more tensile stress was relieved when a crack formed in the control deck compared to the Type K deck. This difference clearly shows that the Type K deck had less tensile stress stored in concrete. By linking the small-scale test results with the large-scale results, the discussion below explores a possible reason for this difference in the stored tensile stress level in concrete.

After a thorough comparison of the results from both studies, a few major themes can be discerned. First of all, the small-scale tests resulted in much higher strain values than the large-scale tests. A comparison of the control mix results from Figures 8 and 40 shows that the small-scale mix experiences 100 microstrains in expansion and 700 microstrains in shrinkage. In other words, it showed a “shrinkage potential” of 800 microstrains (100 plus 700 microstrains). Meanwhile, in the large-scale tests, an expansion of 50 microstrains was recorded, along with a shrinkage of 200 microstrains. This means that the large-scale model, with a total shrinkage of 250 microstrains is missing 550 microstrains of shrinkage potential compared to the small-scale results due to increased restrain in the large-scale model. It is theorized, that the missing shrinkage potential is what causes development of tensile stress in concrete, because if one lets the concrete shrink freely, there will be no stress. When the full potential for shrinkage strain is prevented due to restraint (referred here as the missing shrinkage potential), it causes stress to develop and possible cracking in the future.

Using the same figures (Figure 8 and Figure 40), a similar comparison can be made for the Type K deck. The small-scale tests showed about 600 microstrains of shrinkage potential (500 microstrains in expansion and 100 microstrains in shrinkage), whereas the large-scale lab test only showed 275 microstrains of shrinkage potential (75 microstrains in expansion and 200 microstrains in shrinkage). So, for the Type K deck, the large-scale lab test is missing 325 microstrains of shrinkage potential when compared to the total 600 microstrains of shrinkage potential observed from the small-scale test.

The high strain values recorded in the small-scale tests do not show up in the large-scale tests because the deck has much more restraint to movement. Instead, these missing shrinkage strains are stored as tensile stress in concrete and it is constantly searching for ways to relieve this excess stress. The Type K mix design does a much better job of reducing this excess tensile stress than the control mix (since the missing strain in Type K deck was only 325 microstrains compared to 550 microstrains in the control deck). When the deck cracks later on, the restraint against movement is finally removed. Opening up of a crack allows the missing shrinkage potential to take effect. This will relieve the stored tensile stress in concrete in exchange of strain that was measured by gage 7 (for Type K mix) and gage 10 (for control mix). The fact that there was less stored tensile stress in Type K deck explains why the strain observed in gage 7 once the crack formed is only 150 microstrains

(Figure 41) compared to the 250 microstrains strain observed in the gage 10 (Figure 42). Further research is necessary to understand the link between the small-scale and large-scale test better and to understand the mechanism behind the reduction in the excess or missing shrinkage strain potential in the Type K deck.

Another careful look at the difference between the observed levels of strains in the small-scale and the large-scale testing showed further insight on the role of external and internal restraint against movement of concrete deck. The external restraint provided by the four C channels placed along the edges of the concrete deck and bolted to the rebars, and the internal restraint provided by the frictional bond between the rebars and concrete and by shear studs attached to the steel girders are much larger in case of the large-scale deck compared to the small-scale beams tested at the UIUC lab. Now the external restraint is more effecting in preventing expansion than shrinkage, whereas the internal restraint will reduce both expansion as well as shrinkage. Large-scale model is showing only about 15% (75 microstrains compared to 500 microstrains) of the expansion and 45% (275 microstrains compared to 600 microstrains) of the shrinkage observed from the small-scale testing. During expansion at early age, the concrete is fresh, and the bond between concrete and rebars may not have achieved its full strength. However, the reduction observed in expansion is still more than the reduction observed in shrinkage. This possibly means that the external restraint in the large-scale testing was much stronger compared to the internal restrain. Also, the restraint placed on the large-scale lab tests do not accurately replicate the situation for a bridge with expansion joints throughout. Expansion joints and integral abutment will alter the external restraint against expansion of Type K concrete. As external restraint can be more effective in preventing expansion than shrinkage, it seems by altering the relative amount of the internal and external restraint, one can adjust the magnitude of the missing shrinkage potential and hence stored tensile stress in concrete. However, the exact role the internal and external restraint play on controlling the missing shrinkage potential still need to be studied. Further research on effects of internal and external restraint in relation to a bridge with and without integral abutment or expansion joints will be necessary to determine full potential of Type K mix. Furthermore, the difference in the modulus of elasticity of concrete under compression and tension may create difference in overall stiffness of the deck and hence difference in internal restraint against movement. Effect of such difference in internal restraint against expansion and shrinkage should also be studied in the future.

CHAPTER 7 FINITE ELEMENT ANALYSIS

Once the experimental results had been collected for the large-scale lab tests, the next step was to formulate a finite element model (or FE model) to mimic the strains within the deck. This can be tricky, though, because the strains throughout the deck vary considerably and that must be reflected in the model. Once the modelling of the experimental deck is completed, the computer model can then be expanded to model a full-scale bridge.

There were two different programs used to conduct this part of the research. The first was SAP2000, which was used to model both of the experimental bridge bays. The second was Abaqus, which is considerably more in depth but proved to be much more appropriate for modeling the full-scale bridge.

7.1 SAP2000 MODEL

To create the experimental bridge model's Finite Element analysis (FEA), all parts of the concrete bay—steel channels, girders, rebar, and concrete—had to be included and connected to achieve an accurate representation of the experiments. Three-dimensional solid elements were used to create the concrete, while shell elements were used for the steel girders and channels. Frame elements were used for the rebar, as they only provide any real stiffness along the axial direction. Figure 48 shows a picture of the SAP model used for both the control and the Type K experimental decks. The concrete is in red and the c-channels in blue. The rebar shows through in green, but that is merely a problem with the SAP display; the rebar is fully embedded within the concrete in the model.

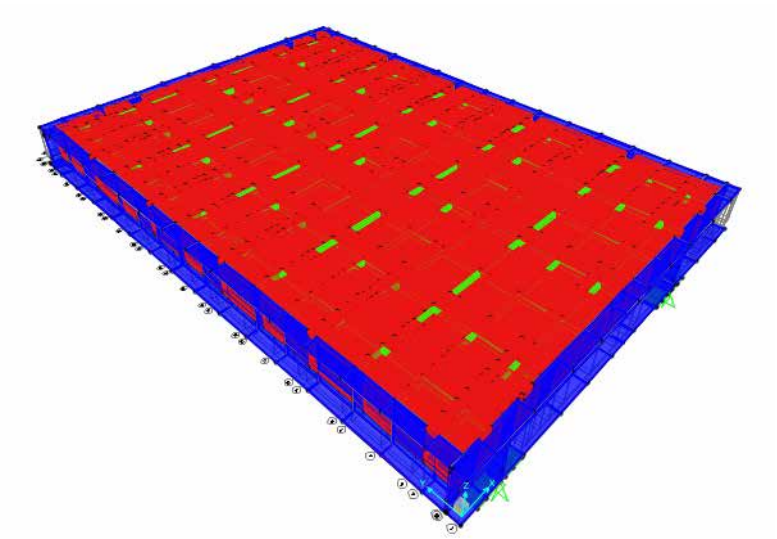

Figure 48. SAP2000 model.

Each element was given a material designation, either steel or concrete. The material properties, which were the same for both experiments, are shown in Table 2.

Table 2. Material Properties for Steel and Concrete

	Steel	Concrete
Weight per Unit Volume (lb/in^3)	0.2836	0.0868
Modulus of Elasticity (ksi)	29000	3605
Poisson's Ratio	0.3	0.2
Coefficient of Thermal Expansion (/°F)	6.5E-6	5.5E-6
f'_c (ksi)	N/A	4
Minimum Yield Stress (ksi)	50	N/A
Minimum Tensile Stress (ksi)	65	N/A
Effective Yield Stress (ksi)	55	N/A
Effective Tensile Stress (ksi)	71.5	N/A

7.1.1 Control Mix Experimental Finite Element Model

The only difference between the decks was in the temperature loading used to model the experimental strain results. Because applying a strain directly to the deck is not possible, temperature loading was used to replicate the strains in the concrete. An initial temperature loading was found based on the coefficient of thermal expansion of the concrete. The initial temperature loading, though, produced extremely large percentage errors (on the order of 80% to 100%) between the recorded strain and the strain produced by the finite element model. These errors were most likely the result of complex interactions of the temperature loadings throughout the deck, which make it impossible to use the coefficient of thermal expansion to determine local strain. Therefore, a ratio was used to relate the recorded shrinkage strain from the experimental lab testing to a temperature to be applied to the deck.

Using the coefficient of thermal expansion as an initial starting point, the percentage errors were meticulously whittled down until an average of 5% to 15% was found. This means that, for the control mix, the SAP and experimental strains very closely mirrored each other, allowing a very high confidence in the results from the finite element model.

Figures 49 and 50 show that the SAP strain and the experimental strain for gage 9 (a typical longitudinal gage) and gage 15 (a typical transverse gage) very closely matched each other (for the rest of the finite element results for the control mix, see Appendix C). The only area that caused discontinuities between the two graphs was during the initial pour, but it was in the transverse rebar only. Because the main concern for this study is the strain in the longitudinal rebar (which corresponds to the longitudinal strain in the deck), this was not a major problem. The SAP strain does return to the correct values once shrinkage begins to take over, which means that long-term shrinkage can still be modeled with excellent accuracy.

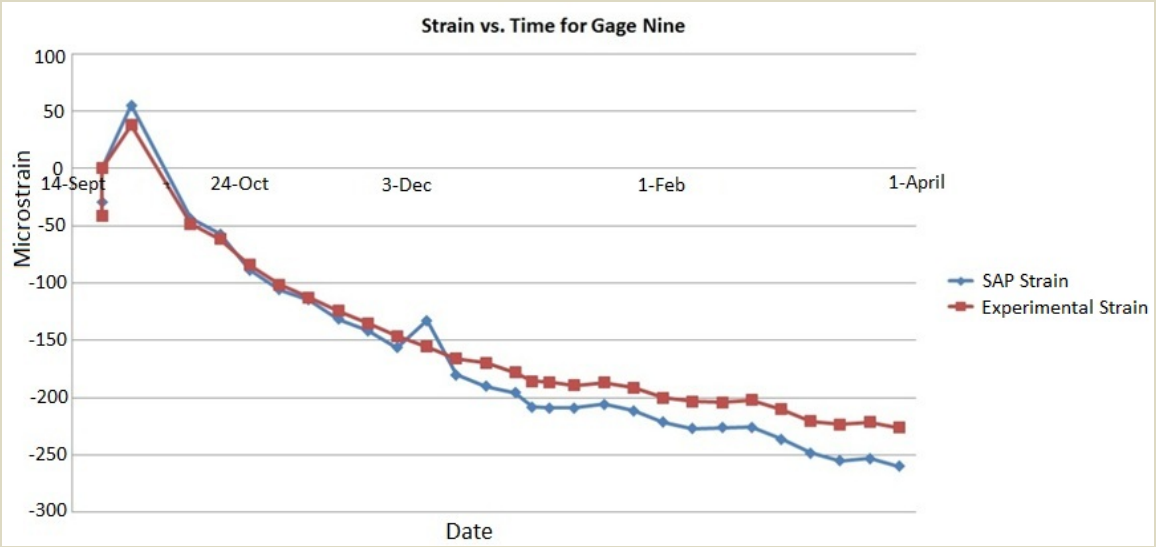

Figure 49. SAP and experimental strain vs. time for a typical longitudinal gage (gage 9).

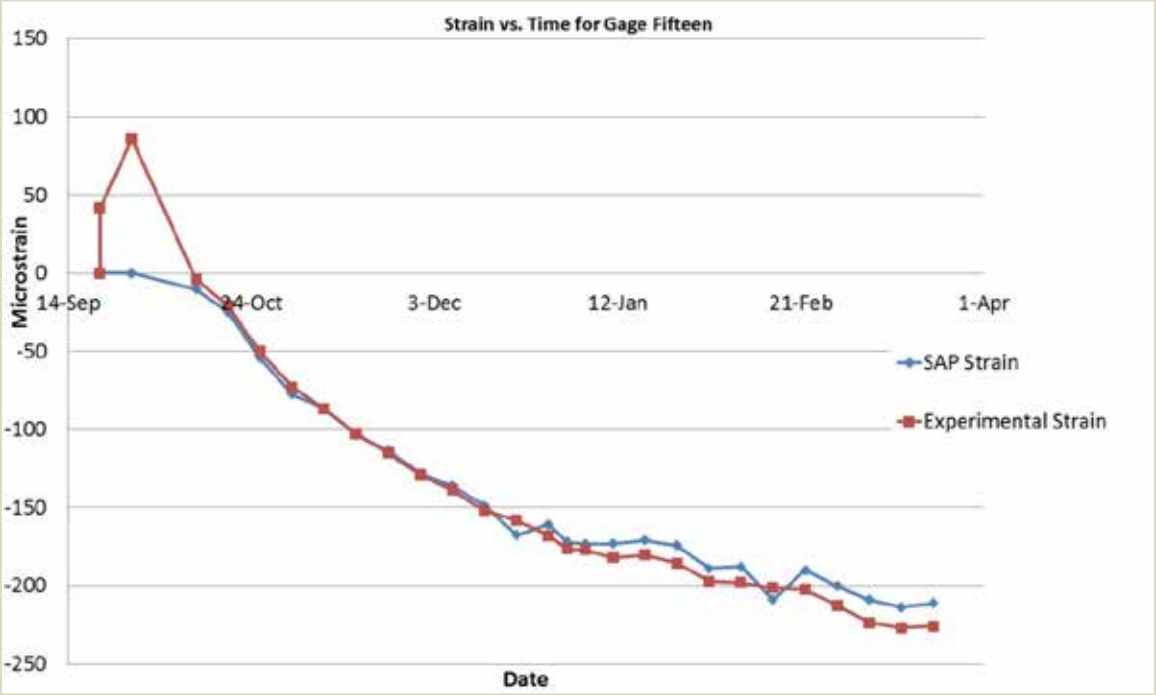

Figure 50: SAP and experimental strain vs. time for a typical6Transverse gage (gage 15).

7.1.2 Type K Mix Experimental Finite Element Model

A finite element model was also necessary for the Type K deck. The same model was used—the only difference was the temperature loads applied. A first attempt was made to model the strains using the same ratios between strain and temperature loading found for the control deck. After applying the subsequent temperature loads, it was found that the

strains predicted by SAP, though plausible, created percentage errors in the range of 70% to 80%. After studying these results, it was decided that this percentage error was unacceptable and that a new model was required to accurately depict the strains for the Type K cement.

This determination meant that new ratios must be found in order to accurately simulate the new loads in the Type K deck. Initially, the coefficient of thermal expansion of concrete (5.5E-6/°F) was used to find the ΔT that must be applied to each region of the model based on the strain readings from the gages. Multiple attempts were made in the same fashion as for the control deck until our model converged on the appropriate loads. The average percentage error for the final data was between 5% and 15% on most dates, which is extremely close when considering that the measurements are in microstrains.

Data were still being collected for this deck when this report was completed, so even though the strains have been modeled for some dates, the final model data cannot yet be completed. The Type K finite element model will be completed and reported during phase II of this project.

7.1.3 Girder Temperature Loading

Over the course of the experiment, questions arose about how the daily temperature changes and the sun's heat would affect the bridge deck and the steel girders. As the sun rose, its rays began to hit the steel girder early in the morning, heating it up to a higher temperature than the deck. This heating caused the girder to expand, while the concrete stayed at a relatively constant size. Non-uniform strains begin to form because of this unequal expansion and could possibly be a factor in deck cracking. This concept was explored using the SAP2000 program and the already-created bridge deck.

A particular date was selected (6/5/2012), and the temperature loads to mimic the strain found were applied. The idea was to use the strains that were found experimentally and add the load caused by the change in girder temperature from exposure to the sun to find the final strains in the deck. After running a control model, the girder was given an additional temperature load of 10 degrees, 20 degrees, and 30 degrees to determine any effects it had on the bridge deck strains. The girder was uniformly heated in each trial.

As expected, the bridge deck showed a non-uniform strain field. The majority of the strain was taken on by the longitudinal rebars closest to the heated girder. The transverse bars showed very little change in strain, which can be expected as a result of the girder expanding the bridge deck longitudinally. Figures 51 through 54 show the results of these test runs. The y-axis shows the strain in microstrains, while the x-axis shows the change in temperature introduced to the girder. The longitudinal rebars took on stresses resulting in 30 to 40 microstrains, while the transverse rebars took on strains of only around 2 or 3 microstrains.

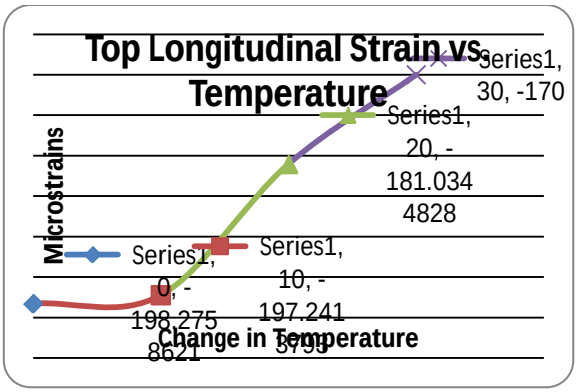

Figure 51. Girder temperature top longitudinal.

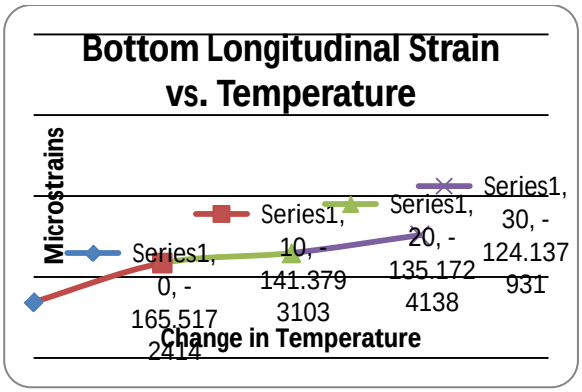

Figure 52. Girder temperature bottom longitudinal.

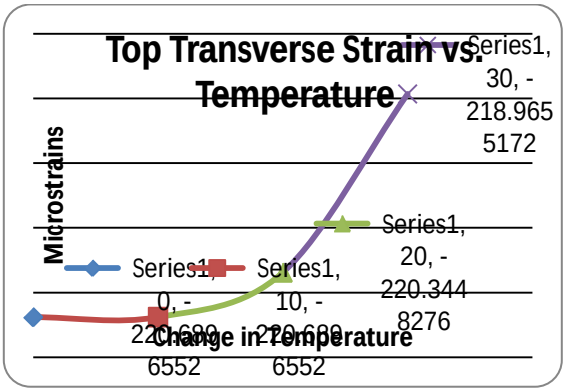

Figure 53. Girder temperature top transverse.

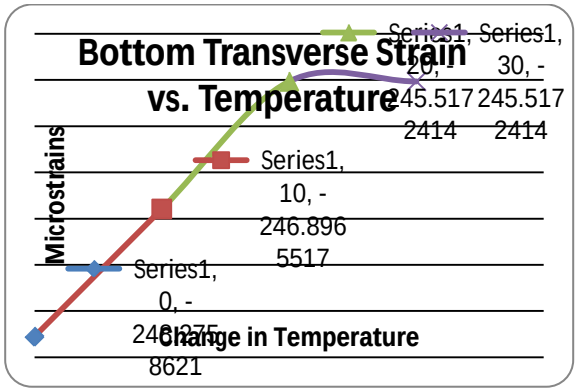

Figure 54. Girder temperature bottom transverse.

After running this analysis, it was readily apparent that the rising sun is probably not a major factor in the formation of cracks. First, to see any significant strain in the rebars, there must be a temperature difference of around 20°F between the girder and the bridge deck. Even though there can certainly be a large temperature change between day and night, this change will affect the whole deck, not just the girder. Second, as the sun heats the girder, tensile stresses form as the girder expands. These tensile stresses fight the compressive stresses formed by shrinkage and drive the strain readings closer to zero instead of further away. If a crack was already formed in the right place, then a very hot girder may cause the crack to expand slightly, but the 30 to 40 microstrains that it creates is not enough to actually form a crack itself. The only possibility left is that the sun heating the girders is a daily loading, and this cyclic loading is capable of doing some damage. It is a very slow load, though, so the effects it has may be minimal. Further study might be done to investigate the cyclic effects of this temperature load.

7.1.4 Shrinkage Strain Determination

The experimental strain that was recorded over the course of this experiment has three distinct processes contributing to it: thermal strain, gravity strain, and shrinkage strain. Our study focused on the shrinkage strain, which is difficult to find on its own. To find only the shrinkage strain, the other two processes must be filtered out of the results, leaving only the shrinkage.

The gravity strain is fairly easy to remove through a series of dead load calculations and then a check using the computer models. Differentiating between thermal strain and shrinkage strain, though, is a much more difficult process. Theoretically, if one can model just the thermal strains and remove those values from the experimental results, all that should be left would be the shrinkage strain. This, though, proved extremely difficult to do for the control deck because of the thermocouple locations.

The thermocouples for the control deck were located on the top and bottom of the concrete. The belief was that the temperature within the concrete could be found through a linear trend between the temperature on top and the temperature on bottom. The problem with this approach is that concrete is a fairly poor conductor of heat, which means that even though the thermocouple on the outside of the concrete may read 40°F, the temperature 1 in. into the concrete is actually much higher.

Many iterations of applying the temperature loads in different ways were attempted, but none of them provided realistic results. Therefore, it was decided to place thermocouples along the top and bottom rebar in the Type K model. This provided exact temperature measurement, which could be used to determine the strain on each gage that was caused by temperature. With this temperature strain removed, the exact value of shrinkage strain can be found for the Type K deck.

7.2 FULL-SCALE BRIDGE MODEL

The next step in the research process was to use the experimental data and the results found from the SAP2000 simulations to effectively model the shrinkage in a full-scale bridge. A bridge had been previously selected to be the first bridge poured in Illinois with the newly designed concrete mixture used for the second experimental deck. This made it easy to choose a bridge to model.

The bridge selected is a highway bridge located in Wayne County, Illinois, along IL 15 (Figures 55 and 56). It is a three-span integral abutment bridge with precast concrete girders and an 8-in. concrete slab that is integrated into the girders using stirrups. The rebar design, as well as a more thorough discussion of the concrete design, will be discussed in detail later.

This bridge was created in stages so as not to completely cut off the flow of traffic. Initially, the southern half of the bridge was poured using the experimental Type K mixture, which was allowed to cure according to the same standards used in the lab [Standard 1020.13(a)(5) from the IDOT Standard Specifications for Road and Bridge Construction]. However, an issue with the balling of Type K concrete mix which noticed during pouring which is believed to be due to improper mixing. For future practice, it is advisable that the Type K and portland cement must be blended properly before adding water. After the southern half had cured, though, it was decided that the northern half should be poured using a concrete mixture typically used by IDOT, which is similar to the control mixture used for the first experimental deck in this project.

Figure 55. Rebar location and stirrup spacing on top of girder.

Figure 56. Southern half of bridge deck with cotton mat on top.

The staged construction, along with the different mix designs, created a problem for modeling the full-scale bridge. First, the southern half of the bridge must be modeled according to the results for the Type K experimental deck. Then, after a certain period of time, the second half of the bridge deck had to be added and, to appropriately model the strains, the results from the control mix experiment had to be used for the northern half . Though the time and mix design discrepancy could theoretically be modeled, it was decided that the results would be too variable to trust. Therefore, only the southern half of the bridge was modeled for the purposes of this research.

Though SAP2000 had proven to be an ideal tool for modeling our experimental deck, it was extremely difficult to use SAP2000 to model the full-scale bridge deck. A real-world-sized bridge was far too complicated for the software to handle, and it repeatedly shut down, even when it was running on extremely powerful computers. Therefore, the validity of transferring the SAP2000 results into the Abaqus framework required delving into.

Accordingly, a new model was created in Abaqus to mirror the one built in SAP2000. It was the same size and used the same element types as the SAP2000 model (see Figure 57). It was also partitioned the same way as the SAP2000 model so that temperature loads could be applied. Finally, a random date was chosen (12/28/2011) on which to take the temperature loads. The stress profiles (in psi units) produced by both programs can be seen in Figures 58 and 59. Not only are these results extremely similar, but they also accurately predict the strain in the laboratory experimentation. Therefore, Abaqus clearly behaves comparably to SAP2000 and, from the evidence presented, it was determined that using a different finite element program would yield minimally different results. This led to tremendous confidence in the choice to use Abaqus as the finite element program for modeling the full-scale bridge.

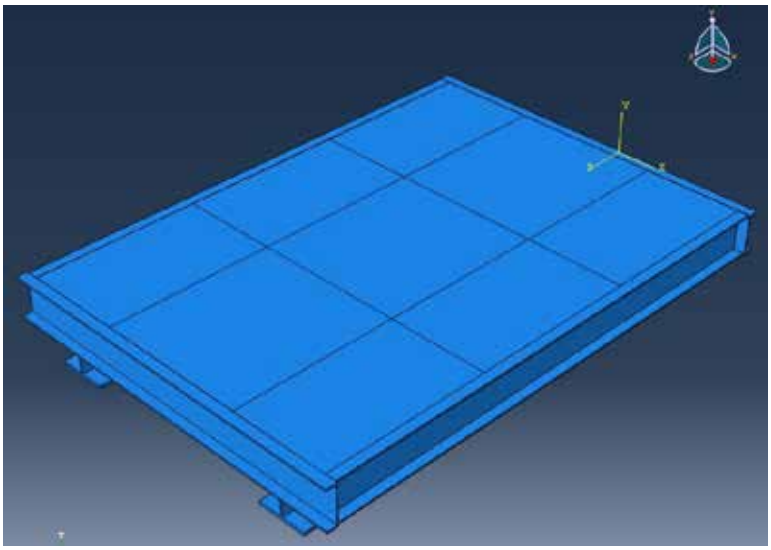

Figure 57. Abaqus model.

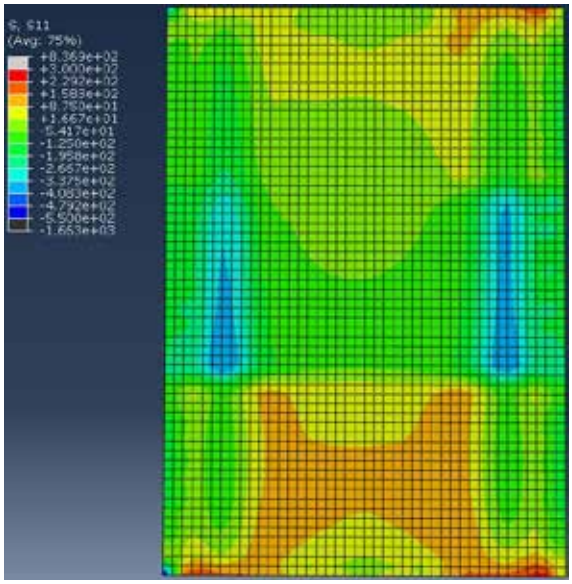

Figure 58. Abaqus stress color contours.

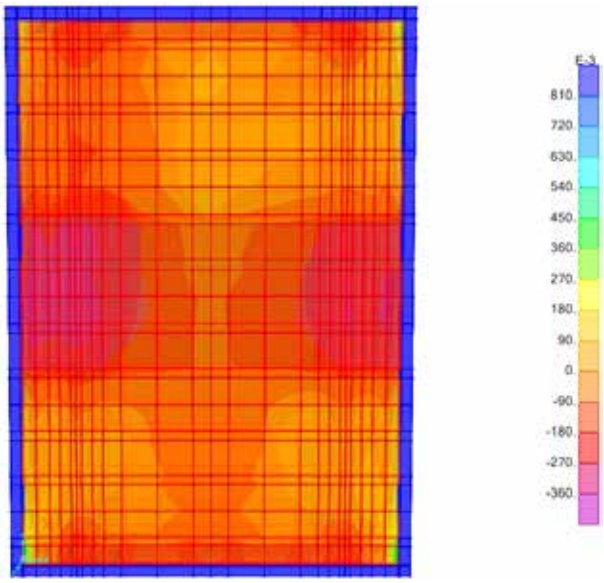

Figure 59. SAP2000 stress color contours.

7.2.1 Abaqus Element Selection

The first decision to be made before modeling the full-scale bridge was what element type to use for the concrete deck, girders, parapet, and the steel rebar. The deck, girders, and parapet were designated 8-node solid elements because they all are concrete sections, and the steel rebar was designated a truss element. These element types were chosen not only because they are the most appropriate for modeling purposes but also because they closely match those used for the experimental model.

Next, it was necessary to determine how to handle the fact that the bridge not only used precast concrete girders (instead of the steel girders used in the experimental model) but it also had a parapet on the end, which created a torsional load. These girders were reinforced with #5 steel rebar and were cast in place with ample time to cure before the deck

was poured. Though the girders contained rebar, this study is concerned with shrinkage strain and the cracking it causes within bridge decks. Therefore, because the dead load does not create failure or excessive deflection, for the purposes of this study the rebar was removed. The girders could then be modeled as non-shrinking concrete objects because of the amount of time they had been given to cure before the concrete was even poured. Therefore, no temperature loads were applied to the girders (just as in the experimental model) to mimic any sort of shrinkage strain. The parapets were dealt with in a similar manner.

Because the parapets require special forms, they are poured after the concrete deck has had time to cure. Also, they might not be a part of the bridge structural elements, which means that cracking in the parapet is of much less concern. This, coupled with the fact that no data for shrinkage within the parapet existed from the experimental model, led to the decision to not apply any shrinkage loading to the parapet. The parapet does, however, contribute a significant amount to the dead load of the structure and provides extra restraint, similar to the girders. Consequently, the parapet could not be ignored when modeling the full bridge.

Figures 60 and 62 display the concrete design in the Abaqus model. In Figure 61, the orange arrows display the locations of the parapets and the ends of the bridge, which were modeled as boundary conditions placed on the model.. The two ends of the bridge model were fixed in order to represent the slab and girders embedded in the soil on either side. The deck is held up by two piers, each 42 ft from either end. These two piers were poured separately; therefore, they are represented by rollers.

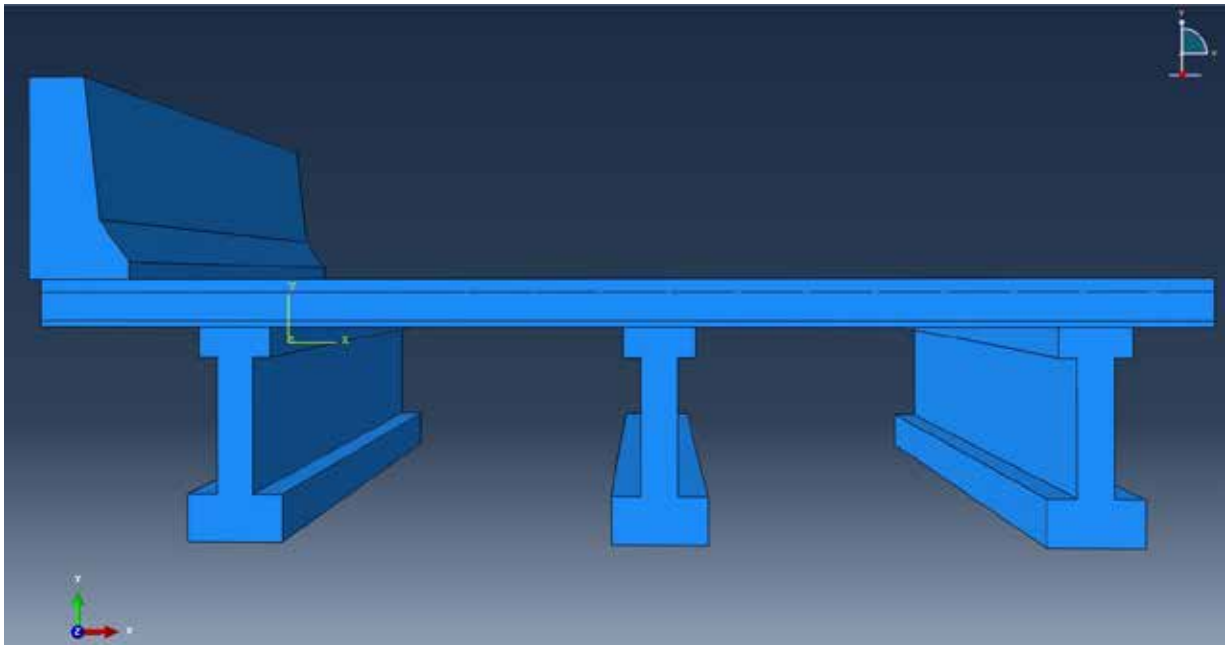

Figure 60. Full-scale model section view.

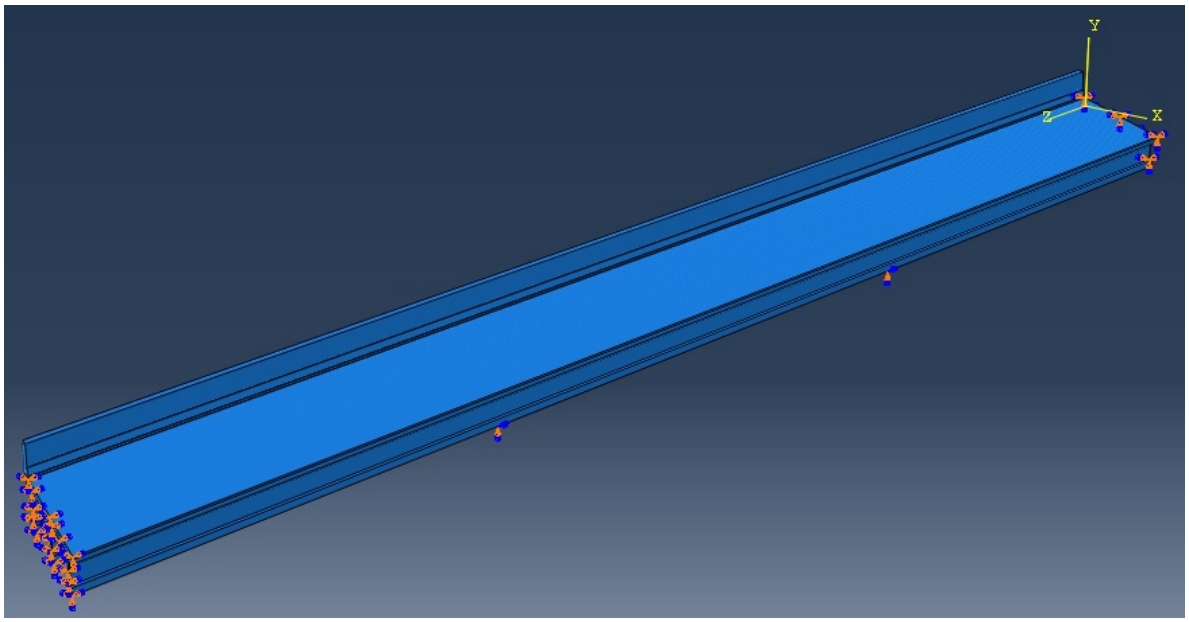

Figure 61. Full-scale model 3D view.

The final, and most difficult, step was to model the rebar within the bridge deck. Just as in the experimental deck, there are four main types of rebar: top longitudinal, top transverse, bottom longitudinal, and bottom transverse. Another similarity with the experimental deck was the location of the rebar: 2.25 in. from the top of the concrete for the top rebar and 1 in. from the bottom of the concrete for the bottom rebar. Though this is not exactly the same, the 0.25-in. difference should not affect the shrinkage loading too much.

The main difference between the models was the spacing of the rebar. In the full-scale model, the rebar spacing was not constant throughout and changed whenever it passed over a pier or other structural components. The average rebar spacing was 6.5 in. for the top transverse and 10 in. for the bottom transverse. The top longitudinal was generally spaced at 12 in. on center, whereas the bottom longitudinal bars were commonly spaced at 12.5 in.

The main rebar size used was still #5 steel rebar, but some of the top longitudinal rebars were #6 because extra steel was needed. Therefore, the shrinkage loading should still transfer properly to the full-scale model because the rebar distribution is fairly similar to the experimental model. Again, just as in the experimental model, a frame element was used for the rebar to simulate the purely axial loading that it resists.

Once all of the materials were in place, a dead load analysis of the full bridge was run. The results matched the predicted longitudinal strain values, which proved that the model was ready assess temperature loading. Figure 62 is a section view taken from the center of the bridge, and Figure 63 is an overhead view. Both display longitudinal strain.

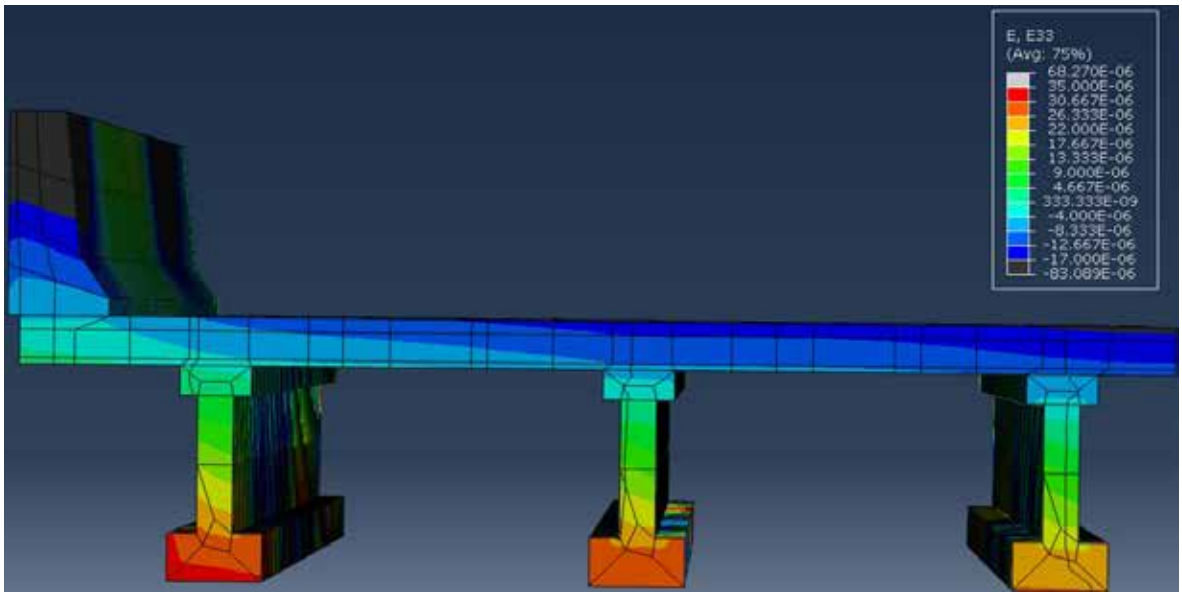

Figure 62. Longitudinal strain section view at middle of bridge.

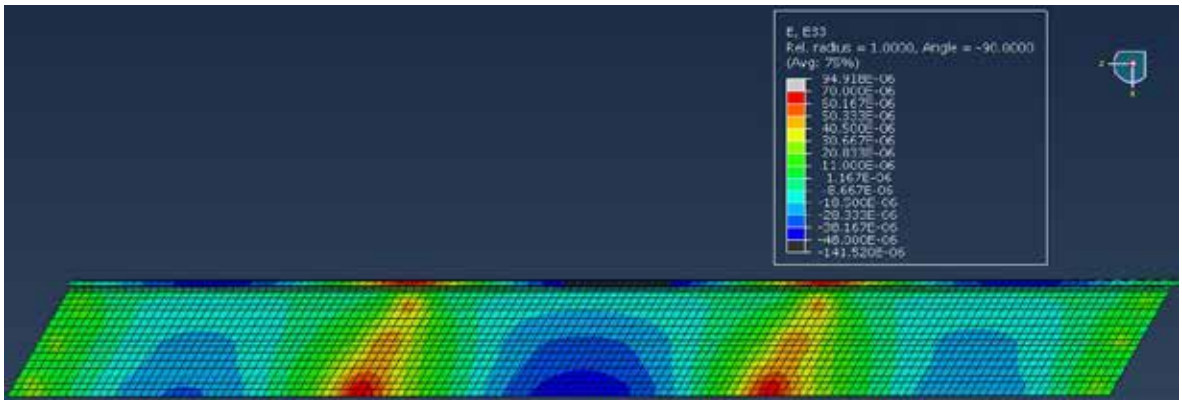

Figure 63. Longitudinal strain overhead view.

7.2.2 Mesh Size and Deck Partitioning

The experimental model had an enormous variety of mesh sizes. They ranged from a cubic inch to about a cubic foot. This was mostly due to the rebar spacing and the restrictions of SAP2000. Luckily, Abaqus provided much more leeway in its meshing parameters and a more uniform spacing could be chosen. Owing to the immense size of the full-scale model, a mesh spacing of 10 in. was chosen for the concrete. Accordingly, the girders, deck, and parapet were all meshed using roughly 10 x10 x10-in. solid elements. This mesh spacing, though, was strategically broken up at the locations on the top and bottom rebar, as well as at the connection sites for the parapet and girders. This configuration ensured that the rebar was appropriately embedded within the deck and that the girders and parapet were well connected to the slab.

After the mesh was completed, the size of the deck partitions had to be determined. These partitions would break up the top concrete, middle concrete, and bottom concrete, which refer to the top 2.25 in. of concrete, middle 4.75 in. of concrete, and bottom inch of

concrete, respectively. To correspond to the experimental model, similar section sizes were used. There are two types of sections: the sections located above the girders and those located in the center spans. Because the experimental model used c-channels around the outside to simulate continuity, the shrinkage loading within each section was expected to translate fairly well to the full-scale model. To mimic the experimental model, each layer of the deck was first split into sections, as shown in Figure 64 (because the locations are the same for the top, middle, and bottom layers, only one figure is provided). Each section corresponds to a section in the experimental model and had the same temperature load applied as those used the trial decks.

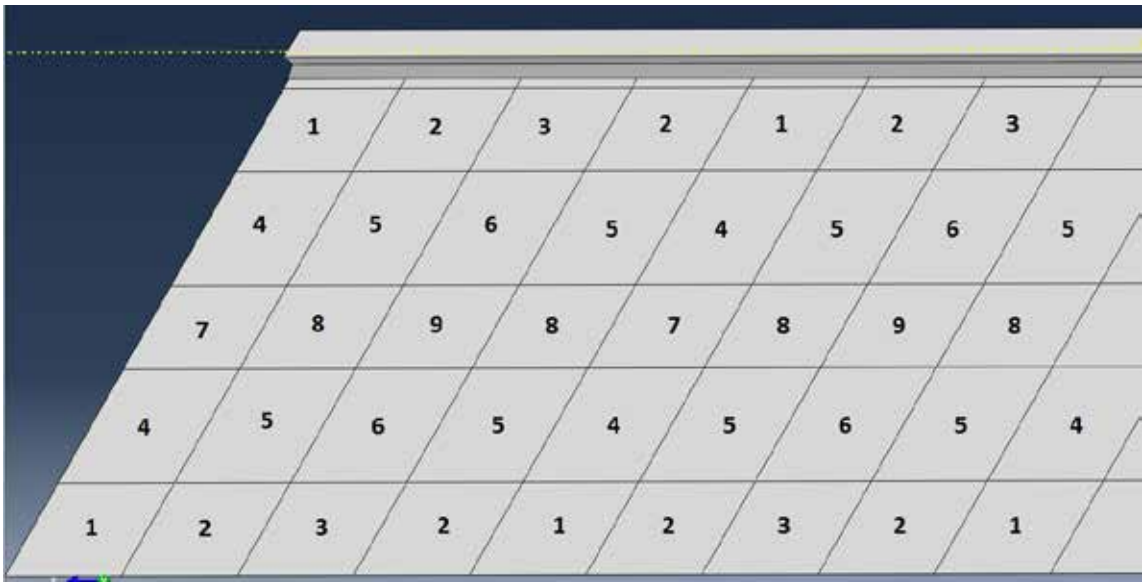

Figure 64. Full-scale model section location and numbering.

7.2.3 Sources of Error

Even though many safeguards were implemented to decrease error when transferring results from the experimental model to the full-scale model, it is unwise to blindly forge ahead based on these results. Some possible sources of error were unavoidable, the most important being the difference in dimension between the experimental model and the full-scale model. Shrinkage in a bridge deck is highly unpredictable because of the non-homogenous nature of concrete. Although the experimental model was designed to simulate discontinuity and it was scaled up appropriately, it still could not precisely predict how the shrinkage in the rest of the bridge would pull on each 10 x 7-ft portion and how they all interacted.

Our results from the experimental portion of this research can still be used to assess the strength of a given mix design, as well as to determine the general trend of the strains that will be found within a full-scale bridge deck, but the chain-reaction aspect of the shrinkage strain is not yet well understood. Finally, the idealization of non-shrinking girders, along with the difference between the steel girders used in the experimental model and the concrete girders used in the full-scale model, cannot be overlooked.

Even with these sources of error, the predictive power of the full-scale model cannot be ignored. It provides a look at an incredibly erratic material. Though the full-scale model

might not be completely accurate, it should offer engineers improved knowledge about the future shrinkage strains expected within this and other bridge decks and ways to reduce or counteract them.

CHAPTER 8 CONCLUSIONS

The main conclusions of this study are as follows:

- The use of Type K and Type G in plain concrete can effectively compensate for drying shrinkage. The 15% replacement of Type K and 6% addition of Type G in portland cement concrete resulted in minimal shrinkage strain after 100 days.
- The Class F fly ash increased the restrained expansion of Type K concrete, whereas silica fume resulted in a decrease in the extent of expansion. Similar behavior was observed for the unrestrained expansion of Type K cement pastes. In the case of Type G cement pastes/concretes, both the Class C fly ash and Class F fly ash increased expansion, whereas no significant difference was noticed for silica fume.
- The behavior of Class C fly ash in Type K concrete was found to be only slightly different than its behavior in the pastes. In Type K concrete, the Class C fly ash resulted in higher expansion than plain concrete. In both cases, studies highlighted that the expansion stops earlier in Class C fly ash–based mixes.
- Expansion characteristics in the presence of mineral admixtures could be explained based on the difference in material resistance. For example, the Class F fly ash seems to have reduced the material resistance (hence, increased expansion), whereas silica fume increased the material resistance to deformation (thereby decreasing expansion). The difference in material resistance was also evident from the 28-day compressive strength results of Type K and Type G concretes.
- The slump loss is rapid in Type K concrete; hence, it should be taken into account when calculating transportation time. However, Type G concrete did not exhibit any significant slump loss.
- The extent of expansion was reduced with enhanced mixing time in Type K concrete, which is also important in transporting the concrete to the job site.
- According to ASTM C878, the use of retarder did not show much difference in the level of expansion of Type K and Type G concretes. However, the delay in setting time must be taken into account when retarder is used because it is expected to influence the expansion. The use of ASTM C878 does not account for the delay in setting caused by the retarder. Also, a higher dosage of retarder may affect the expansion and therefore should be investigated in the future.
- The total heat of hydration of Type K-based cement was lower than that of the portland cement, whereas Type G-based cement had a similar amount of heat release after 72 hours.
- The Type G component does not seem to increase the potential for alkali–silica reaction. Total alkalis were reduced in the presence of Type G. In addition, the beneficial effect of using Class C fly ash was observed at later ages.
- Compressive strengths of Type K and Type G concretes after 28 days were found to be similar or higher than the compressive strengths of plain concrete. Addition of Class F fly ash and Class C fly ash resulted in lower 28-day strength of Type K concrete. However, silica fume increased the 28-day strength of Type

K and Type G concretes. For both the Type K and Type G concretes at w/cm 0.44, 28-day compressive strength was found to be higher than 4000 psi.

- The effectiveness of SRAs in reducing the shrinkage cracking was verified. The use of an SRA can significantly lower the vulnerability of concrete to cracking. However, high dosage of an SRA seems to reduce the compressive strength of concrete.
- The strain monitoring of the bridge deck model without and with Type K highlighted the reduction in tensile strain on the order of 40 to 50 microstrains at early-age. Also the resulting strain due to cracking caused by the release of the stored tensile stress in concrete was smaller for Type K deck.
- Linking the small-scale test results with large-scale test results, it was observed that the excess shrinkage potential due to the higher restraint against movement in the large-scale model was reduced in the Type K deck which is hypothesized to reduce stored tensile stress in concrete. Further research is necessary to understand completely how small-scale tests relate to the large-scale tests.
- The experimental decks could be effectively modeled using finite element analysis, making it possible to model the shrinkage strains associated with both Type K and plain concrete. By using the finite element model, it was determined that girder temperature loads seem to have little effect on strain in the deck until a differential of 30°F is reached. To ensure the validity of these claims, a future study can be conducted using the full-bridge model instead of just the laboratory model.
- Applying results from the experimental models to a full-scale bridge model provides greater insight into the strains found within a real-world bridge deck and could help predict future shrinkage strains when modeled accurately.

REFERENCES

ACI 223-R. *Guide for the Use of Shrinkage-Compensating Concrete*. 2010. American Concrete Institute. Farmington Hills. MI. 5 pp.

Aitcin, P. 2003. "The Durability Characteristics of High Performance Concrete: A Review." *Cement and Concrete Composites* 25(4-5):409-420.

Aktas, K., H. Nassif, and H. Najim. 2007(Dec.). *"Concrete Shrinkage Analysis for Bridge Deck Concrete."* Technical Report FHWA-NJ-2007-007. New Jersey Department of Transportation.

Ali, M. M., Shri Gopal, and S. K. Handoo. 1994. "Studies on the Formation Kinetics of Calcium Sulphoaluminate." *Cement and Concrete Research* 24 (4): 715-720.

Altoubat, S. A. and D. A. Lange. 2001. "Creep, Shrinkage, and Cracking in Restrained Concrete at Early Age." *ACI Materials Journal* 98(4):323-331.

Andac, O. and F. P. Glasser. 1995. "Microstructure and Microchemistry of Calcium Sulfoaluminate Cement." *Materials Research Society*, 1994.

Babaei, K., and R. L. Purvis. 1995(Nov.) *"Prevention of Cracks in Concrete Bridge Decks: Report on Laboratory Investigations of Concrete Shrinkage."* Wilbur Smith Associates Report. Pennsylvania Department of Transportation. Project No. 89-01.

Barneyback Jr., R. S. and Sidney Diamond. 1981. "Expression and Analysis of Pore Fluids from Hardened Cement Pastes and Mortars." *Cement and Concrete Research* 11 (2): 279-285.

Bentur, A. and M. Ish-Shalom. 1974. "Properties of Type K Expansive Cement of Pure Components--2. Proposed Mechanism of Ettringite Formation and Expansion in Unrestrained Paste of Pure Expansive Component." *Cement and Concrete Research* 4 (5): 709-721.

Bentz, D. P., K. H. Hansen, and M. R. Geiker. 2001b. "Shrinkage-Reducing Admixtures and Early Age Desiccation in Cement Pastes and Mortars." *Cement and Concrete Research* 31(7):1075-1085.

Bentz, Dale P., Ole Mejlhede Jensen, Kurt Kielsgaard Hansen, John F. Olesen, Henrik Stang, and Claus-Jochen Haecker. 2001. "Influence of Cement Particle-Size Distribution on Early Age Autogenous Strains and Stresses in Cement-Based Materials." *Journal of the American Ceramic Society* 84 (1): 129-135.

Beretka, J., M. Marroccoli, N. Sherman, and G. L. Valenti. 1996. "Influence of C_4A_3S Content and W/S Ratio on the Performance of Calcium Sulfoaluminate-Based Cements." *Cement and Concrete Research* 26 (11): 1673-1681.

Bloom, Ronit and Arnon Bentur. 1995. "Free and Restrained Shrinkage of Normal and High-Strength Concretes." *ACI Materials Journal* 92 (2): 211-217.

Brown, M. D., C. A. Smith, J. G. Sellers, K. J. Folliard, and J. E. Breen. 2007. "Use of Alternative Materials to Reduce Shrinkage Cracking in Bridge Decks." *ACI Materials Journal* 104(6): 629-637.

Chatterji, S. 1995. "Mechanism of Expansion of Concrete due to the Presence of Dead-Burnt CaO and MgO." *Cement and Concrete Research* 25 (1): 51-56.

Chen, Irvin A., Craig W. Hargis, and Maria C. G. Juenger. 2012. "Understanding Expansion in Calcium Sulfoaluminate-Belite Cements." *Cement and Concrete Research* 42 (1): 51-60.

Cohen, M. D. and C. W. Richards. 1982. "Effects of the Particle Sizes of Expansive Clinker on Strength-Expansion Characteristics of Type K Expansive Cements." *Cement and Concrete Research* 12 (6): 717-725.

Collepardi, M. R., M. R. Turriziani, and A. Marcialis. 1972. "Paste Hydration of 4Ca0.3Al2O3.SO3 in Presence of Calcium Sulphate, Tricalcium Silicate and Dicalcium Silicate." *Cement and Concrete Research* 2 (2): 213-223.

Deshpande, S., D. Darwin, and J. Browning. 2007 (Jan.). *"Evaluating Free Shrinkage of Concrete for Control of Cracking in Bridge Decks."* SM Report No. 89. University of Kansas. Lawrence. Kansas.

El Hindy, Elie, Buquan Miao, Omar Chaallal, and Pierre-Claude Aitcin. 1994. "Drying Shrinkage of Ready-Mixed High-Performance Concrete." *ACI Materials Journal* 91 (3): 300-305.

Eppers, L. J., C. W. French, and J. F. Hajjar. 1998 (July). *Transverse Cracking in Bridge Decks: Field Study.* Minnesota Department of Transportation. Final Report.

Folliard, K., C. Smith, G. Sellers, M. Brown, and J. E. Breen. 2003 (Oct.). *"Evaluation of Alternative Materials to Control Drying-Shrinkage Cracking in Concrete Bridge Decks."* Texas DOT Report No. FHWA/TX-04/04098-4.

Folliard, Kevin J., Makoto Ohta, Ellen Rathje, and Patrick Collins. 1994. "Influence of Mineral Admixtures on Expansive Cement Mortars." *Cement and Concrete Research* 24 (3): 424-432.

French, C. W., L. J. Eppers, Q. Le, and J. F. Hajjar. 1999a. "Transverse Cracking in Concrete Bridge Deck." *Transportation Research Record* 1688:1-29.

French, C. W., L. J. Eppers, Q. Le, and J. F. Hajjar. 1999b (Jan.). *Transverse Cracks in Bridge Decks.* Report No. MN/RC-1999-05. Minnesota Department of Transportation. St. Paul. Minnesota. 37 pp.

Gulyas, R. J., K. A. McCabe, and J. A. Katlin. 2008. High Performance Bridge Deck: Use of ASTM C 845 Type K Shrinkage Compensating Cement with Lightweight Aggregate for Optimized Internal Curing, Excellent Durability, and Performance Benefits. In *2008 Concrete Bridge Conference*.

Holt, Erika. 2005. "Contribution of Mixture Design to Chemical and Autogenous Shrinkage of Concrete at Early Ages." *Cement and Concrete Research* 35 (3): 464-472.

Jensen, O. M., and P. F. Hansen. 1996. "Autogenous Deformation and Change of Relative Humidity in Silica Fume Modified Cement Paste." *ACI Materials Journal* 93(6):539-543.

Justnes, H., B. Ardoullie, E. Hendrix, E. J. Sellevold, and D. V. Gemert. 1998. "The Chemical Shrinkage of Pozzolanic Reaction Products," pp. 191-205 *Fourth CANMET/ACI/JCI Conference: Advances in Concrete Technology*. SP-179. American Concrete Institute.

Kalousek, G. L., and E. J. Benton. 1970. "Mechanism of Seawater Attack on Cement Pastes." *ACI Journal* 67 (2): 187-192.

Kasselouri, V., P. Tsakiridis, C. Malami, B. Georgali, and C. Alexandridou. 1995. "Study on the Hydration Products of a Non-Expansive Sulfoaluminate Cement." *Cement and Concrete Research* 25 (8): 1726-1736.

Lange, D. A., J. R. Roesler, M. D. D'Ambrosia, Z. C. Grasley, C. J. Lee and D. R. Cowen. 2003(July). *"High Performance Concrete for Transportation Structures,"* Final Report. Illinois Cooperative Highway Research Program.

Lawler, J., P. Krauss, and C. Abernathy. 2006. "HPC Mixture Development for Montana Using Local Material." *HPC Bridge Views*. 43. 4 pp.

Le, Q., C. W. French, and J. F. Hajjar. 1998 (July). *"Transverse Cracking in Bridge Decks: Parametric Study."* Minnesota Department of Transportation. Final Report.

Lefchik, T. E. 1994 (Dec.). *"Performance of Bridge Decks in Ohio."* The Ohio DOT Report.

Lobo, Colin and Menashi D. Cohen. 1992. "Effects of Silica Fume on Expansion Characteristics of Expansive Cement Pastes." *ACI Materials Journal* 89 (5): 481-491.

Mehta, P. K. 1973. "Effect of Lime on Hydration of Pastes Containing Gypsum and Calcium Aluminates Or Calcium Sulfoaluminate." *Journal of the American Ceramic Society* 56 (6): 315-319.

Mehta, P. K., and Faichung Hu. 1978. "Further Evidence for Expansion of Ettringite by Water Adsorption." *Journal of the American Ceramic Society* 61 (3-4): 179-181.

Naik, T. R., Y.-M. Chun, and R. N. Kraus. 2006. *"Reducing Shrinkage Cracking of Structural Concrete Through the Use of Admixtures."* Report No. WHRP 06-08. Department of Civil Engineering and Mechanics. University of Wisconsin at Milwaukee, Milwaukee, Wisconsin.

Polivka, M. 1973."Factors Influencing Expansion of Expansive Cement Concretes." *Klein Symposium on Expansive Cement Concretes*. ACI SP-38: 239-250.

Russell, H. G., R. A. Stadler, and H. G. Gelhardt III. 2002 (Aug.). "Shrinkage-Compensating Concrete Made with an Expansive Component." *Concrete International* 24(8):107-111.

Sant, G., F. Rajabipour, P. Lura, and J. Weiss. 2007. "Volume Changes in Pastes Containing Shrinkage Reducing Admixtures under Autogenous and Drying Conditions." *Proceedings of the 12th International Congress on the Chemistry of Cement*. Montreal, Canada.

Setter, N. and D. M. Roy. 1978. "Mechanical Features of Chemical Shrinkage of Cement Paste." *Cement and Concrete Research* 8 (5): 623-634.

Shing, P. B., and N. Abu-Hejleh. 1999 (Aug.).*"Cracking in Bridge Decks: Causes and Mitigation"* Report No. CDOT-DTD-R-99-8. Colorado Department of Transportation.

Streeter, D. A. 1996. "Developing High-Performance Concrete Mix for New York State Bridge Decks." *Transportation Research Record*. 1532: 60-65.

Subramaniam, K. V., R. Gromotka, S. P. Shah, K. Obla, and R. Hill, R. 2005. "Influence of Ultrafine Fly Ash on the Early Age Response and the Shrinkage Cracking Potential of Concrete." *Journal of Materials in Civil Engineering*. ASCE. 17(1):45-53.

Subramaniam, K., and A. K. Agrawal. 2009 (Jan.). *"Concrete Deck Material Properties."* Final Report. SPR Project C-02-03. New York State Department of Transportation.

Tazawa, E., and S. Miyazawa. 1995. "Influence of Cement and Admixture on Autogenous Shrinkage of Hydrating Cement Paste." *Cement and Concrete Research* 25(2):288-292.

Weiss, W. J. 1999. *Prediction of Early-Age Shrinkage Cracking in Concrete Elements.* PhD thesis. Northwestern University, Evanston, IL.

Whiting, D. A., R. J. Detwiler, and E. S. Lagergren. 2000. "Cracking Tendency and Drying Shrinkage of Silica Fume Concrete for Bridge Deck Applications." *ACI Materials Journal*. 97(1): 71-78.

APPENDIX A MATERIALS AND METHODS

A.1 RAW MATERIALS

Table A.1 shows the phase composition (Bogue Composition) of Type I portland cement from 12 different sources. After preliminary investigation, Type I portland cement from Continental Hannibal was selected for further investigation. The Bogue's phase composition of portland cement (Continental Hannibal) included 57.82% C_3S, 16.38% C_2S, 7.20% C_3A, 8.26% C_4AF, 2.44 % SO_3 and 0.52% Na_2O_{eq}.

Table A.1. Phase Composition of Type I Cement from Different Sources

Cement Source	C_3S (%)	C_2S(%)	C_3A(%)	C_4AF(%)	Na_2O_{eq}(%)	Fineness
Lafarge Alpena (LFA)	63.88	10.49	7.43	8.33	0.57	394
Buzzi Cape Girade (BUCG)	58.55	14.52	6.8	9.26	0.52	393
Cemex Kosmosdale (CEK)	54.70	18.40	6.44	10.00	0.68	387
St. Mary Charlevoix (SMC)	55.57	15.41	7.85	9.04	0.93	400
Lafarge Joppa (LFJ)	60.34	12.62	6.86	9.33	0.54	408
Buzzi Festus (BUF)	55.31	16.94	7.06	9.90	0.48	376
Holcim Bloomsdale (HOB)	66.04	7.18	6.64	9.55	0.51	390
Lehigh Mitchell (LHM)	53.38	18.79	7.23	9.70	0.7	401
Lafarge Davenport (LFD)	58.00	15.00	6.00	10.00	0.48	407
Illinois LaSalle (ILC)	61.35	8.90	10.13	6.52	0.98	388
Continental Hannibal (COH)	57.82	16.38	7.20	8.26	0.52	398
Buzzi Greencastle (BUG)	62.74	7.50	8.68	9.05	0.89	371

Table A.2 presents the typical chemical composition of various raw materials utilized in the current study. A calcium sulfoaluminate (or CSA) based expansive component or Type K (sold as Komponent by CTS Company) and calcium oxide-based expansive component or Type G (sold as Conex by Euclid Chemical Co.) were utilized along with portland cement and three other mineral admixtures: Class C fly ash, Class F fly ash and silica fume. The phase composition of Komponent consisted of $C_4A_3\hat{S}$ (ye'elimite), $CaSO_4$, C_2S and C_4AF whereas Conex contained CaO, fly ash and portland cement.

Table A.2. Chemical Composition of Raw Materials

Oxide Composition	OPC*	Komponent	Conex	F FA	C FA	SF
SiO_2	20.93	7.70	12.61	59.08	37.76	93.0
Al_2O_3	4.45	7.00	5.68	22.43	19.43	0.7
Fe_2O_3	2.72	1.17	1.87	8.39	5.33	0.5
CaO	63.28	50.07	62.61	1.59	25.56	0.7
MgO	3.03	0.08	0.92	1.06	4.09	0.7
SO_3	2.44	26.04	—	0.20	2.23	—
Na_2O	0.13	—	—	0.64	1.07	0.4
K_2O	0.59	—	—	2.18	—	0.9
Na_2O_{eq}	0.52	0.56	0.89	2.07	1.07	1.00
LOI	1.98	2.10	—	2.99	0.58	6.0

*OPC - Continental Hannibal

A.2. CONCRETE MIXTURE PROPORTIONING

Tables A.3 and A.4 show the proportions of various concrete mixtures used in this study. The mix design procedure followed by IDOT was used to design the concrete mixtures. Table A.3 shows mixture proportions of concrete without any mineral admixtures whereas Table A.4 presents the mixture proportions of concrete incorporating mineral admixtures like Class C fly ash, Class F fly ash and silica fume. The replacement level (by mass) for Class C fly ash, F fly ash and silica fume was 15%, 15% and 5% of total cementitious material, respectively. The base concrete mix was finalized as the one with cement factor of 610, mortar factor of 0.86, and w/cm ratio of 0.44. Type K concrete was prepared at two w/cm ratios (0.44 and 0.5), and for Type G concrete, two dosages of Conex (4.5% and 6%) were examined. The cement factor of 610 lb/yd^3 is higher than the minimum requirement for Class BS concrete according to IDOT specification. Fine aggregate (FA 1) and coarse aggregates (CA7) confirming to IDOT specification were utilized in concrete proportioning. Air entraining admixture (Micro Air, BASF) was used to entrain air in the range of 4-7%. For preliminary examination of the influence of retarder, Delvo Stabilizer (BASF) was used at its recommended dosage. In this study, Tetraguard (BASF) was also utilized as a shrinkage-reducing admixture. Table A.5 presents the proportion of three different control mixtures with varying cement and mortar factor.

Table A.3. Mixture Proportions of Plain, Type K and Type G Concrete Without Mineral Admixtures

	Plain	OPC+K (0.44)	OPC+ K (0.5)	OPC+G (G-4.5%)	OPC+G (G-6%)
Water*	268	268	305	268	268
OPC*	610	518.5	518.5	583.7	575.5
Komponent*	0	91.5	91.5	0	0
Conex*	0	0	0	26.3	34.5
Fine Agg*(SSD)	1130	1130	1033	1130	1130
Coarse Agg*(SSD)	1826	1826	1826	1826	1826
w/cm	0.44	0.44	0.5	0.44	0.44
AEA (fl oz/cwt)**	2	3.2	2	2.0	1.5
Slump (in)	3.5	3.0	4	4.5	6
Air Content (%)	5.5	6.2	6	4.5	5.5

* Quantities are in lb/yd3 (1 lb/yd^3 = 0.59 Kg/m^3)
** AEA – Micro Air (BASF)

Table A.4. Mixture Proportions of Type K and Type G Concrete Containing Mineral Admixtures

	OPC+K+ F FA	OPC+K+ C FA	OPC+K+ SF	OPC+G+ F FA	OPC+G+ C FA	OPC+G+ SF
Water*	268	268	268	268	268	268
OPC*	427	427	488	546.7	489.2	546.7
F FA*	91.5	0	0	28.8	0	0
C FA*	0	91.5	0	0	86.3	0
SF*	0	0	30.5	0	0	28.8
Komponent*	91.5	91.5	91.5	0	0	0
Conex*	0	0	0	34.5	34.5	34.5
Fine Agg*(SSD)	1130	1130	1130	1130	1130	1130
Coarse Agg*(SSD)	1826	1826	1826	1826	1826	1826
w/cm	0.44	0.44	0.44	0.44	0.44	0.44
AEA (fl oz/cwt)**	4.1	4.3	3.7	2.2	2.5	2.2
Slump (in)	4	6.5	2	6	8.5	3.5
Air Content (%)	4.2	6.6	4.7	5	5.7	6.5

* Quantities are in lb/yd3 (1 lb/yd^3 = 0.59 Kg/m^3)
** AEA – Micro Air (BASF)

Table A.5. Mixture Proportions of Concrete Mixtures with Varying Cement and Mortar Factors

	Control	Mix-I	Mix-II
Water*	268	268	277
OPC*	610	610	630
Fine Agg*(SSD)	1130	1081	1042
Coarse Agg*(SSD)	1826	1875	1875
w/cm	0.44	0.44	0.44
AEA (fl oz/cwt)**	2.0	2.39	2.02
Slump (in)	3.5	3.5	6.0
Air Content (%)	5.5	4.5	4.5
CA/FA	1.62	1.73	1.80
Mortar Factor	0.86	0.82	0.82

* Quantities are in lb/yd3 (1 lb/yd^3 = 0.59 Kg/m^3)
** AEA – Micro Air (BASF)

A.3 TEST METHODS

A.3.1 Mixing Procedure

The paste/mortar samples were mixed according to ASTM C305 in a Hobart mixture. The mixing procedure for concrete complied with ASTM C192. The coarse and fine aggregate were initially dried in an oven and subsequently cooled before using in concrete. The amount of water to reach the saturated surface dry condition for aggregates was added separately to the mixing water. The oven dry condition of aggregates was adopted to reduce the variation due to subjectivity of SSD test.

A.3.2 Fresh Properties

Slump and air content of freshly made concrete was determined according to ASTM C143 and 231 respectively. The target air content ranged from 4 -7%.

A.3.3 Restrained Expansion of Type K and Type G Concrete

Restrained expansion of expansive concrete was monitored according to ASTM C878.The concrete samples of size 3 in. (75 mm) x 3 in. (75 mm) x 10 in. (254 mm) were prepared and cast in a mold shown in Figure A.1. The steel rod placed at the center with attached end plates provides a restraint for the concrete. The samples were demolded after 6 hours, and immersed in saturated lime water for a period of 7 days. Length measurements were taken after 6 hours (demolding time) and after 7 days of saturated lime water curing as per the code. Intermediate length measurements were often taken to get more information regarding the rate of expansion. The 7-day expansion value provides useful information as it can be related to the maximum expansion experienced by a structural member in the field [ACI 223-R 2010]. The test procedure was further modified to understand the drying behavior of expansive concrete. Hence, the concrete prisms were exposed to a drying environment of 23±2^{o}C and 50% RH after the saturated lime water curing for 7 days. The

length measurements were taken at regular intervals after exposing concrete samples to drying.

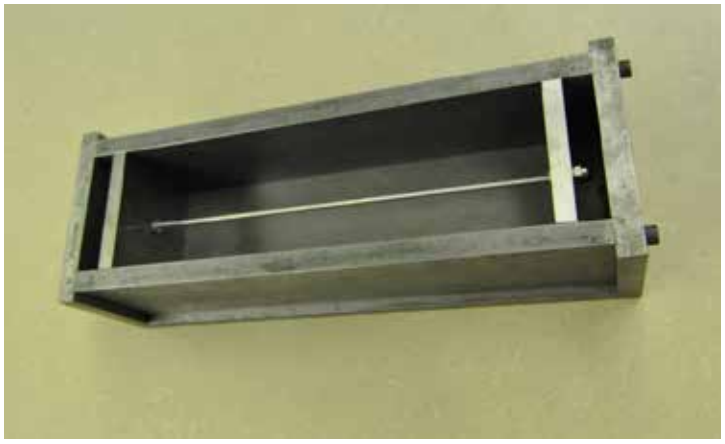

Figure A.1. A typical mold for restrained expansion according to ASTM C878.

A.3.4 Unrestrained (Free) Expansion of Type K and Type G Cement Paste

To study the rate of expansion more carefully at the early-age (within 24 hours), the unrestrained (free) expansion of cement paste was measured following ASTM C1698. The paste was prepared according to ASTM C305. Then, the paste was encapsulated in corrugated polyethylene tube according to ASTM C1698 (Figure A.2). This test method allows monitoring the linear deformation by providing increased restraint against lateral deformation and minimizing the restraint of the fresh paste in the linear direction only. The length measurements were started after final set (as determined by Vicat needle test according to ASTM C191).

Figure A.2. A dilatometer for monitoring the unrestrained deformation of cement pastes according to ASTM C1698.

A.3.5 Compressive Strength

Compressive strength of 4 in. (100 mm) x 8 in. (200 mm) cylinders was determined after 28 days of moist curing according to ASTM C39.

A.3.6 Drying Shrinkage of Mortar and Plain Concrete

The drying shrinkage of mortars containing portland cement and graded sand were monitored using ASTM C596 (Figure A.3). For this test, 1 in. (25 mm) x 1 in. (25 mm) x 11¼ in. (285 mm) mortar prisms using standard Ottawa sand were prepared, and cured for 3 days in moist environment before starting the shrinkage measurements. Free shrinkage was measured at constant temperature (22 ± 2^{o}C), and constant relative humidity (50 ± 4%).

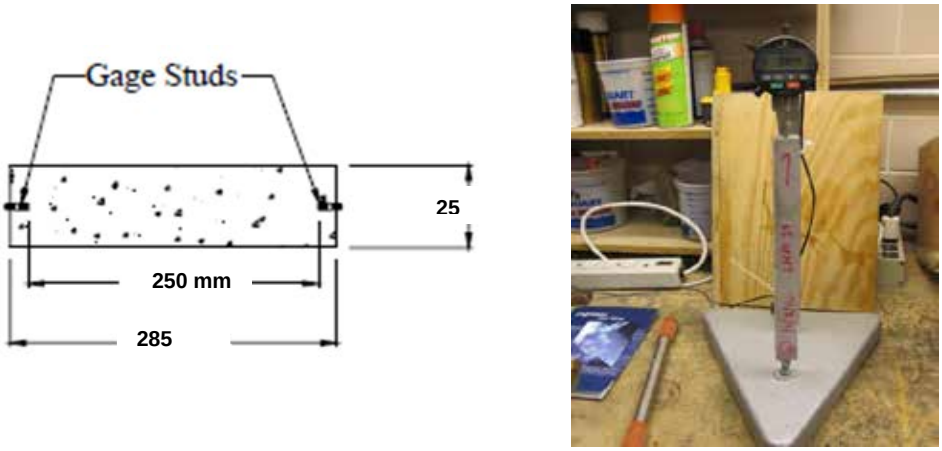

Figure A.3.Typical mortar sample and digital length comparator for free shrinkage measurement.

The free drying shrinkage of plain concrete (without any expansive component) was determined using ASTM C157. Samples of size 3 in. (75 mm) x 3 in. (75 mm) x 11 ¼ in. (285 mm) were prepared, and cured in sealed environment for 24 hours. Afterwards the samples were demolded and cured in saturated limewater for 7 days before exposing them to constant temperature (22 ± 2^{o}C) and relative humidity (50 ± 4%). The length measurements were carried out intermittently over the period of time.

A.3.7 RING TEST

The restrained shrinkage of plain concrete was determined using ASTM C1581. Figure A.4(a) shows the schematic of this test method. The concrete is cast around a steel ring on which four strain gages (placed on mid height) are mounted on diametrically opposite locations. Steel ring provides the restraint for the concrete when it shrinks during drying. Figure A.4(b) shows the data acquisition system and test setup used for the ring test.

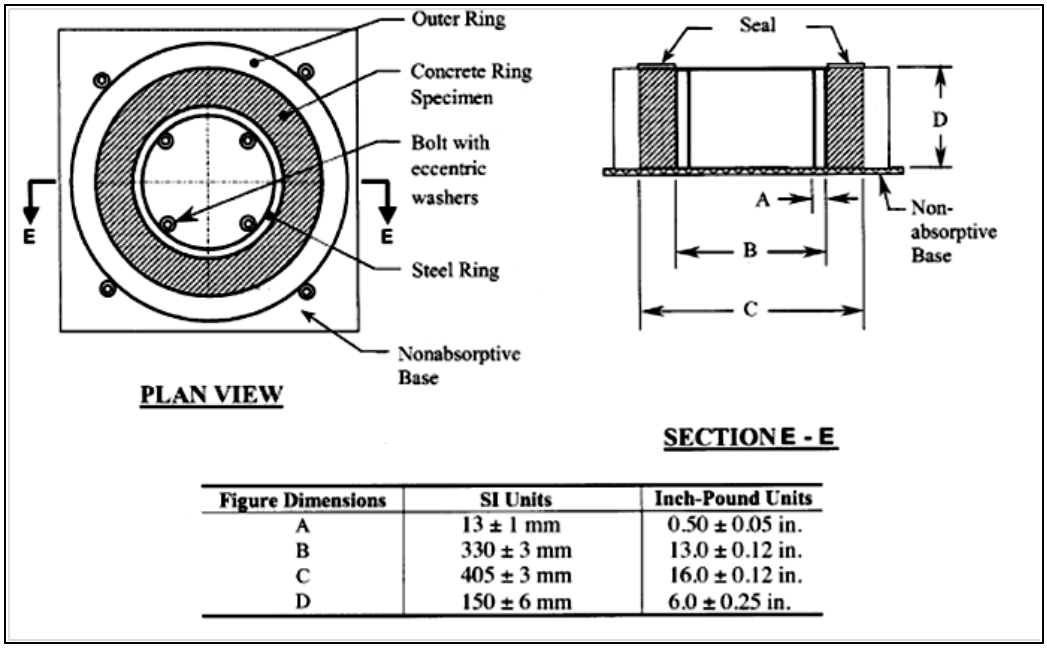

Figure Dimensions	SI Units	Inch-Pound Units
A	13 ± 1 mm	0.50 ± 0.05 in.
B	330 ± 3 mm	13.0 ± 0.12 in.
C	405 ± 3 mm	16.0 ± 0.12 in.
D	150 ± 6 mm	6.0 ± 0.25 in.

(a)

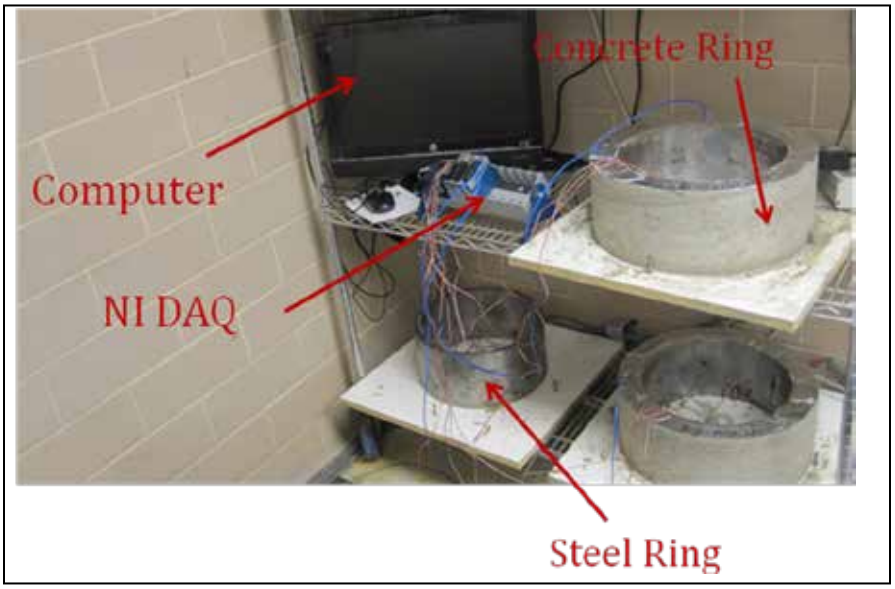

(b)

Figure A.4. (a) Schematic showing the ring setup according to ASTM C1581, and (b) photograph showing the data acquisition system in the laboratory.

A.3.8 Heat of Hydration

Isothermal conduction calorimeter (TAM Air, TA Instruments) was used to monitor the heat evolution of expansive cements. The cement pastes were externally mixed for a period of 2 minutes before inserting them in the respective channels. It is noted that the data for the first 45 minutes was not considered for analysis in order to avoid the heat associated with mixing and placing the externally prepared cement paste samples and allow it to stabilize with the set temperature of 22^0C.

A.3.9 Alkali-Silica Reaction

The role of Type G component in alkali-silica reaction was investigated using ASTM C227 test method and pore solution analysis. ASTM C227, a mortar-bar test method, is used for evaluating the cement-aggregate combination with regard to alkali-silica reaction. Figure A.5 shows the test set up used for ASTM C227. The goal of the investigation was to examine the influence of Type G (source of calcium hydroxide crystals) on the expansion due to ASR. To expedite the ASR process, reactive sand (supplied by IDOT) was used in ASTM C227 test. It is expected that the ASR might occur, as the reactive aggregates were used. The difference in expansion levels is believed to shed the light on the influence of Type G in the expansion due to ASR. The test method ASTM C1293 (concrete-prism test) is intended to evaluate the reactivity of an aggregate. In this test method, alkali content is enhanced to expedite the alkali-silica reaction. As the goal of current study was not to check the reactivity of aggregate, ASTM C227 was used to investigate the influence of Type G on the expansion process.

Figure A.5. Test set up used for ASTM C227 to investigate ASR.

Since the alkalis play important role in triggering the alkali-silica reaction in concrete, the concentration of alkalis in pore solution can provide useful information. In order to extract the pore solution, the extraction device (Barneyback and Diamond 1981) was utilized, as shown in Figure A.6.

(a) (b)

Figure A.6. (a) and (b) Photographs showing pore solution extraction device.

APPENDIX B TYPE K AND CONTROL DECK STRAIN GAGE RESULTS

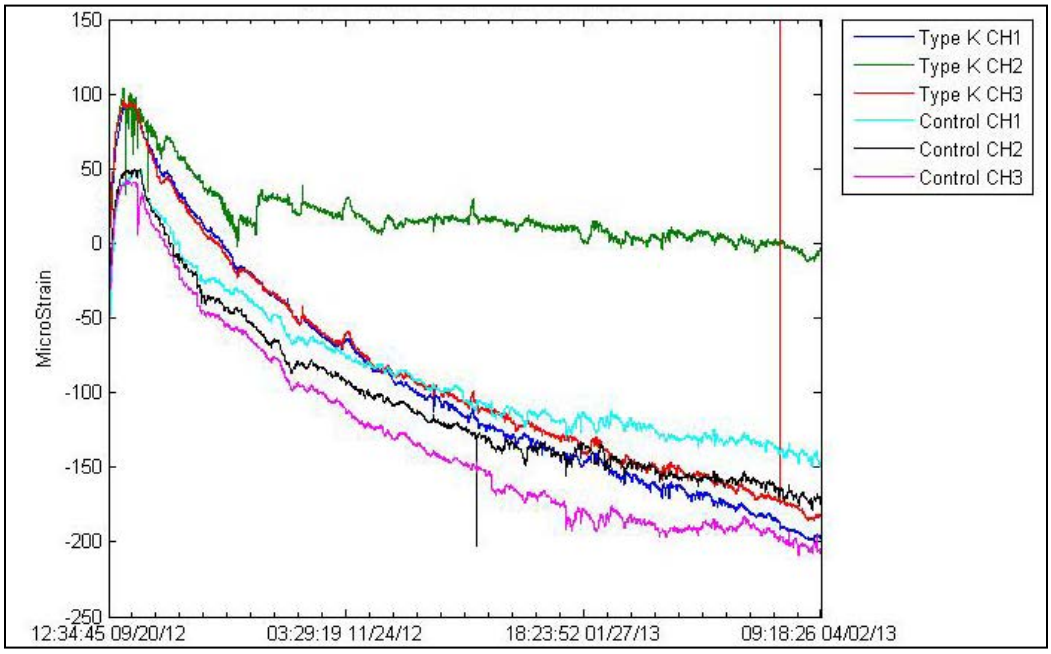

Figure B.1. Top longitudinal Type K and control strain gages.

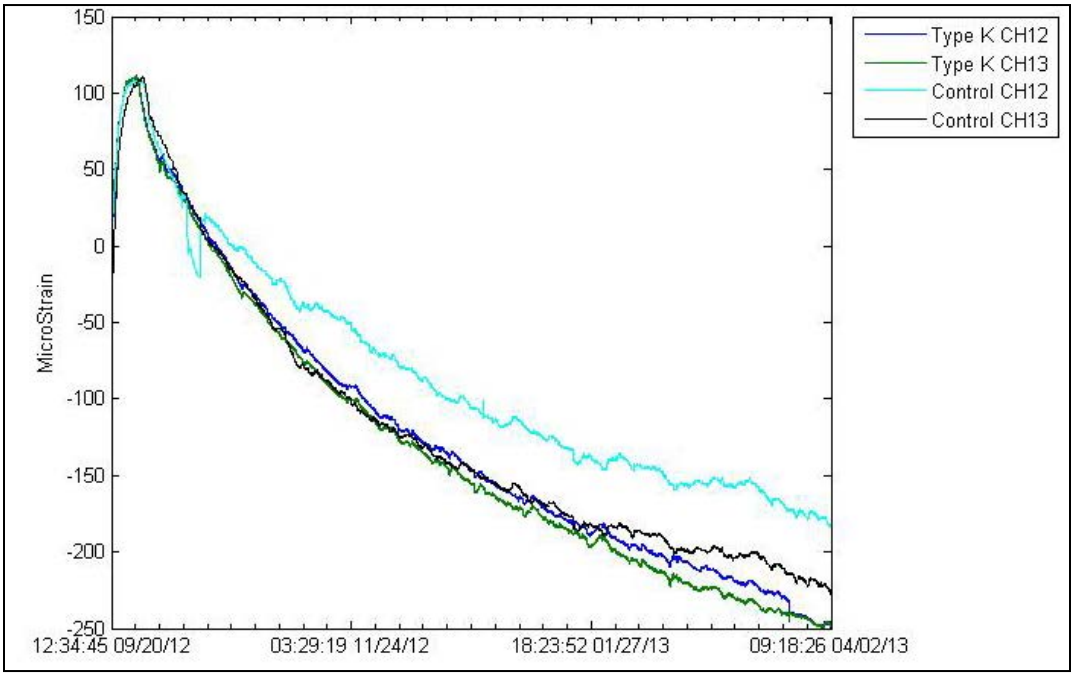

Figure B.2. Top transverse Type K and control strain gages.

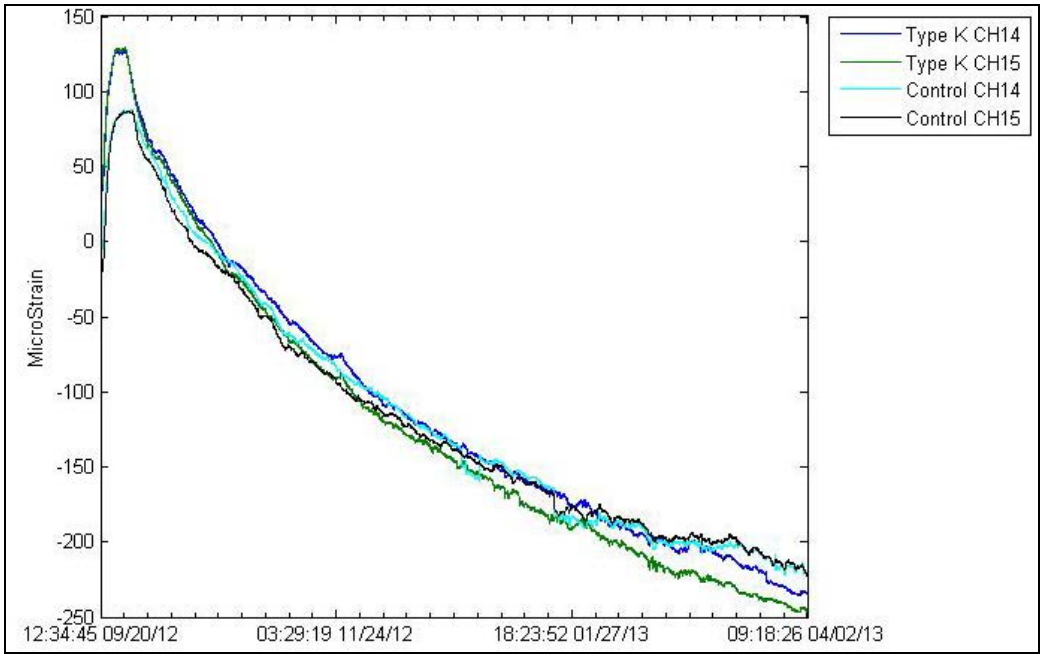

Figure B.3. Top transverse Type K and control strain gages.

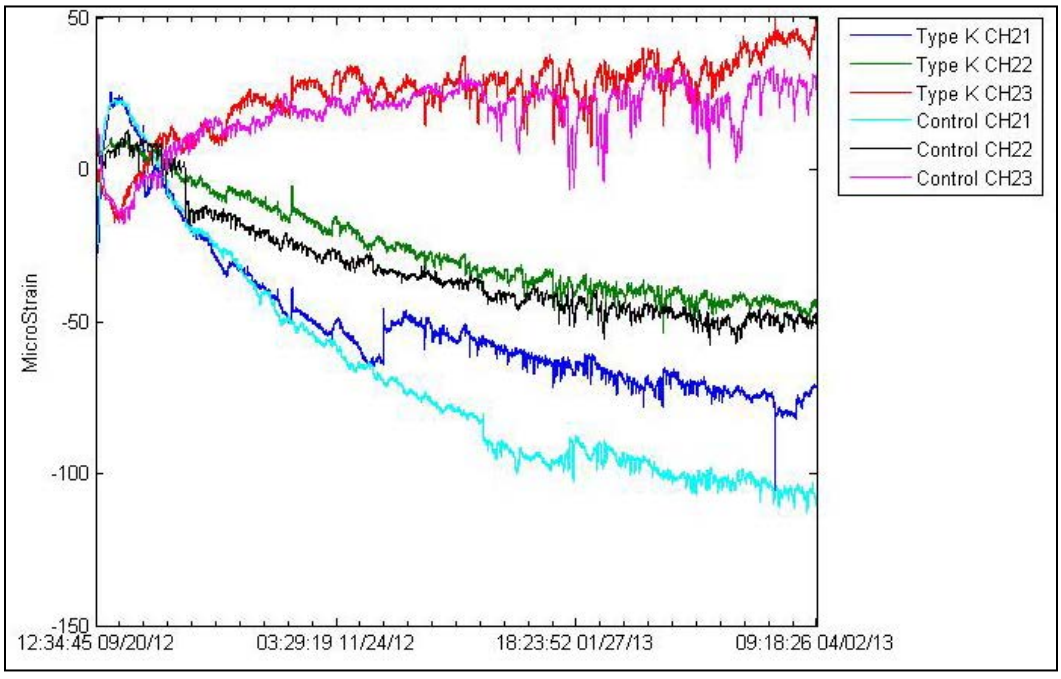

Figure B.4. Girder Type K and control strain gages.

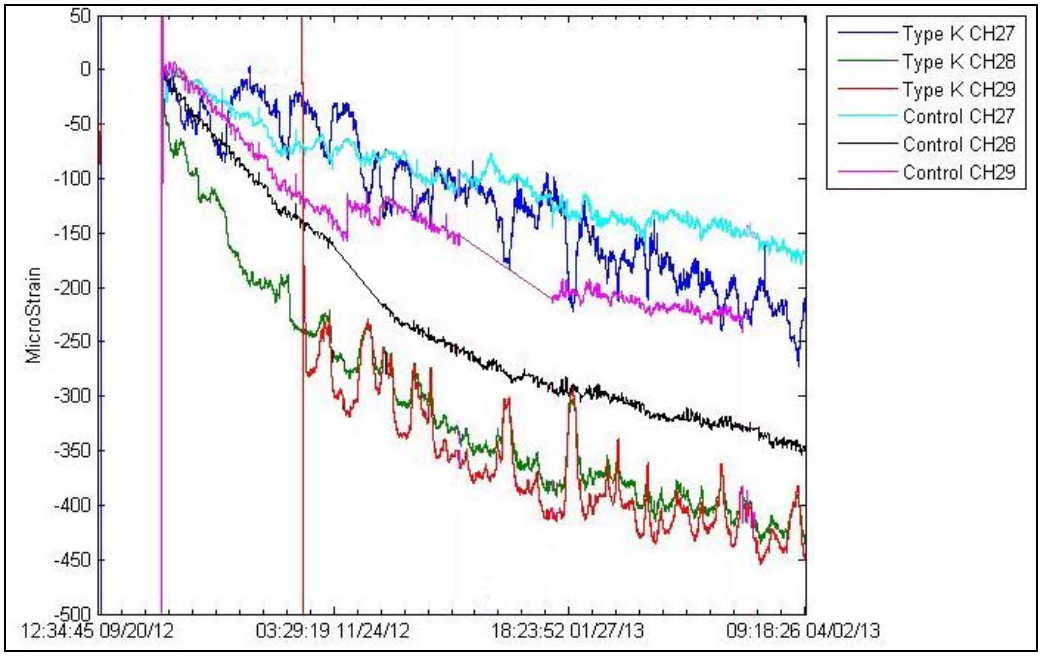

Figure B.5. Top Concrete Longitudinal Type K and control strain gages.

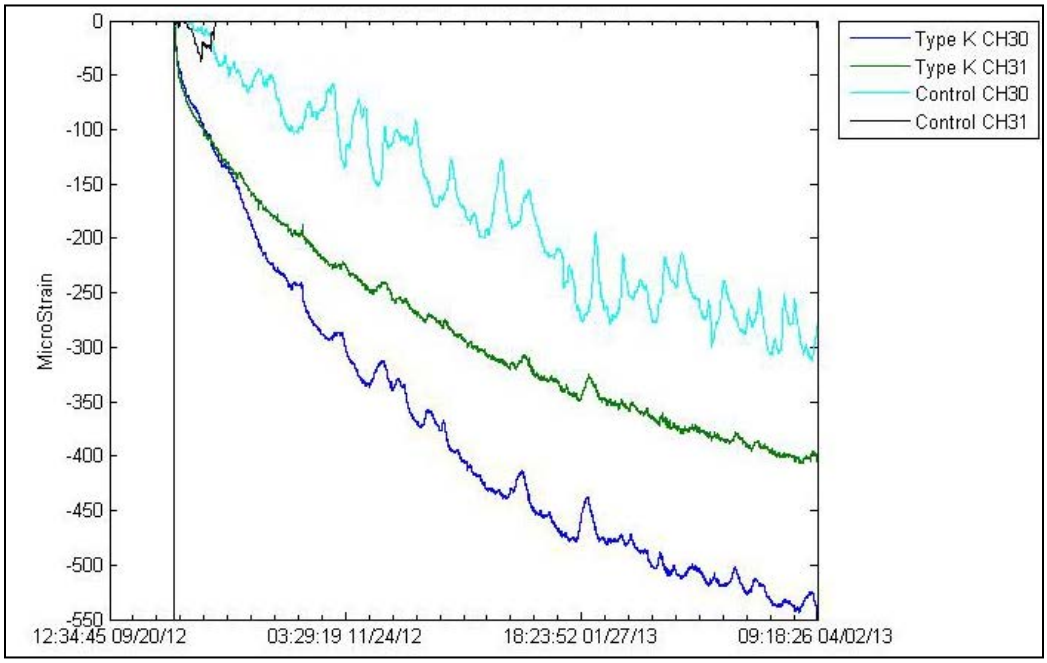

Figure B.6. Top Concrete Transverse Type K and control strain gages.

APPENDIX C CONTROL MIX FINITE ELEMENT MODEL RESULTS

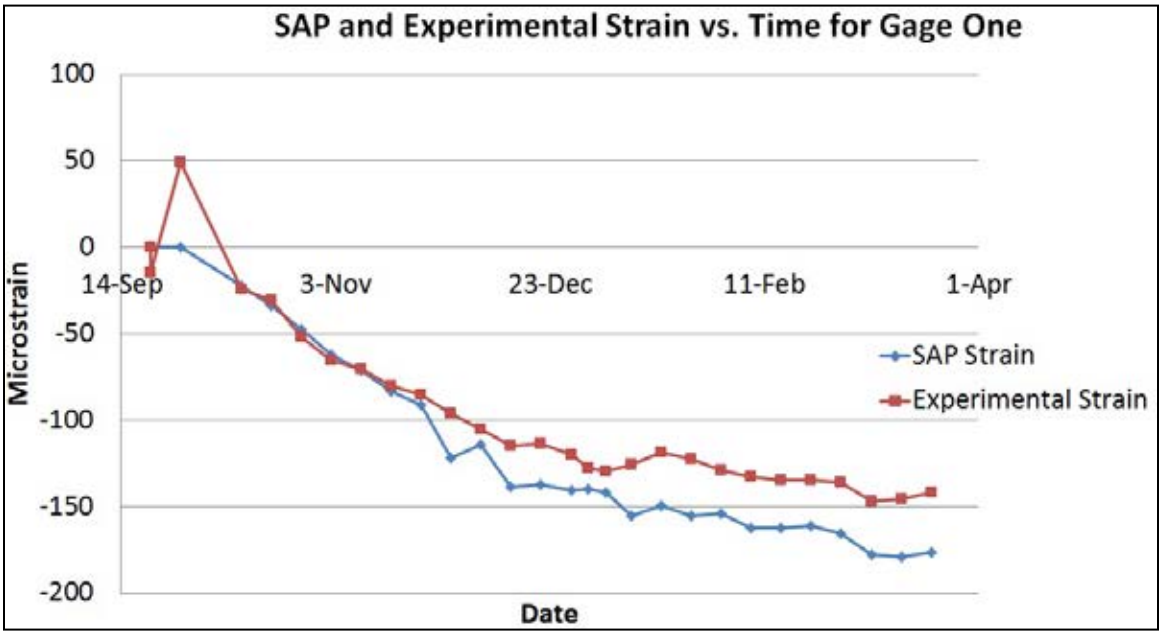

Figure C.1. Gage one SAP and experimental strain.

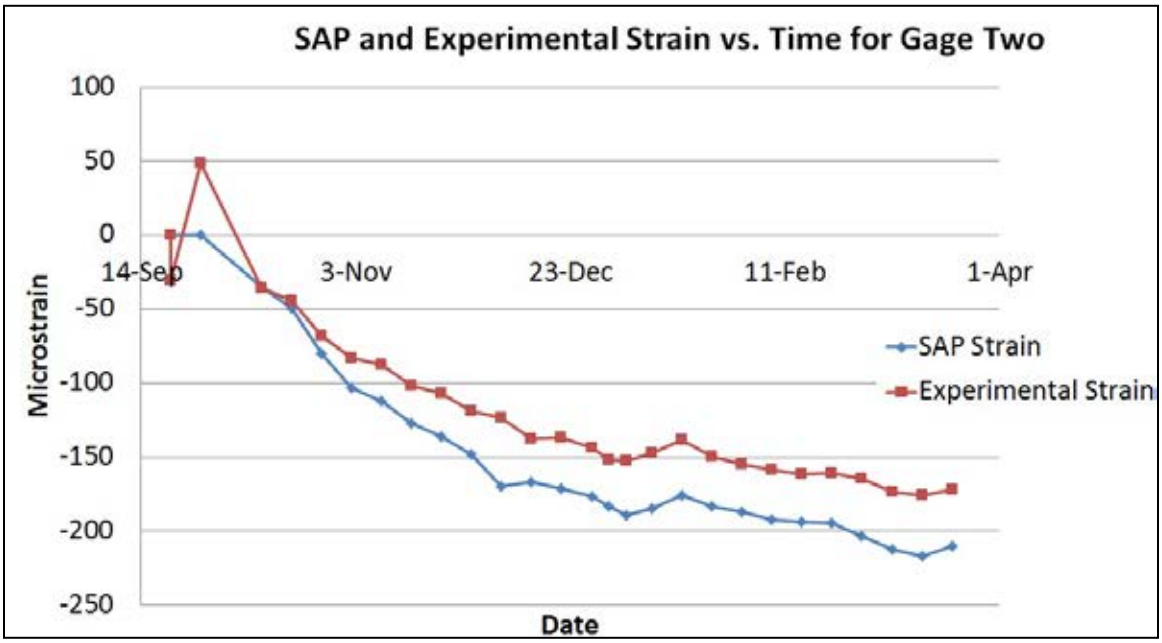

Figure C.2. Gage two SAP and experimental strain.

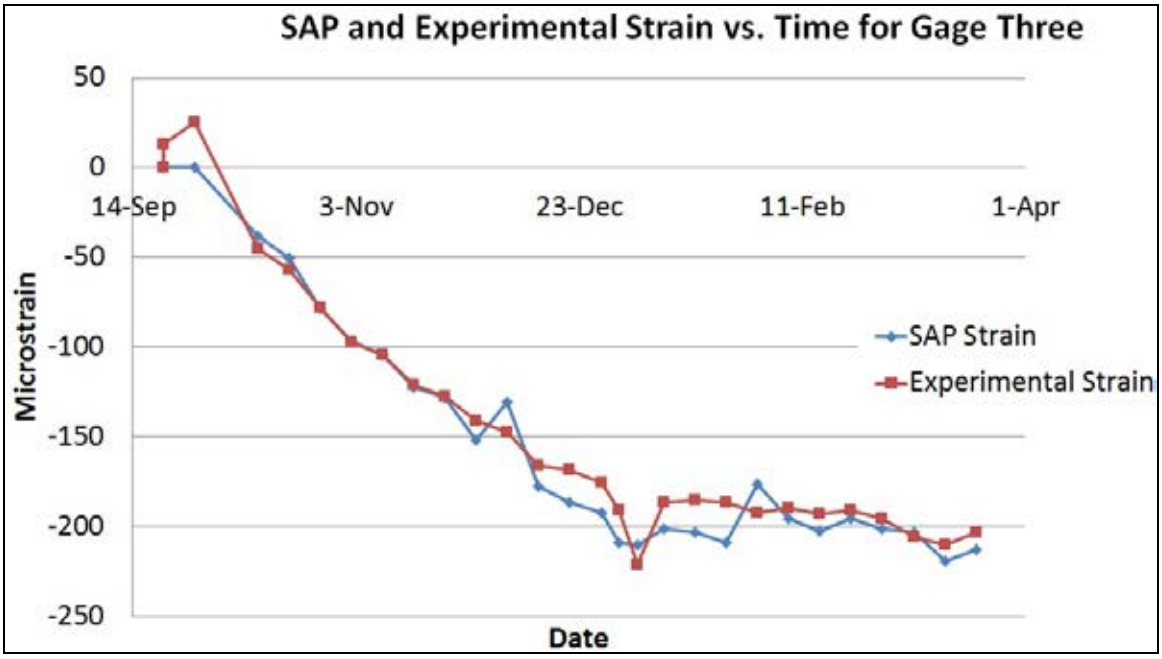

Figure C.3. Gage three SAP and experimental strain.

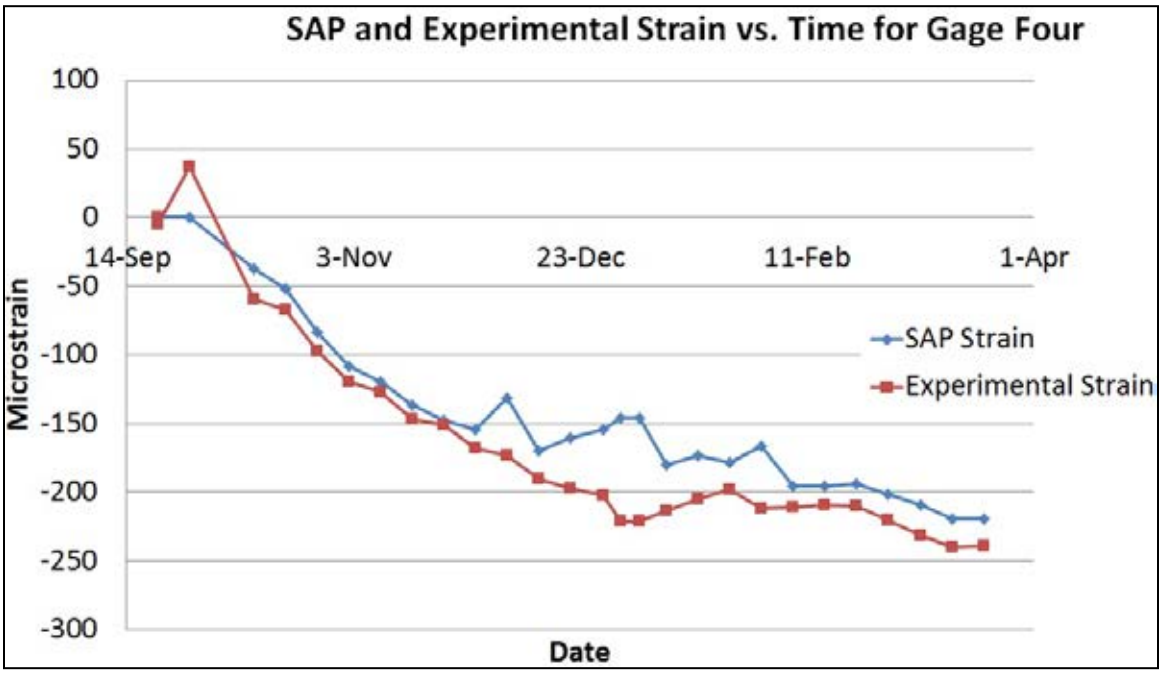

Figure C.4. Gage four SAP and experimental strain.

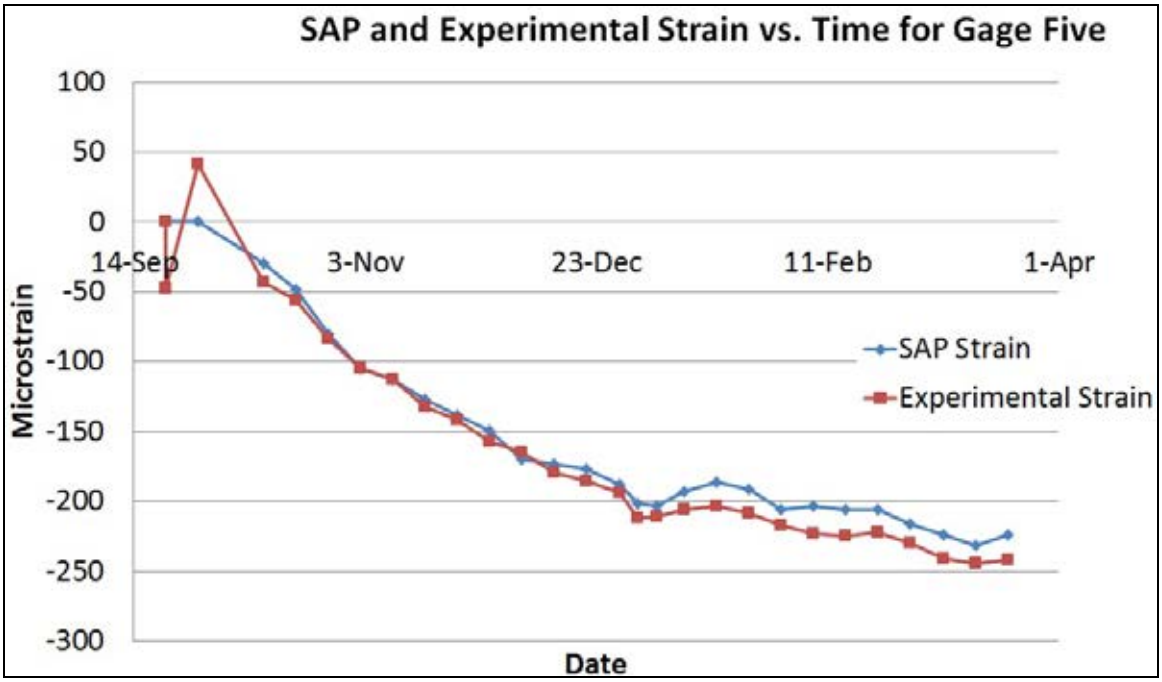

Figure C.5. Gage five SAP and experimental strain.

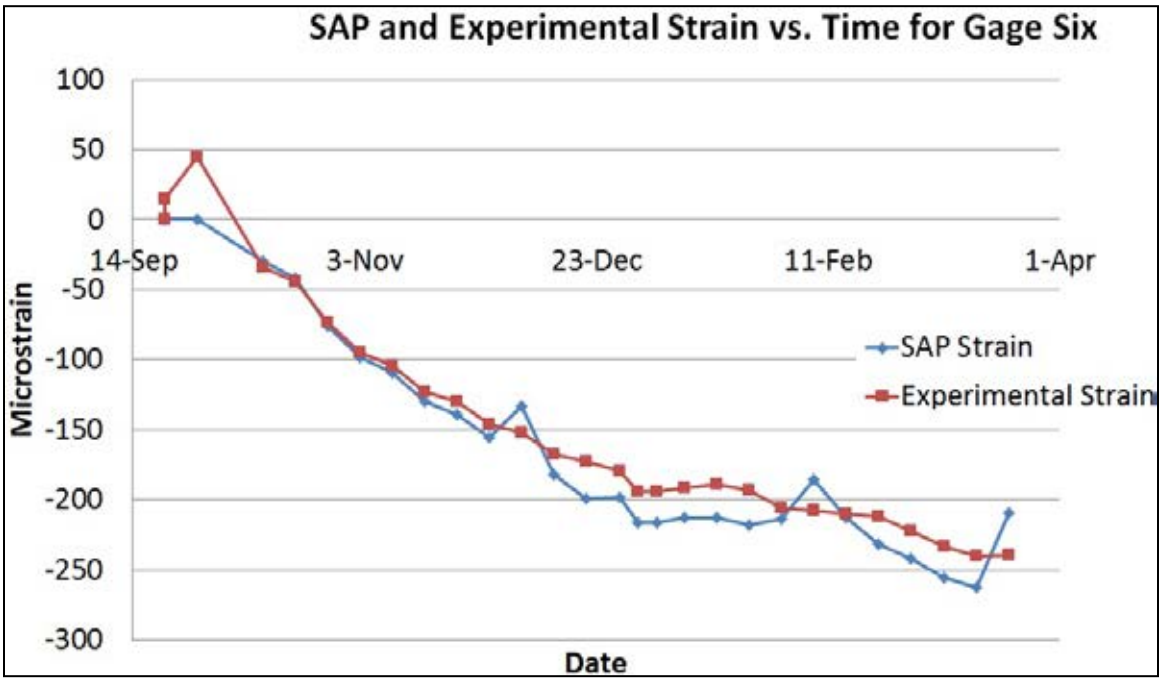

Figure C.6. Gage six SAP and experimental strain.

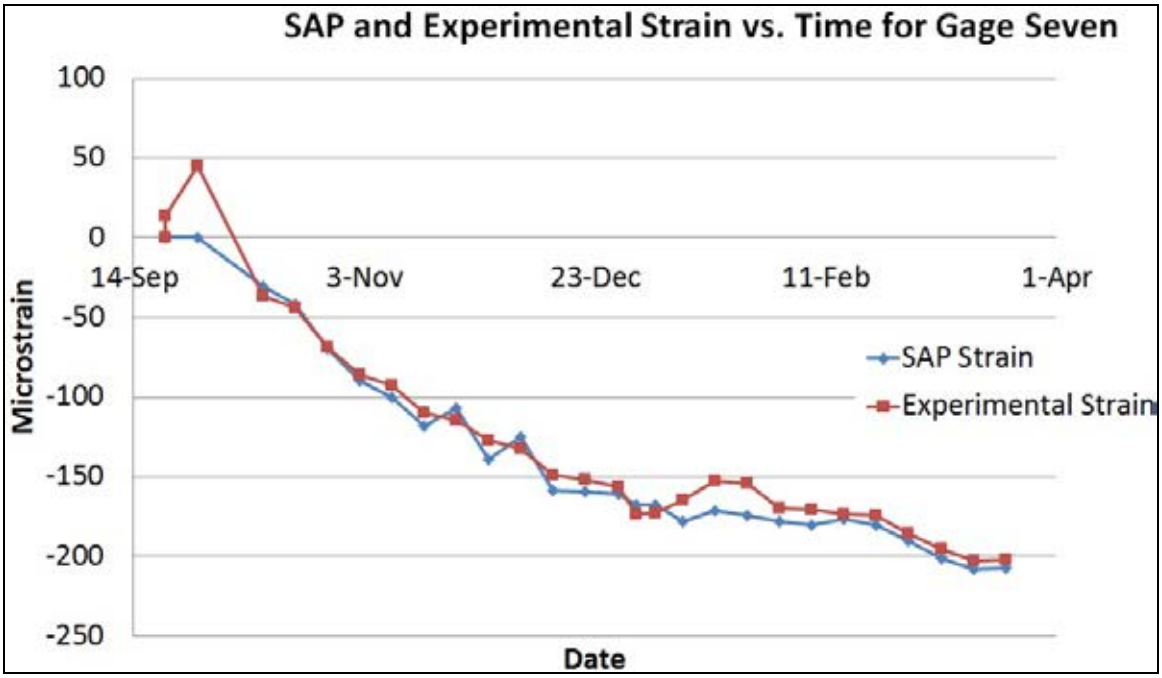

Figure C.7. Gage seven SAP and experimental strain.

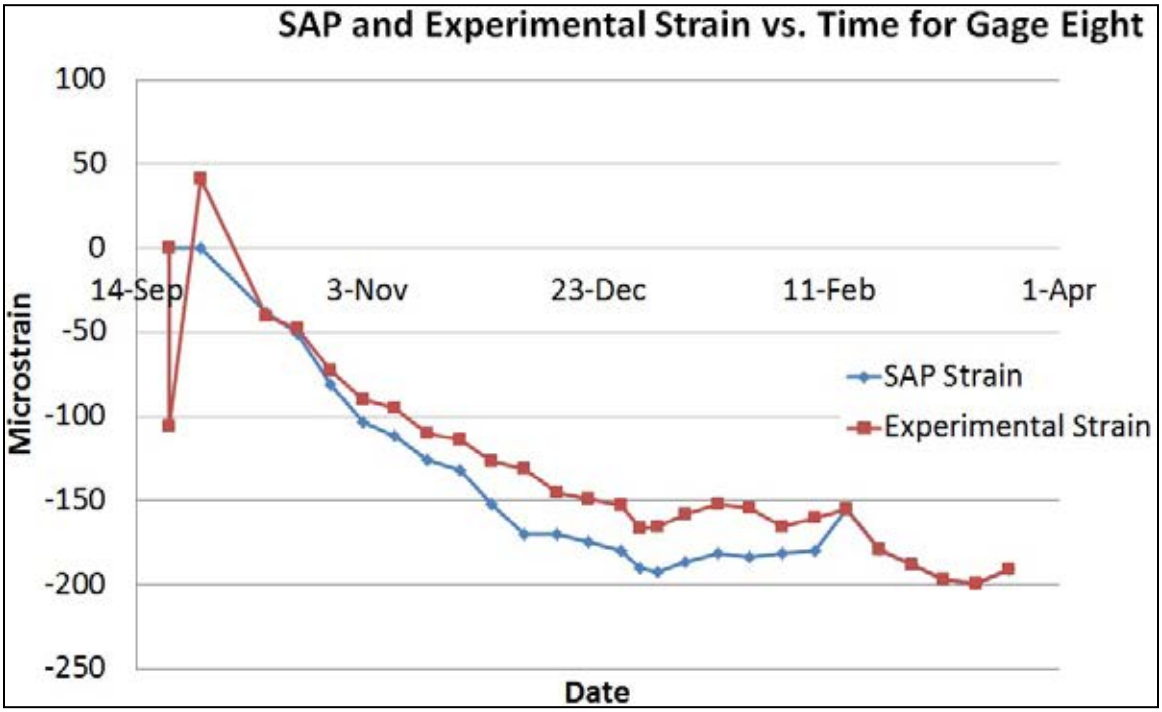

Figure C.8. Gage eight SAP and experimental strain.

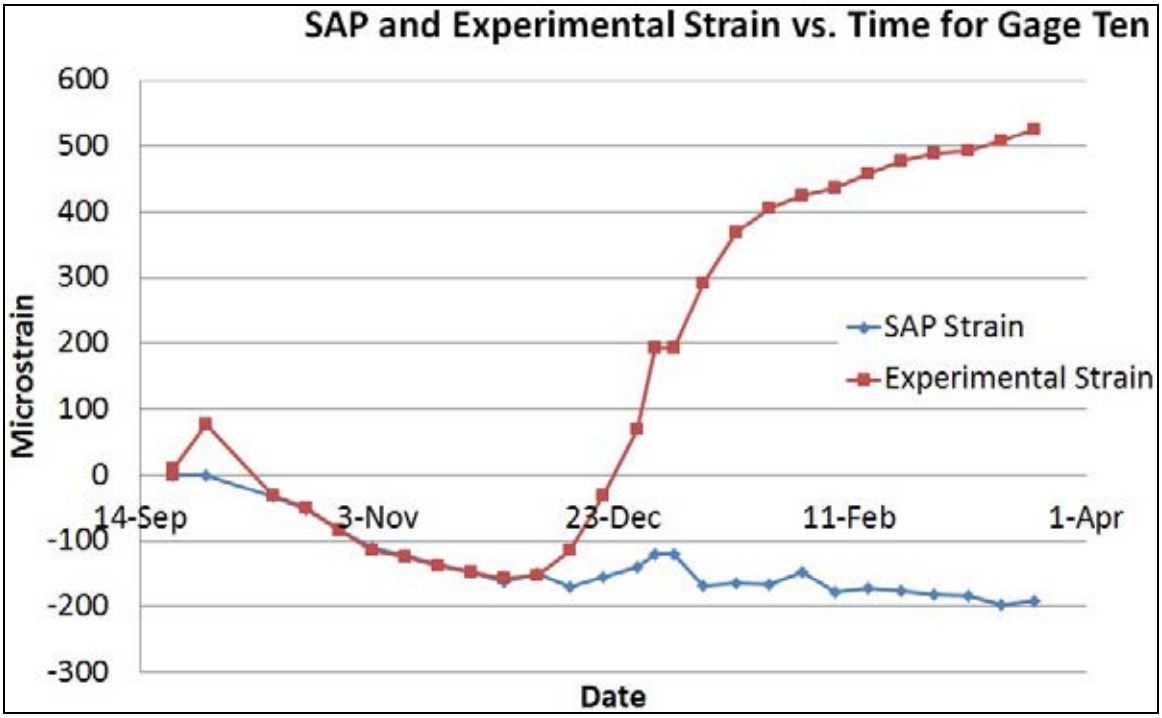

Figure C.9. Gage ten SAP and experimental strain.

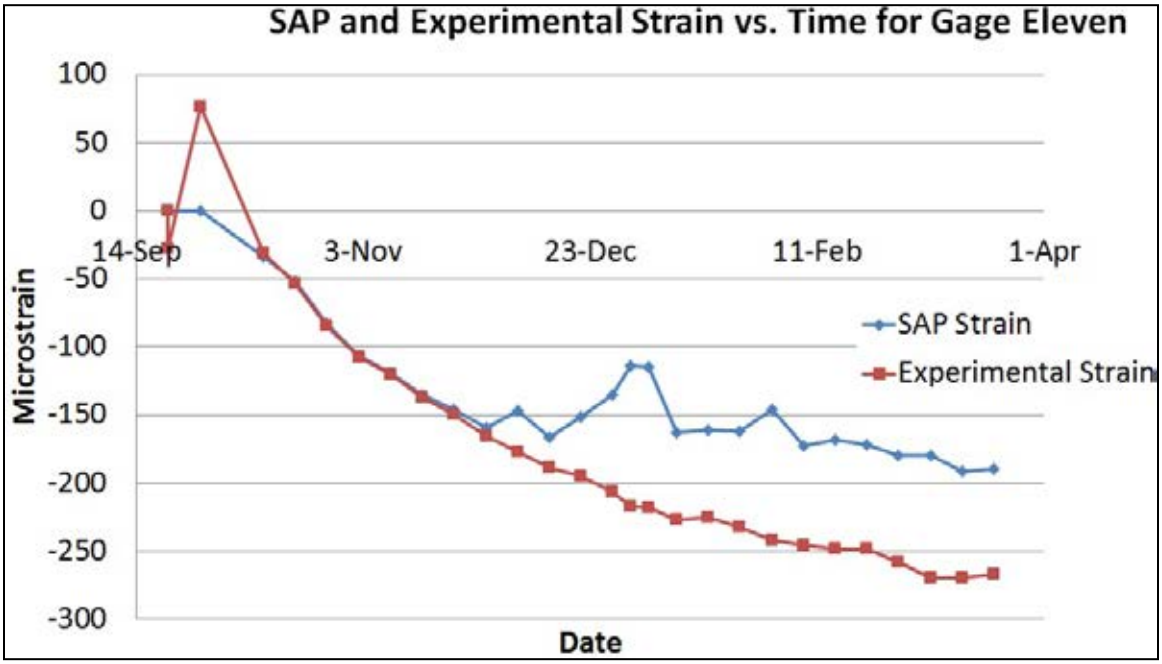

Figure C.10. Gage eleven SAP and experimental strain.

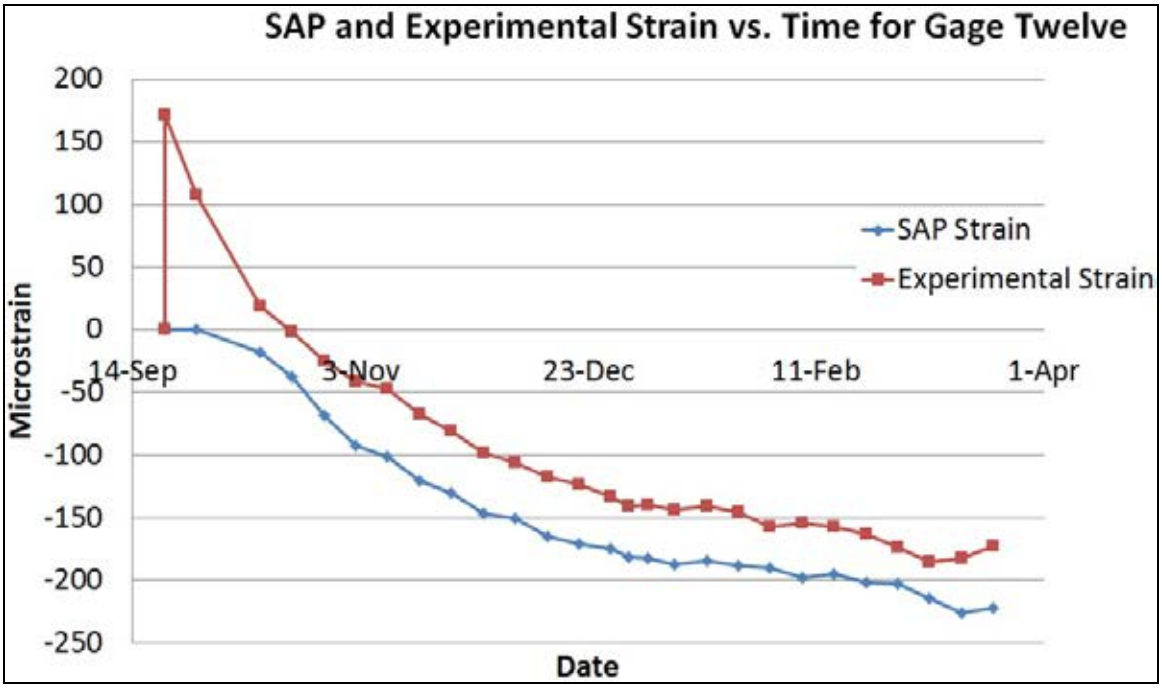

Figure C.11. Gage twelve SAP and experimental strain.

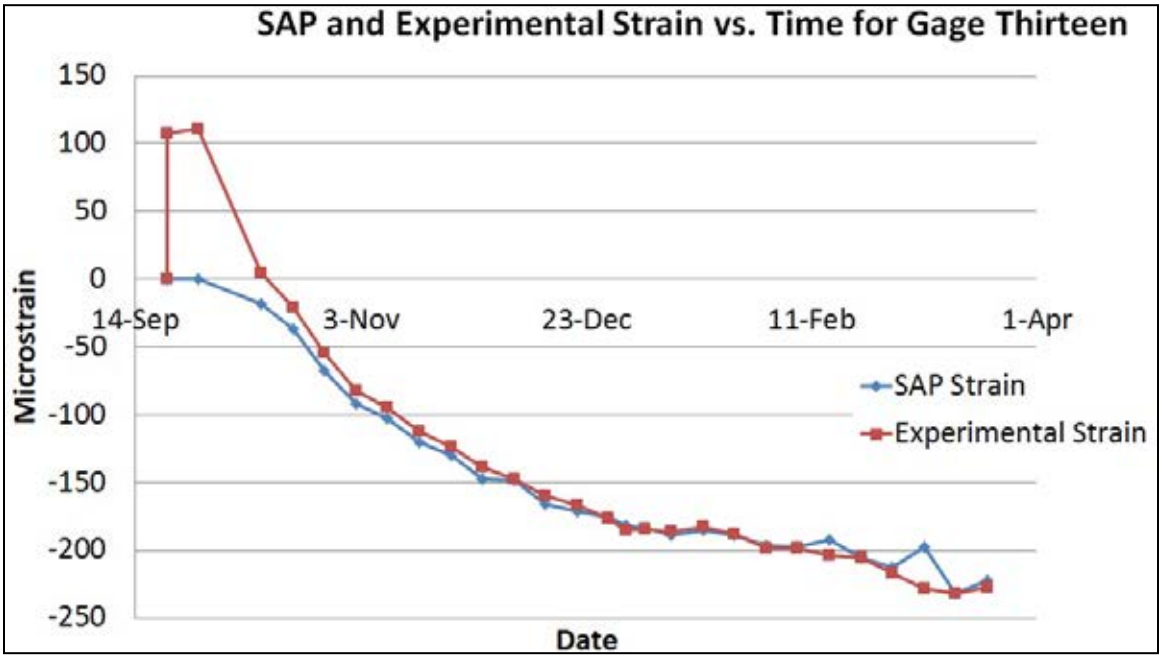

Figure C.12. Gage thirteen SAP and experimental strain.

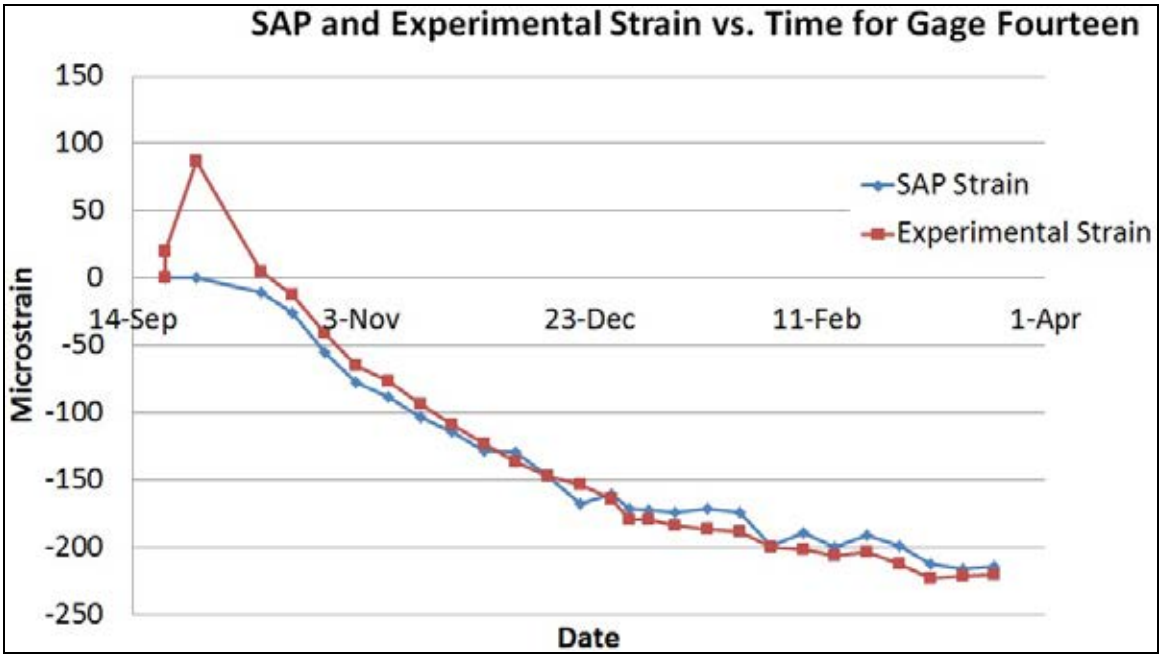

Figure C.13. Gage fourteen SAP and experimental strain.

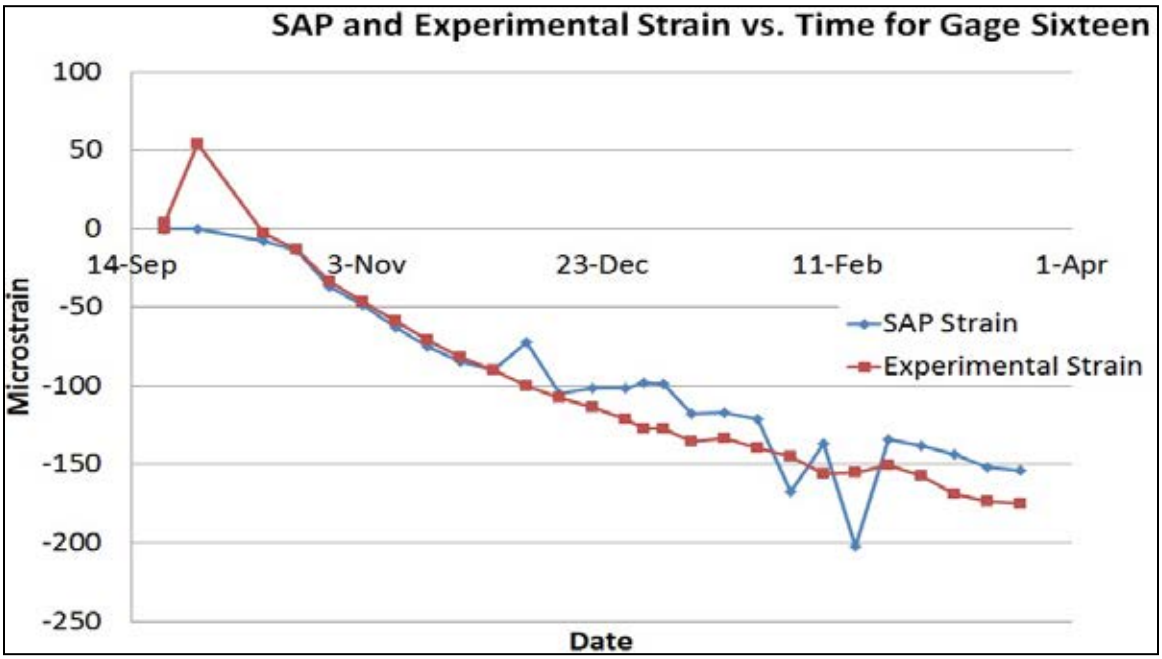

Figure C.14. Gage sixteen SAP and experimental strain.

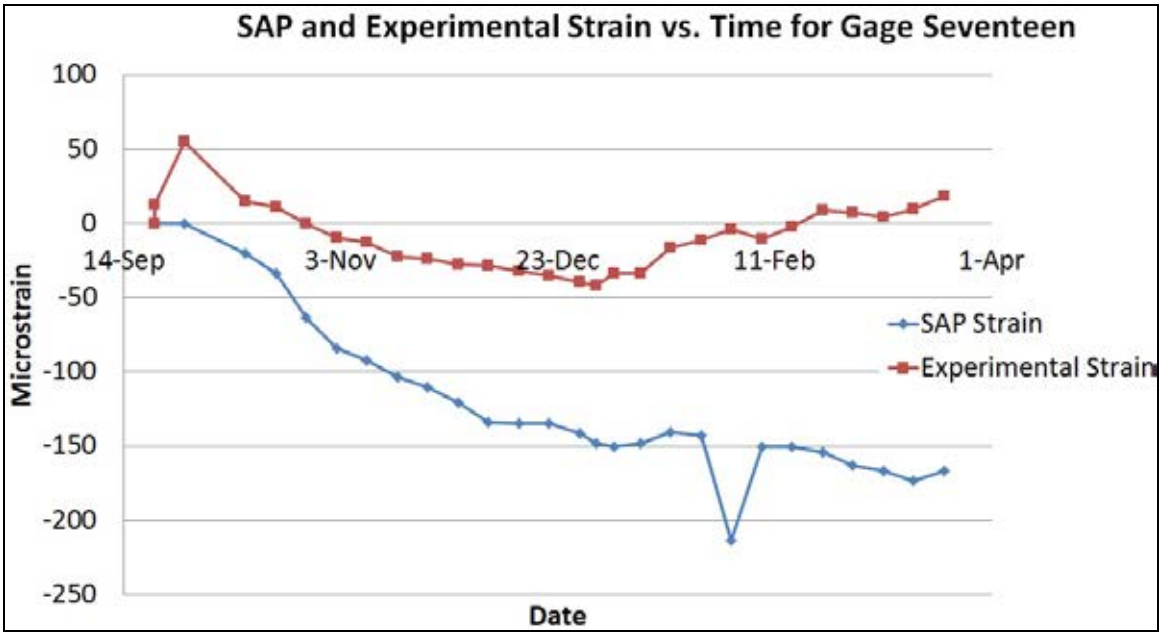

Figure C.15. Gage seventeen SAP and experimental strain.

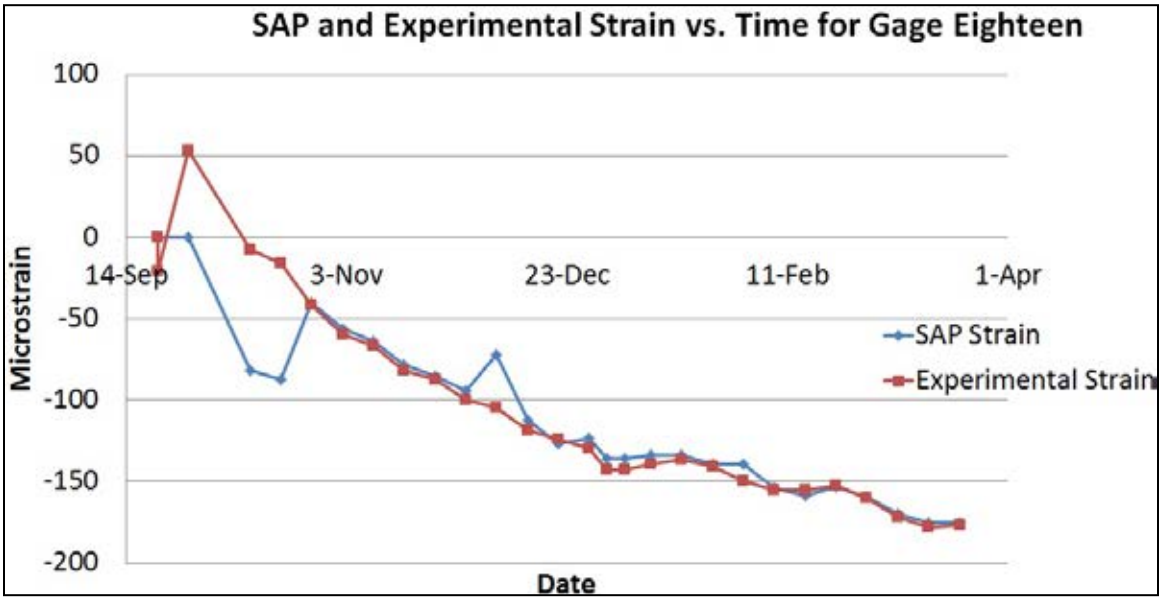

Figure C.16. Gage eighteen SAP and experimental strain.

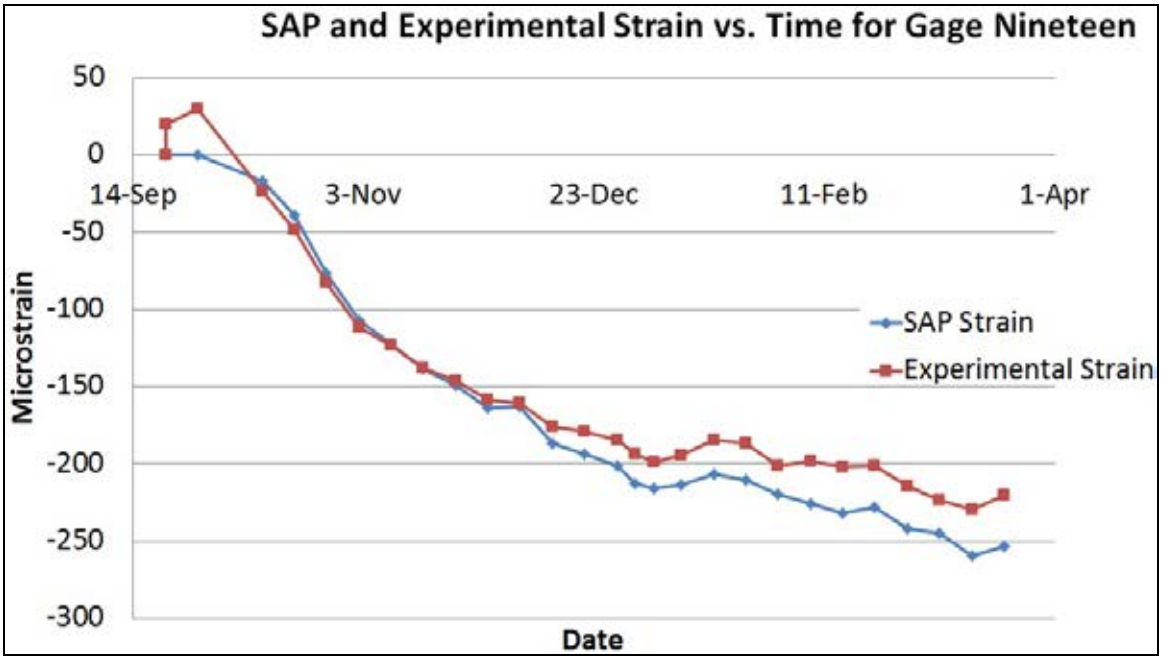

Figure C.17. Gage nineteen SAP and experimental strain.

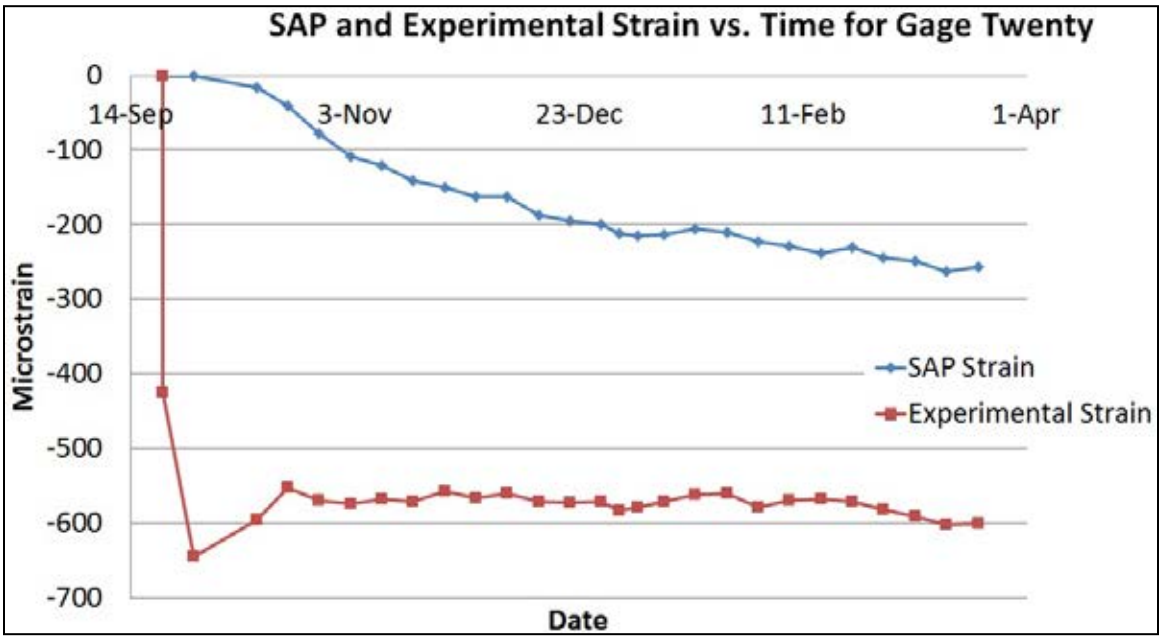

Figure C.18. Gage twenty SAP and experimental strain.


Illinois Department
of Transportation


ILLINOIS
UNIVERSITY OF ILLINOIS AT URBANA-CHAMPAIGN